2018

Linking Microbial Phylogenetic and Functional Gene Diversity to Microbial Mat Ecosystem Function Following Environmental Disturbance

Eva Christine Preisner
University of South Carolina

LINKING MICROBIAL PHYLOGENETIC AND FUNCTIONAL GENE DIVERSITY TO MICROBIAL MAT ECOSYSTEM FUNCTION FOLLOWING ENVIRONMENTAL DISTURBANCE

by

Eva Christine Preisner

Bachelor of Science
University of Duisburg-Essen, 2010

Master of Science
University of South Carolina, 2012

Submitted in Partial Fulfillment of the Requirements

For the Degree of Doctor of Philosophy in

Environmental Health Sciences

The Norman J. Arnold School of Public Health

University of South Carolina

2018

Accepted by:

Robert Sean Norman, Major Professor

Alan W. Decho, Committee Member

Anindya Chanda, Committee Member

James Pinckney, Committee Member

Cheryl L. Addy, Vice Provost and Dean of the Graduate School

DEDICATION

This work is dedicated to the beautiful microbial mats on San Salvador Island, The Bahamas that have gained, besides the attention from scientists, little acknowledgement from the general public and locals who have called the Ponds harboring mats “the stinky ponds”.

ACKNOWLEDGEMENTS

This work could not have been done without the help of many people. First and foremost I want to acknowledge my family in U.S. and back home in Germany, who supported me in many ways. Especially my husband who has been there for me and always had an open mind to discuss my research, sat through plenty of practice talks, and motivated me to keep going when I wanted to give up. My son, the light of my life, who put things in perspective the moment he was born. A great thank you to all my other grad-student friends who can easily relate to the hard work of being in graduate school and who always supported me. My lab peers have been wonderful throughout the years and helped me develop into a better scientist by teaching me new methods and discussing research. A special acknowledgement to Erin Fichot and Gargi Dayama who both were not only my lab mates but became my closest friends. The people from the RCI, Paul, Nathan, and Ben at the University of South Carolina were more than supportive of our lab and helped us tremendously with the computational resources to handle the bioinformatics side of our research. A special thank you to Ben Torkian, who did not mind my endless questions and quickly wrote an R or Phython script for me to help with the analysis. I also want to thank Dr. Jay Pinckney's lab group for helping me with sample preparation and photopigment analysis. I am very grateful to have Dr. Pinckney on my doctoral committee; he always had an open door to talk about my research and the sample site, and was a great help with statistical analysis. I want to give a special acknowledgement to Dr. Anindya Chanda for agreeing almost last minute to serve on my

doctoral committee. To the last member of committee Dr. Alan Decho, for helping us with this study by sharing knowledge and lab equipment. I also want to thank everyone we have worked with and all the staff at the Gerace Research Station on San Salvador Island, the Bahamas; we certainly couldn't have done all the research without their help. Lastly, I want to give a big thank you to my adviser and mentor Dr. Sean Norman, who invited me to come study in his lab and didn't let me go until I had my PhD, it has been a pleasure to be your student.

ABSTRACT

The ability of ecosystems to adapt to environmental perturbations depends on the duration and intensity of change and the overall biological diversity of the system. In this study, a microbial mat ecosystem located on San Salvador Island, the Bahamas was used as a model to examine how environmental disturbance affects microbial community resistance, their protein synthesis potential (PSP), ecosystem function as measured by biogeochemical cycling, community stability, and resilience. This ecosystem experienced a large shift in salinity (230 to 65 g kg^{-1}) during 2011–2012 following the landfall of Hurricane Irene on San Salvador Island. High throughput sequencing and analysis of 16S rRNA and rRNA genes from samples before and after the pulse disturbance showed significant changes in the diversity and an increase in PSP of abundant and rare taxa, suggesting overall compositional and functional sensitivity to environmental change. Together, these findings show complex community adaptation to environmental change and help elucidate factors connecting disturbance, biodiversity, and ecosystem function that may enhance ecosystem models. Based on these findings, a long-term study was conducted to answer questions about the impacts of seasonal and pulse disturbance on the community resistance, ecosystem function and stability, and resilience using a comparative metagenomic approach. Over the course of four years the microbial mat community was monitored and vertical sections were taken at eight time points. We found that a wide range of environmental factors play a role in shifting the microenvironment of the mat resulting in compositional changes over time leading to

vertical niche differentiation within the mat. Community composition did not significantly change on Archaea and Bacteria phyla level but on class level. The microbial community of the deepest layer was resistant to environmental disturbance, while upper layers changed in community composition and did not return to its pre-disturbed state, suggesting that the community was not resilient to the disturbance event after one year. Assessing apparent functional capacity of the archaeal metagenomes over time showed that the metagenome of the first three time points were distinct from all other time points and pre-and postdistubance metagenome were different.

TABLE OF CONTENTS

LIST OF TABLES

LIST OF FIGURES

CHAPTER 1

INTRODUCTION

1.1 Ecosystem Ecology

The term ”ecosystem” was first defined by Sir Arthur Tansley in 1935 as a biotic community or assemblage, including its physical (abiotic) characteristics, located in a specific place. There are three major facets to an ecosystem. First, an ecosystem includes the interactions between the biotic community, which can consist of any forms of living species (e.g. animals, plants, microbes, etc.), and the abiotic factors that demonstrate the physically unique environment in a given place (e.g. temperature, salinity, UV, pH, etc. (Tansley, 1935). Second, an ecosystem is scale-independent, meaning it can be of any size so long as organisms, their physical environment, and biotic/abiotic interactions can exist within (Allen and Hoekstra, 1992). Hence, an ecosystem can be small--such as a microbial mat or a patch of soil--or as large as an ocean. According to (Thiel, 1994) Likens (1992) and (Odom, 1993), when defining a specific ecosystem, an explicit extent (area, size etc.) must be specified and bounded. Third, an ecosystem is not restricted by equilibrium, complexity, or stability (Holling, 1973), meaning that it can be dynamic or in steady state, simple or complex. Tansley’s basic definition of an ecosystem covers an unimaginably broad array of spatial scales—from microbial to biospheric, temporal scales—from instantaneous to geological, and disciplines--from biodiversity to evolution (Jones C. G. 1995). Identifying a changing ecosystem can be difficult, so (Rykiel, 1985) proposed the need to state a reference condition in order to quantify the change (e.g.

stress, perturbation or disturbance). The reference state determines the significance of those changes, including some measure of biological and ecological impact on the system. There are two proposed ways to define a reference state. First, the reference state can be the system's steady state which is defined under optimal conditions (idealization), or secondly, the reference state can be the current state of the system despite its dynamic status. Based on the reference state, ecosystem change can be quantified and seen in terms of cause (disturbance) and effect (perturbation).

It is often understood that disturbances initiate ecosystem change through damage or destruction to the system (e.g. wildfire) after which the system has to recover to reach the initial reference state (Bazzaz 1983). However, the intermediate disturbance hypothesis (IDH) by Connell (1978) states that disturbances can improve ecosystem stability. Specifically, the hypothesis has 2 parts: 1) a "disturbance of a certain intensity and frequency may prevent one or a few species from dominating resources" and 2) a disturbance is "not so biologically damaging that only a few species can use the resulting resources" (Connell 1978). He suggests that the highest number of different species (highest richness) will be reached at intermediate level of disturbance (Figure 1.1) and that both high and low levels of disturbance would lead to reduced diversity. According to his hypothesis, diversity will decline if disturbances are infrequent and of low intensity. But at intermediate levels of disturbance there is enough time between disturbances for a wide variety of species to colonize but not enough time to allow competitive exclusion. Those ecological community changes following a disturbance are termed *succession*. There are three distinguishable types of successions: 1) primary and 2) secondary as well as 3) cyclic successions. 1) A habitat that is uninfluenced by pre-

existing communities and is then newly colonized is termed primary succession. 2) Secondary succession is started by an event (disturbance) and reduces the already established ecosystem to smaller population of species (Bard 1952). 3) Cyclic succession can be described as a state where major disturbances are absent and is driven by pattern of smaller scale changes in which a smaller number of species replaces each other over time (Morin 1999). Climate cycles for example can result in cyclic successions by directly altering physical changes (Glenn-Lewin 1992).

Connell's IDH predicts that in early successional stages, disturbance leads to reduction in diversity. Overall, the IDH has been a topic of many studies and appears in ecological textbooks (Ricklefs 1999; Begon 2005; Lampert 2007); however, 100 published empirical studies as reviewed by Mackey and Currie (2001) show that the peak in diversity at intermediate disturbance levels hardly occurs (< 20% of studies), a result corroborated in another review published in 2007 by Hughes et al. (2007). In Fox's (2013) opinion, the IDH should be "abandoned". He argues that it is theoretically invalid and most of the time can not be explained by empirical data. However, models that were developed recently predict various diversity‐disturbance relationships, including different shaped relationships (Miller et al. 2011). That is why Fox suggests focusing on testing the assumptions and predictions of logically valid models of diversity and coexistence in fluctuating environments.

Definitions for resilience and stability of ecological systems are challenging and depend highly on how one defines equilibrium of a system. Ecological stability concepts are very diverse in the literature (for more information see review of 163 definitions of stability by (Grimm and Wissel 1997)). Grimm and Wissel synthesize three major

different categories for the definition of stability: (1) "staying essentially unchanged", (2) "returning to the reference state after a temporary disturbance" and, (3) "persistence through time of an ecological system". While definitions of the category 1 are based on a specific reference state, category 3 is founded on the question of whether a system persists as an identifiable entity (Shrader-Frechette, 1993; Grimm and Wissel, 1997).

In the literature, resilience reflects different aspects of stability (Holling, 1973, 1996; Ludwig *et al.*, 1996). Holling (Holling, 1996) defines stability as the persistence of a system near or close to an equilibrium state (Walker et al. 2004). In other words, stability quantifies the extent to which a community "stays the same" over a long period of time (depending on the time scale) or during some disturbances. Resilience, however, is how far a system has moved from equilibrium state and how quickly it returns (Walker 1981). However, other sources describe the return times as a measure for stability Holling (Holling 1973). Walker and Holling state that resilience involves the following four aspects: latitude, resistance, precariousness, and panarchy (Walker et al. 2004). Latitude of systems is the maximum amount of disturbance a system can deal with before losing its ability to recover. Resistance describes how easy or hard it is for the system to change. Precariousness explains in which state the system is and how close it is to a limit or "threshold." Panarchy explains how latitude, resistance, and precariousness are "influenced by the states and dynamics of the systems at scales above and below the scale of interest." A guide to avoid terminological confusion was published by Grimm and Wissel (1997) (Table 1.1), and is used in this study as a guide to define terminology.

According to Pielou (1966), diversity refers to the number of species (species richness) or to a diversity index based on the number of species weighted by relative abundance (species evenness). The most widely used diversity index is Shannon-Weaver (H'):

$$H' = - \Sigma p_i \ln p_i$$

where i=species, and p=proportion of total cover (Shannon 1949). Whittaker (1972) defined three levels of diversity, alpha, beta, and gamma diversity. Alpha diversity describes the diversity within a particular area or ecosystem, and is usually expressed by the number of species (e.g. species richness) in that ecosystem. The difference in species diversity between two ecosystems is a measure of beta diversity; specifically, the total number of species unique to each of the ecosystems is compared. Gamma diversity measures the overall diversity for the different ecosystems within a region ("landscape-level" diversity).

Many diversity studies focus on eukaryotes, but it is critical to understand the patterns of prokaryotic (bacteria and archaea) biodiversity due to the following reasons: 1) bacteria and archeaea display the majority of the Earth's species diversity and 2) they are involved in the most important environmental cycles that sustain life on Earth. In plant- and animal- dominated systems, primary productivity is thought to be the major determinant for species diversity (Rosenzweig, 1999) The following studies showed that link in prokaryotes in field systems as well (Benlloch *et al.*, 1995; Øvreås and Torsvik, 1998; Schäfer and Muyzer, 2001; Claire Horner-Devine *et al.*, 2003). In vitro studies showed that microbial diversity peaked after intermediate disturbance (Buckling *et al.*,

2000) so that the IDH is valid for bacterial systems in lab settings. However, in field studies, it was shown that bacterial community composition and diversity may respond to gradients in disturbance (Müller *et al.*, 2002), but it is difficult to assess the applicability of the intermediate-disturbance hypothesis to bacteria outside the laboratory (Fierer *et al.*, 2003).

High-throughput sequencing has broadened our understanding of the scope of biodiversity in ecological systems Sogin et al. (2006). Using operational taxonomic units (OTUs), an *abundant species* has been defined as a microorganism with sequences comprising more than 1% of the sequencing effort (Pedrós-Alió, 2006). Likewise, *rare species* have been defined as OTUs representing 0.1% to <1% of the sequences in a sample (Fuhrman, 2009). The rare biosphere and its functions in ecosystems are mostly undiscovered. Two main hypotheses have been proposed to explain its role. The first hypothesis states that the rare biosphere stays inactive and in low abundance until environmental conditions change, suggesting that the rare biosphere acts like a "seed bank" (Brown and Fuhrman, 2005; Pedrós-Alió, 2006). The second hypothesis claims that rare taxa are active and well adapted to their environmental niche and play a role in ecosystem function (Galand *et al.*, 2009). However, both hypotheses have not been well tested. The rare biosphere might not be as large as previously believed due to the findings of methods for error correction in metagenomic sequencing datasets by Reeder and Knight (2009) . It has also been suggested that the rare biosphere has a biogeography and that it might be subjected to ecological processes such as selection, speciation, and extinction (Galand *et al.*, 2009).

1.2. Photosynthetic Microbial Mats

Microbial mats are complex, densely, layered microbial communities (Stal *et al.*, 1985). Different types of microbial mats can exist almost all over the world in places such as marine intertidal and sub tidal zones and in fresh water rivers and lakes, but microbial mats are mostly found under extreme conditions such as, hot springs, saline lagoons, hypersaline ponds (Des Marais, 1990) (Figure 1.2). In this study we focus on microbial mats in hypersaline ponds on San Salvador Island (The Bahamas) (Figure 1.2 B). Physical characteristics that impact the type of organisms in the mat include, temperature, water content, and flow rate; while chemical characteristics such as pH, alkalinity, oxidation reduction potential (E_0), and concentration of different chemical compounds (e.g. salts, oxygen, hydrogen sulfide, nitrate etc., as well as organic carbon) can also impact the microbial mat. In general, microbial mats are self-sustaining communities that take part in all major biogeochemical cycles and are believed to be analogous to some of the earliest communities on Earth (Cohen *et al.*, 1989). The complex community structure fulfills the definition of an ecosystem because there are interactions between biotic and abiotic elements in a particular space but more importantly due to the presence of all trophic levels (primary producers, consumers, decomposers). Nematodes and diatoms are eukaryotes that are usually found in microbial mats but the eukaryotic diversity in mats is lower than prokaryotic depending on environmental conditions (Nübel *et al.*, 1999; Feazel *et al.*, 2008).

Due to the unique layered structure of microbial mats, it was thought that each of the layers harbors different microorganisms that have distinct metabolic activities (Cohen

et al., 1984). However, when sulfate reducing bacteria (SRB) typically associated with anoxic layers, were found at the surface level of mats (Canfield and Des Marais, 1991), this view had to be revised. Mat microorganisms can be classified into six major functional groups: oxygenic phototrophs, anoxygenic phototrophs, aerobic heterotrophic bacteria, fermenters, anaerobic heterotrophs, and sulfide oxidizing bacteria (van Gemerden, 1993; Visscher *et al.*, 1998; Visscher and Stolz, 2005).

Primary producers (e.g. cyanobacteria) belong to the first functional group of the system (light induced CO_2 and N_2 fixation) (Paerl *et al.*, 2001). Filamentous cyanobacteria trap and bind sediment and sand grains together with extracellular polysaccharide (EPS), thus establishing the foundation for microbial mats. Primary producers use photosynthetically active radiation (PAR = 400–700 nm), which has been found to penetrate the first two mm of the mat, in oxygenic and anoxygenic photosynthesis. The second functional group, anoxygenic phototrophs (e.g. purple and green bacteria), is also involved in photosynthesis but it uses HS^- instead of O_2 as an electron donor. The aerobic heterotrophic bacteria gain energy from respiration of oxygen and organic carbon and can exist in the range of near infra-red radiation (NIR = 700–1100 nm) which is deeper in the mat than PAR (van Gemerden, 1980). Using organic carbon or sulfide compounds as electron donor and acceptor, fermenters build the fourth functional group (Bak and Cypionka, 1987; Visscher *et al.*, 1999). The fifth group consists of anaerobic heterotrophs, predominantly SRB, that respire organic carbon with sulfate and produce hydrogen sulfide ions (HS^-). The last functional group, sulfide oxidizing bacteria (SOB), has many chemolithoautotrophs that oxidize reduced sulfur compounds with oxygen or nitrate while fixing carbon dioxide. Most of the 6 functional

groups can be found in microbial mats, however, they are mainly photosynthetically driven systems and are mostly dominated by cyanobacteria (Stal, 1994).

Photopigments secreted by phototrophic bacteria and archaea result in color banding visible in depth sections of mats. Diatoms and cyanobacteria are mostly found in the upper brownish layer. The underlying dark green layer (~2 - 4 mm) has the highest photosynthetic activity and is dominated by filamentous cyanobacteria such as, oscillatorians (*Microcoleus*, *Oscillatoria*, *Lyngbya*, *Spirulina*) and *Chroococcales* (*Mesrismopedia*, *Chroococcus*) (D'Amelio *et al.*, 1989). All functional groups are involved in element cycling. Because microbial mats can function with sunlight as energy input into the system, they can be considered as semi-closed systems(Fenchel, 1998). These attributes have made microbial mats attractive models for better understanding elemental cycling, microbial interactions, and the evolution and the ecology of microbial systems supporting the processes that now sustain our biosphere.

1.3. Biogeochemical cycling in microbial mats

Biogeochemical cycling describes the transport and transformation of substances (chemicals or molecules) in biotic and abiotic parts of the ecosystem. Microorganisms play a major role in element cycling (Butcher 1992). In microbial mats, oxygen, carbon, nitrogen, phosphorous, and sulfur cycles are present and found to be inextricably interconnected within microbial communities (Canfield and des Marais 1993). For instance, the oxidation and reduction of nitrogen and sulfur compounds are directly coupled to the reduction and oxidation of carbon, respectively, all carried out by different microbial communities.

The water in which microbial mats grow is usually nutrient depleted (Javor 1983), but the mat itself is a highly productive system involved in all major biogeochemical cycling. Figure 1.3 explains how microbially driven biogeochemical processes are interconnected based on photosynthesis. The major energy input into the system is sun light, which triggers both oxygenic and anoxygenic photosynthesis. During oxygenic photosynthesis, an electron donor, H_2O, is oxidized and CO_2 fixation occurs ($[CH_2O]_n$). In anoxygenic photosynthesis the electron donors are HS^-, H_2, or Fe^{2+} (Figure 1.3). Electrons and protons from oxygenic and anoxygenic photosynthesis are then used to reduce inorganic carbon to organic matter. Resulting compounds serve as electron acceptors in either aerobic/anaerobic respiration or can be used by photosynthetic organisms (Blankenship *et al.*, 1995).

Phototrophic organisms form the foundation of the carbon cycle, where organic matter (CH_2O) is generated through photosynthesis [$CO_2 + H_2O \rightarrow (CH_2O) + O_2$]. The resulting carbohydrates can be degraded in either a respirational or a fermentative process. Methane and carbon dioxide are formed through the activity of methanogens and chemoorganotrophs during fermentation, anaerobic respiration or aerobic respiration (see Figure 1.3). Methane produced in anoxic environments is oxidized to CO_2 in the oxic zone.

In the nitrogen cycle, nitrogen gas fixation is the only biological process that makes N_2 accessible for the synthesis of proteins and nucleic acids. N_2 is transformed to NH_4^+, this reductive reaction is catalyzed by nitrogenase (Figure 1.4, Step 1). Nitrogenase is an enzyme complex, which is inhibited by oxygen (Postgate, 1998). NH_4^+ is oxidized to nitrate in the presence of oxygen (Step 2). This reaction can happen in a two-stage

pathway by a specific group of Bacteria or Archaea that oxidize ammonia to NO_2^- (via hydroxyamine). Nitrifying bacteria then oxidize NO_2^- to NO_3^- (Falkowski, 1997) (Step 3). Using the small differences in redox potential in the oxidation reactions, nitrifiers reduce CO_2 to organic matter. Opportunistic microbes are involved in the respiration pathway that forms N_2. Under the anaerobic oxidation of organic matter, NO_2^- and NO_3^- are used as electron acceptors if O_2 is absent (Step 4). The nitrogen cycle was believed to be closed, but research within the last decade found that there are more processes involved shown in Figure 1.4. step 5 and 6. Step 5 describes both, a process called anamox where NO is oxidized anaerobically to N_2H_2 (Strous *et al.*, 1999), and NH_4^+ oxidation by crenarchaea (Könneke *et al.*, 2005; Francis *et al.*, 2007) as well as the interaction between these two groups (Lam and Kuypers, 2011). Step 6 shows the dissimilatory nitrate and nitrite reduction to ammonium (Risgaard-Petersen *et al.*, 2006) .

The sulfur cycle takes place in mostly anaerobic conditions. The major aerobic process is the oxidation of sulfate to S^{2-} which occurs intracellularly. Organic S mineralization leads to HS^-, which can then be oxidized by oxygen by facultative chemolithotrophs in a dissimilatory process via O_2 or NO^{3-}, Mn^{4+}, or Fe^{3+} as electron acceptors. Sulfate is the end product but several intermediates can be found. Sulfide can also be oxidized in a photosynthetic process resulting in S^0 and SO_4^{2-} (by phototrophic sulfur bacteria).

Paerl and Pinckney (1996) graphically explained each biogeochemical process within a depth profile of microbial mats where processes of microbial nitrogen, sulfur and carbon transformation occur in regard to the biogeochemical transformation take place (Figure 1.5. A, B, C). With oxygen concentrations decreasing the production of

ammonia/ammonium (NH_4^+/NH_3) increases (see yellow line shifting more to the right as oxygen disappears). Nitrification maximizes at oxic/anoxic interface, here ammonia/ammonium is first oxidized to nitrite (NO_2^-), which is then oxidized to nitrate (NO_3^-). Denitrification is the anaerobic conversion of nitrate to nitrogen (N_2) and depends on high nitrate concentrations within the sediment. N_2 is then converted to ammonium via N_2 fixation.

Sulfate (SO_4^{2-}) concentrations are highest in oxic zone (see yellow line) while in the anaerobic environment sulfide (S_2^-) is reoxidized to elemental sulfur (S), sulfate, or thiosulfate. In the carbon cycle, anaerobic respiration is localized in oxic zone; whereas anaerobic respiration and fermentation as well as methanogenesis are deeper in the anaerobic zone.

1.4. Molecular based tools

Several molecular-based tools exist to study ecosystem function, one of which is the use of transcript analysis. In transcriptomics, the abundance of major genes involved in elemental cycling are quantified to examine the rate of biogeochemical cycling occurring at a given time or over time. Using reverse transcriptase quantitative polymerase chain reaction (RT-qPCR), it is possible to calculate how many copies of the gene of interest were present at the time of sampling, which helps to estimate up- or down- regulation of a specific pathway within the microbial mat. To study nitrogen fixation, researchers can use a part of the nitrogenase pathway, which is encoded by the gene *nif*H (the reductase). The gene involved in the process of archaeal and bacterial nitrification (Step 2 in Figure 1.4.) is called *amo*A (ammonium monoxygenase). The genes believed to take part in denitrification are nitrous oxide reductase genes (*nir*K, *nir*S

and *nos*Z). A functional gene that encodes a key enzyme (reductase AprBA) of the dissimilatory sulfate-reduction pathway can be used to look at the sulfur cycle in sulfate reducing (SRB) and oxidizing bacteria (SOB). The terminal step of the pathway in methanogenesis is the expression of methyl coenzyme-M reductase subunit A (*mcrA*) gene. This can be used as an indicator of the methanogenic activity (Nazaries *et al.*, 2013).

Photopigments can be used as a measure of distribution of oxygenic (oxygenic chlorophyll *a* (Chl *a*)) in relation to anoxygenic photosynthesis (bacteriochlorophyll (BChl)). Both processes together with chemoautotrophy resemble primary production. According to Stal *et al.*, (1985) primary productivity (especially CO_2 fixation) and nitrogen fixation can be an ecophysiological measure for phototrophic community growth. Primary productivity can also be a measure of trophic stability and an indicator of ecosystem recovery after a perturbation (Oksanen *et al.*, 1981). Adenosine triphosphate (ATP), generated during photosynthesis is used for reproduction and cell growth, but after a disturbance it can shift towards stress compensating mechanisms in the cell resulting in lower primary productivity.

There are different approaches to look at the relative abundance of species within the microbial mat. Depending on the research interest, one can use chemosystematic photopigments as indicators of the relative abundance when looking at the phototrophic community of the mat. Analysis of the 16S rRNA genes give information of the total pool of DNA that might consist of DNA derived from living, dormant or even dead cells as well as extracellular DNA (Josephson *et al.*, 1993). DNA has a relatively long life span as compared to RNA, so RNA, which is transient, can serve as an indicator of the

metabolically active fraction of the community (Mills *et al.*, 2005; Moeseneder *et al.*, 2005; Gentile *et al.*, 2006). There is a linear relationship between cellular rRNA content and the growth rate in bacteria (DeLong *et al.*, 1989; Kemp *et al.*, 1993; Kerkhof and Ward, 1993). During starvation, the rRNA content decreases to minimum levels in the cell (Fegatella *et al.*, 1998). The higher amount of rRNA in active than in dormant cells associated with the higher number of ribosome in active cells provides a tool to determine the metabolically active members of the bacterial community (Poulsen *et al.*, 1993). To explore an aspect of activity and dormancy the abundance of the 16S rRNA gene transcripts is compared to the abundance of bacterial and archaeal communities via 16S rRNA genes (rDNA). Here we are using the term rDNA when we describe the 16S rRNA genes to differentiate between transcripts of the gene and the gene itself. The ratio of 16S rRNA to rDNA is an index of the growth rate for specific taxa in natural communities (Jones and Lennon, 2010).

1.5. Comparative Metagenomics

Metagenomics is described as the study of microorganisms by sequencing random pieces of their genomes directly from environmental or clinical samples (Handelsman *et al.*, 1998; Rondon *et al.*, 2000). Metagenomics require no prior cultivation of individual isolates or entire communities, as the method is based solely on nucleic acid extraction of the sample and microbial communities can therefore be studied directly in their natural state (Schloss and Handelsman, 2005). Taxonomic compositions and metabolic profiles of the microbial communities inhabiting a specific environment can be studied using metagenomics. By comparing gene abundance between metagenomes, important

differences in community structure, diversity and biological function can be identified. With the decrease in cost and increase in efficiency within the last decade, high throughput DNA sequencing technologies (or next generation sequencing technologies) have become a widely-used tool for the study of metagenomes. The term metagenomics has been falsely applied to studies performing PCR amplification of certain marker genes and was referred to as "marker gene amplification metagenomics". Direct sequencing of a nucleic acid pool is termed "shotgun metagenomics", as the whole genetic potential of a sample is being analyzed. Shotgun metagenomics has evolved to address the questions of "who" is present in an environmental community, "what" they are doing (function-wise), but also "how" these microorganisms interact to sustain a balanced ecological niche. Post sequencing processing of metagenomic data poses a challenge, as there are many different ways to perform analyses each containing certain caveats. Depending on sequencing technology used different options of post run processing need to be carefully assessed.

One of the first steps after removing any sequences containing errors or those sequences not meeting quality criteria (quality control step, Figure 1.6) is the generation of a metagenomic assembly. During an assembly collinear metagenomic sequences from the same genome are being merged into a single contiguous sequence (i.e., contig) resulting in longer sequence reads, which can simplify bioinformatic analysis relative to unassembled short metagenomic reads. Due to DNA extraction from the sample, whole protein coding genes as well as full operons are unlikely to be intact but can offer invaluable functional knowledge about the community. However, in some cases, complete or nearly complete genomes can be assembled, which provides insight into the

genomic composition of uncultured organisms found in a community. An assembly of shorter reads into genomic contigs and orientation of these into scaffolds is often performed to provide a more compact and concise view of the sequenced community under investigation. Depending on the dataset, there are two approaches for creating an assembly 1) a reference based assembly or 2) a de novo assembly. When following a reference based assembly protocol, one or more already existing reference genomes can be used as a "map" for creating contigs. This approach is often used when metagenomes are taken from extensively studied areas and genomes of closely related organisms are already in an online reference database. In the case of de novo assembly, no reference "map" is being used and contigs from the sequencing run are being assembled. This process is computational extensive but several programs including MetaVelvet-SL (Afiahayati *et al.*, 2015; Namiki *et al.*, 2012) and Meta-IDBA (Peng *et al.*, 2011) or MEGAHIT (Li *et al.*, 2015) address previously arising issues. After assembly and quality control (MetaQuast (Mikheenko *et al.*, 2016)), sequence reconstruction and grouping can be performed through binning using various tools such as emergent self-organization maps (ESOM) (Dick *et al.*, 2009), followed by automated gene or regulatory element prediction of the sequences using Prodigal (Hyatt *et al.*, 2010). Potential protein coding genes can then be functionally annotated using a reference database such as NCBI's maintained "non- redundant" (NR) protein database (NCBI Resource Coordinators, 2017) using BLASTp (Altschul *et al.*, 1990, 1997). With the resulting data functional comparative metagenomics is possible and is based on identifying differential feature abundance (pathways, subsystems, or functional roles) between two or more conditions following a statistical procedure with some normalization step (Rodriguez-Brito *et al.*,

2006; Pookhao *et al.*, 2015). Tools to carry out such comparisons are programs such as MEGAN (Huson *et al.*, 2007), Parallel-META 2.0 (Su *et al.*, 2014), or STAMP (Parks et al., 2014).

Using metagenomics data to investigate the taxonomical composition of one or more samples does not depend on gene-targeted primers or PCR amplification and is therefore not affected by the biases (e.g. chimera formation) these methods pose. For taxonomical composition comparison of metagenomes, phylogenetic marker genes such as the 16S ribosomal RNA genes can be either extracted from the raw sequencing data or later separated based on a blast search of the cleaned sequences against for instance the SILVA rRNA database (Figure 1.6). Extraction from the raw sequencing data by reconstructing 16S rRNA genes through an assembly tool can be done with programs like REAGO (Yuan et al., 2015), however it needs to be noted that the use of REAGO is limited to short (~200 bp) Illumina HiSeq reads and does not support longer (>200 bp) MiSeq sequencing data. The use of reference gene sequences to assemble rRNA genes from metagenomics data is used by EMIRGE (Miller et al., 2011), this program requires large numbers of known rRNA genes for the mapping step and may miss remotely related rRNA genes. When blasting the cleaned sequences against a reference rRNA database such as SILVA, similarities between the gene sequence and the reference database is measured by the score obtained from an alignment algorithm (e.g. BLASTn), this method is computationally expensive and requires a parsing step where the resulting data is separated into those sequences being rRNA genes (hits) and those sequences being different from rRNA genes (no hits).

After all data from the metagenomic analysis described above is obtained, the

next step is to investigate important differences in community structure, diversity and biological function, by comparing gene abundance between the metagenomic datasets. Since this type of analysis is complex, and to avoid false positives and type I errors as well as unbiased estimation of the false discovery rate, several different methods (e.g. MetaStats (White *et al.*, 2009), STAMP (Parks *et al.*, 2014), FANTOM (Sanli *et al.*, 2013)) have been developed to undertake this task. Based on statistical model used for the analysis, results have to be interpreted carefully. Most impactful on gene ranking performance of the methods were found to be group size, effect size and gene abundance (Jonsson *et al.*, 2016). Based on the study by Jonsson et al. (2016) the following programs showed the best overall performance DESeq2 (Love *et al.*, 2014), edgeR (Robinson *et al.*, 2010) and the overdispersed Poisson GLM (OGLM) (Kristiansson *et al.*, 2009). However, performance of programs may differ based on sequencing method chosen for the metagenomic study.

1.6. Statement of Problem

Most ecosystems are subjected to seasonal environmental changes and species may be adapted to frequent cycles of disturbance and recovery. However, disturbance-dependent species deteriorate when disturbance frequency declines. Conversely, if major disturbances occur too frequently or reoccur multiple times during the recovery period, conditions are created that can lead to the formation of alternative community states that are distinct from the initial state. In studies examining ecosystems, the role of microorganisms is often greatly oversimplified because of the complexity of microbial processes. However, microorganisms form the foundation of ecosystems since they are

largely responsible for the biogeochemical cycling of natural systems. Recently, molecular based studies of microbes involved in biogeochemical processes indicated that microorganisms contain enormous diversity, complexity, and functional redundancy. On the one hand, single species carry genes that are involved in different pathways of elemental cycling, and on the other hand, there are different organisms that harbor the same genes (orthologs) carrying out the same functions. There may also be functional equality of whole communities where entirely different microbial communities carry out the same processes. It is therefore highly important to understand the abiotic factors that are responsible for community structure and function and their impact on ecosystem function and resilience. It has been shown that microorganisms that were rare before a major disturbance were highly abundant post-disturbance but that overall functional processes like nitrogen fixation and primary productivity were equal to the pre-disturbed state. These studies suggest that microbial community metagenomes contain functional redundancy within rare members and the diversity of those microorganisms supported the overall recovery of ecosystem function after disturbance.

While the genetic diversity in most ecosystems lies within the rare biosphere, most studies either focus on characterizing the abundant microbial community or characterize the rare biosphere at a single point in time. To fully understand ecosystems, it is important to extensively characterize the contribution of the rare community over time to understand its function in cycles of ecosystem disturbance and recovery. Benthic microbial mats on San Salvador Island (The Bahamas) are subjected to seasonal hurricanes and other tropical storm events. These naturally occurring cycles of disturbance and recovery of the microbial community makes it an excellent ecosystem to

study relationships between community structure and ecosystem function as well as ecosystem resilience.

Molecular biological techniques of 16S rRNA/rDNA (the term 16S rDNA is used to describe the 16S rRNA genes) deep sequencing allow us to monitor changes in active and dormant (both rare and abundant) phyla during cycles of environmental disturbance and recovery of the system. The investigation of redundancy of the overall functional processes during disturbance cycles can be conducted through metagenomic sequencing and comparative bioinformatic analysis. Metadata will be used to understand how abiotic factors trigger taxonomic changes and community function.

Table 1.1: An ecological guide to avoid confusion. The list captures six characteristics of an ecological situation which delimit the domain of validity of a stability statement (Grimm and Wissel 1997).

Features of ecological situation	Checklist question for this feature	Example answer
(1) Level of description	On what level of description is the stability property examined?	Individual, population, community, ecosystem, …
(2) Variable of interest	Which ecological variable of interest is being considered?	Biomass, population size, nutrient cycling rate, …
(3) Reference state or reference dynamic, respectively	What is the reference state or dynamic of the variable of interest without external influences?	Equilibrium, trend, cycles, high or low spatial or temporal variability, …
(4) Disturbance	What does the disturbance look like? What is being disturbed?	Disturbance of the state variable or system parameter, lasting disturbance or short term effect, intensity of disturbance, frequency of disturbance, …
(5) Spatial scale	To which spatial scale does the stability statement refer?	Size of the researched area, ability of researched species to spread, typical lengths in the spatial heterogeneity of the research area, …
(6) Temporal scale	To which temporal scale does the stability statement refer?	Time horizon of statement, longevity of examined organisms, temporal structure in environmental heterogeneity, …

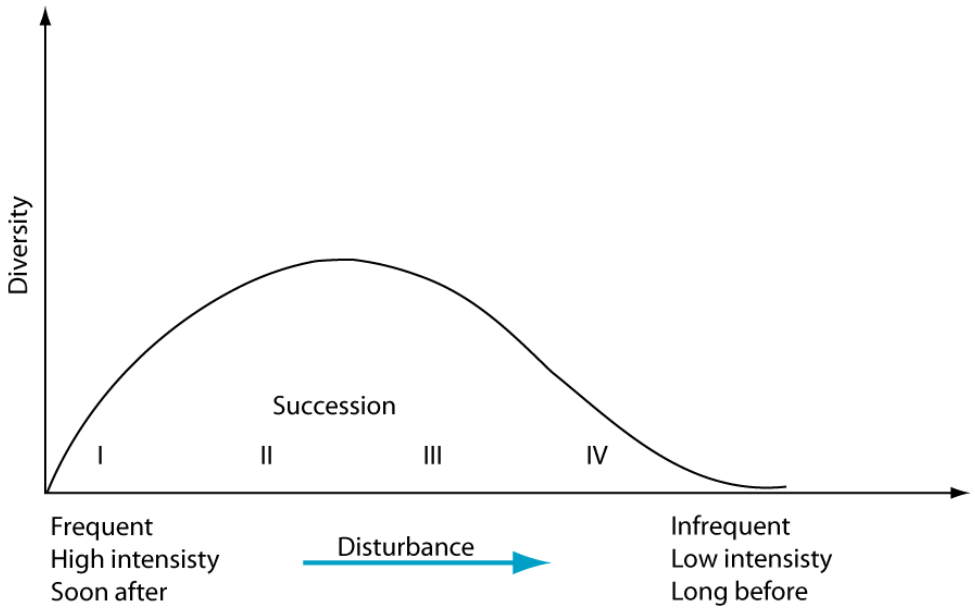

Figure 1.1. The intermediate disturbance hypothesis by Connell (1978). Redrawn from adaptation by Sheils and Burslem (2003).

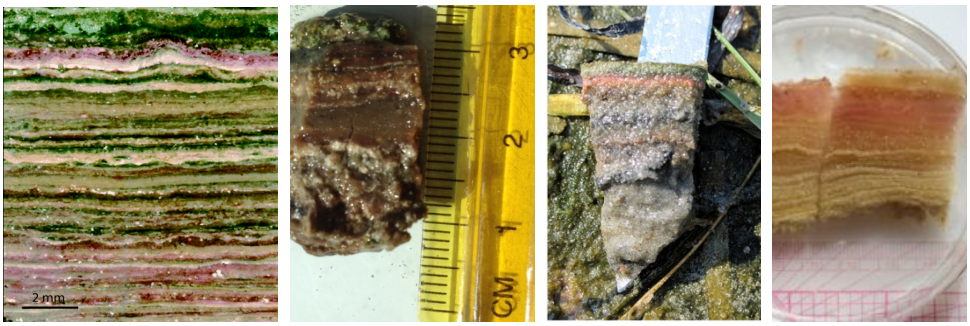

Figure 1.2. Vertical cross sections of microbial mat from different environments **A)** Section of a stratified microbial mat in hypersaline microbial mats at Guerrero Negro, Baja California. Photo by Spear and Pace (2007). **B)** Section of Salt Pond microbial mat collected in March 2013 (Photo by E. Preisner). **C)** Greater Sippewissett salt marsh microbial mat showing typical lamination (Armitage et al., 2012). **D)** Vertically stratified cyanobacterial mat in Lake Hoare Antarctica (Jungblut, 2010).

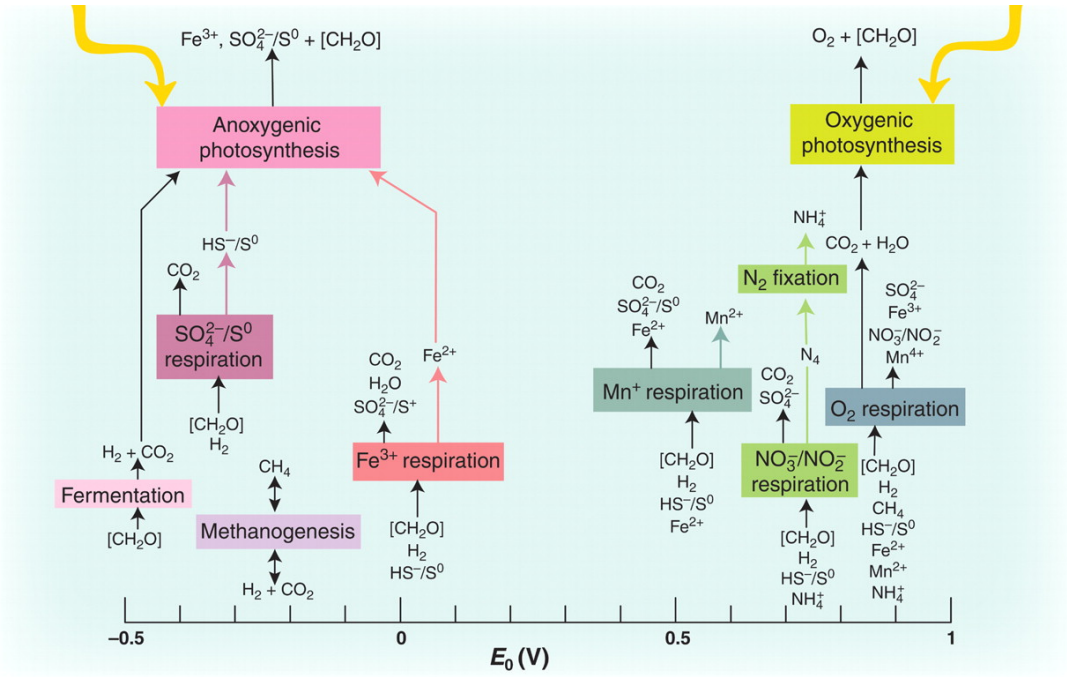

Figure 1.3. A generalized biosphere model of basic inputs and outputs of energy and materials. (Falkowski et al. 2008).

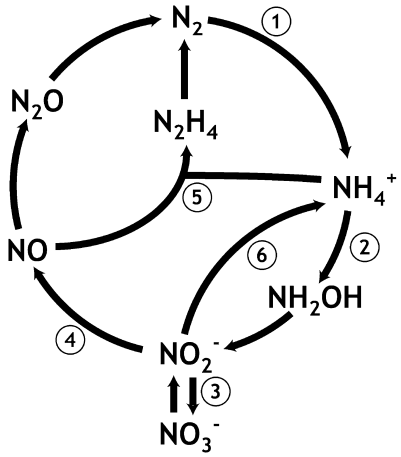

Figure 1.4. Schematic of the microbial nitrogen cycle. 1) N_2 (gas) fixation; 2) aerobic ammonium oxidation by bacteria and archaea; 3) aerobic nitrite oxidation; 4) denitrification; 5) anaerobic ammonium oxidation; and 6) dissimilatory nitrate and nitrite reduction to ammonium (adapted from Jetten, 2008).

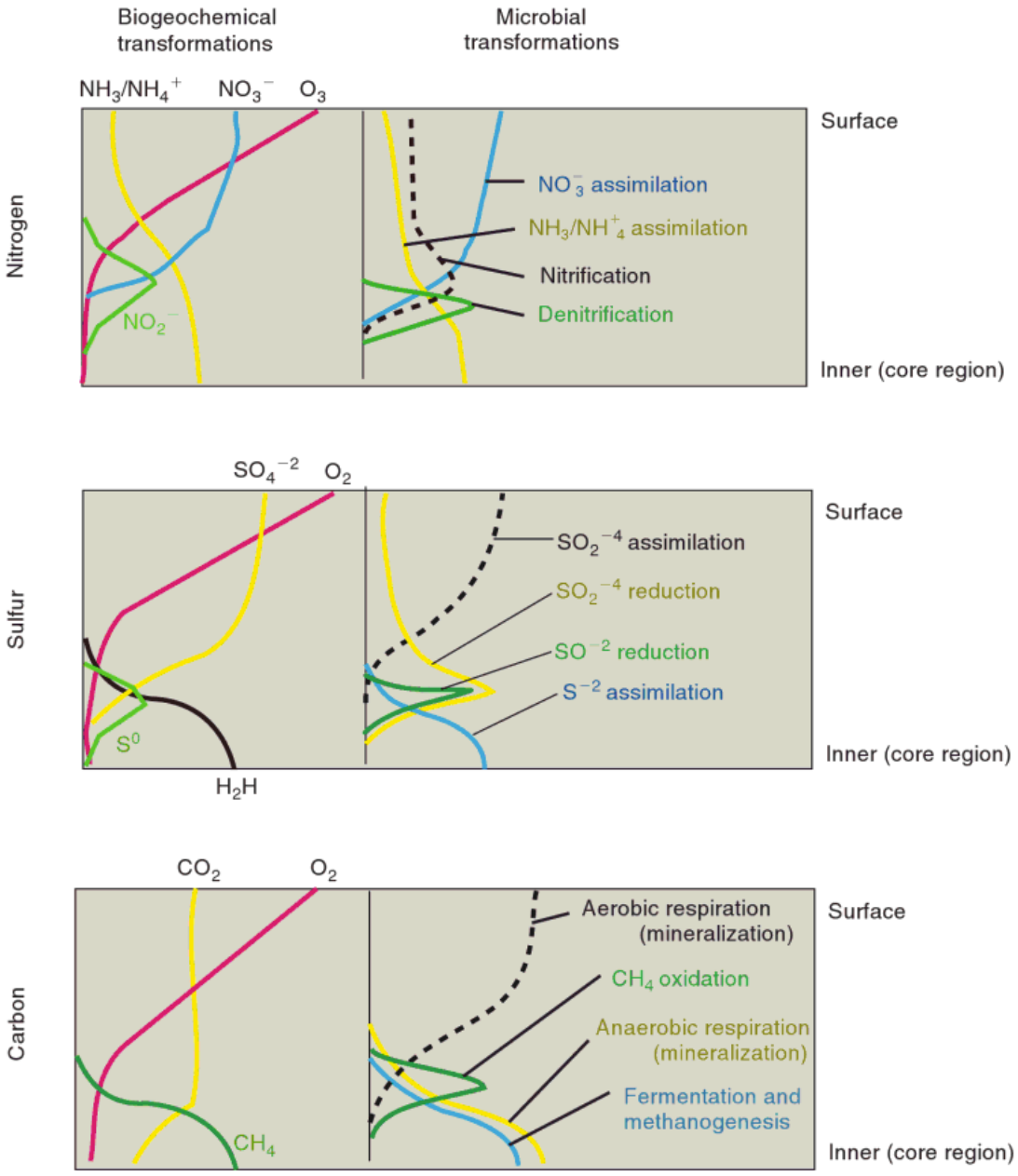

Figure 1.5. Biogeochemical cycling in microbial mats. **A)** Nitrogen biogeochemical transformation and microbial transformation in a microbial mat (Paerl and Pinckney 1996). **B)** Sulfur biogeochemical transformation and microbial transformation in a microbial mat. **C)** Carbon biogeochemical transformation and microbial transformation in a microbial mat.

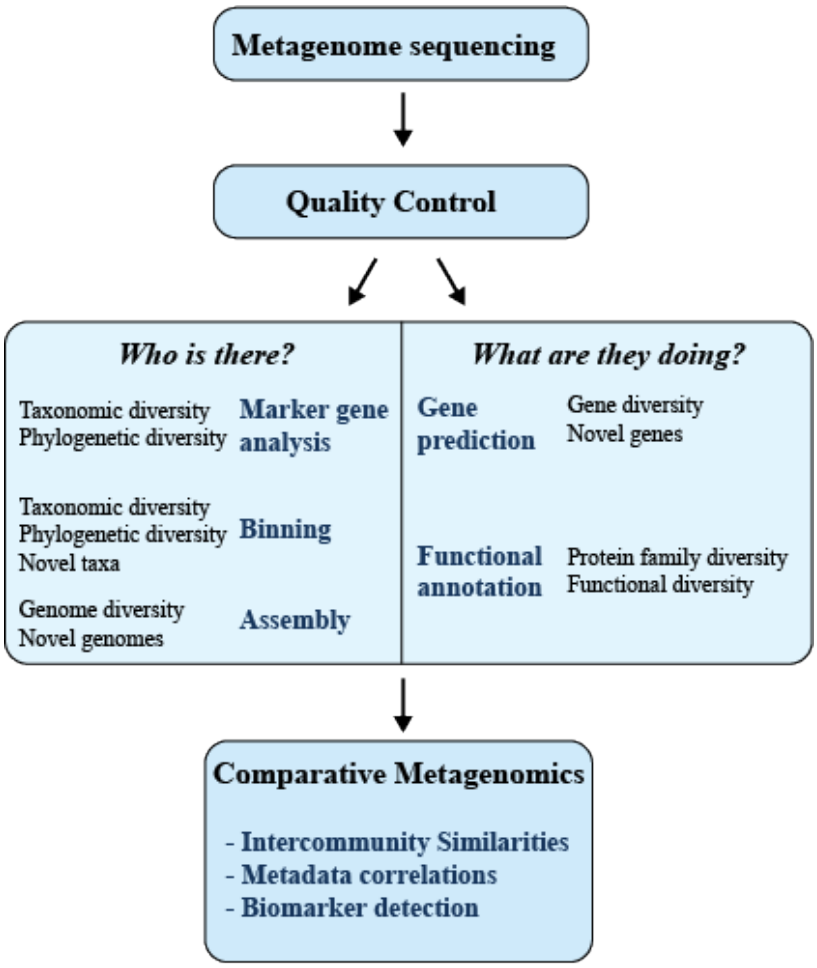

Figure 1.6. Workflow of common metagenomic analytical strategies (Sharpton, 2014). After sequencing of metagenomic nucleic acids, a quality control step is performed followed by analysis based on research question (e.g. taxonomic and functional characterization of the community). The results of these various analyses can be used for comparative metagenomics. Comparative metagenomics can answer questions regarding the similarity between communities, determine how community diversity relates to environmental covariates (metadata), and identify taxa and functions that stratify communities of various types (biomarker detection).

CHAPTER 2

COMPARISON OF NEAR AND FAR SHORE MICROBIAL MAT COMMUNITY IN SALT POND

2.1. Introduction

San Salvador Island is located on the eastern edge of the Bahamian Archipelago, approximately 300 km east of the capital Nassau, New Providence, within The Bahamas. This relatively small (161 km^2) island was formed in the late Quaternary and consist of carbonate (Mylroie and Mylroie, 2007). The island harbors multiple salt lakes and lagoons, ranging in salinity from seawater salinity (35 g kg^{-1}) to hypersaline conditions (250 g kg^{-1}) depending on the season. The two distinguishable seasons within the sub-tropical, semiarid climate are a wet (September – November) and a dry seasons. Seasonal predictable tropical storms and hurricanes occurring in the wet season are responsible for more than half of the mean annual precipitation of approximately 100.7 cm. One of the small coastal lakes, Salt Pond, was used in this study, which received the name due to historical use of the pond as a local source for mining salt. Salt Pond is located on the eastern shore of the island and only separated from the ocean by dunes. The water table of Salt Pond changes throughout the year from more than 1 m depth during the wet season, to completely dry in more dry years. Salt Pond has been the subject of several studies (Pinckney and Paerl, 1997; Paerl and Yannarell, 2010; Pinckney *et al.*, 2011) due to its unique nature of harboring microbial mats. In this study we focus on the community composition of the microbial mats of Salt Pond. After Hurricane Sandy passed over San

Salvador Island, The Bahamas, on October 25/26 (2012) the salinity in Salt Pond was decreased to 30 g kg^{-1} (measured by Erin Rothfus) for reference: Caribbean Sea water 35 g kg^{-1} (Personal measurement, March 2013). By the end of February 2013 the salinity of the Pond had increased to 35 g kg^{-1}. During the Hurricane, the pond likely received inputs of inorganic and organic matter and nutrients from runoff of the surrounding soils resulting in higher levels of pond water prokaryotic and eukaryotic productivity with subsequent increased water turbidity. The fluctuation in salinity allowed the establishment of other primary producers (e.g. sea grass), and other trophic levels (e.g. grazer, fish, and worms) in the pond (personal observation), that are not found at salinities over 45 g kg^{-1} (personal observation), resulting in changes of water chemistry and biology as whole. At lower salinities, primary productivity was found to be increased (Pinckney et al. 1995), thus enhancing oxygen and carbon input into the system and building a foundation for the microbial community to flourish. During March 2013 sampling, two morphologically different microbial mats were found covering the sediment of Salt Pond. The previously sampled site, that is located approximately 15 m from the shore, showed a mat with a brown surface and only few (<3) distinguishable layers, whereas the south side of the pond near shore (approximately 8 m) was covered by a microbial mat with a green surface and multiple (>10) distinguishable layers. Sample site far shore (referred to as sample site 1) was overlaid by approximately 41 cm of pond water, whereas the sample site near shore (referred to as sample site 2) was in a depth of approximately 28.5 cm. The deeper water column of sample site 1 allowed less sunlight to reach the microbial mat surface, as compared to sample site 2. Microsensor oxygen profiles demonstrated reduced oxygen production and smaller aerobic zone by far

shore mats as compared to the sample site near shore. Since microbial mats are photosythetically driven systems we hypothesize that increased water turbidity will result in different light attenuation far shore versus near shore and resulting in shifts in mat community structure. Future studies, comparing the change in microbial mat communities over time need to be done in one sampling area.

2.2. Materials and Methods

2.2.1. Initial Assessment of Microbial Mats

When Salt Pond was assessed for microbial mats covering the sediment, two morphologically different microbial mats were discovered. Within the previous sampling area, located far shore (approximately 15 m) the microbial mat showed reduced layering as compared to the mat sampled in the same area before hurricane Sandy (Figure 2.1 B). This sample site is referred to as sample site 1. The Southside of Salt Pond, near shore (approximately 8 m), was covered by microbial mats with more than 10 distinguishable layers and a green surface (Figure 2.1 A). The Southside sampling side is referred to as sample site 2.

2.2.2. Metadata collection

Environmental parameters of Salt Pond, such as salinity, dissolved oxygen, temperature, photosynthetic active radiation (PAR; 400-700 nm), and pH were measured with an YSI 30 Salinity Meter, a YSI 55 Dissolved Oxygen Meter (YSI, Yellow Springs, OH, USA), a LI-COR LI-250A Light Meter (LI-COR, Lincoln, NE, USA), and a Mettler Toledo SevenGo Portable pH Meter (Mettler-Toledo, Columbus, OH, USA), respectively. All measurements were taken in triplicates together with all other sample

collections at the time point, and average values (± 3 standard deviations) are being reported (Table 2.1, Table 2.2).

2.2.3. Sample Collection and Processing

Samples of each mat type (site 1 and 2) were collected using 7-mm Harris Uni-CoreTM device (Ted Pella, Inc, Redding, CA, USA) and transferred into 3 ml round bottom cryogenic vials (plypropylene, VWR). Five replicate cores were pooled immediately (<1 min), frozen, and kept in the dark after sampling at all times. Samples were thawed and subsequently freeze dried overnight. Freeze dried samples were weighed and 2 ml acetone (90%) and 50 µl carotenal standard were added for pigment extraction, samples were then sonicated for 30 seconds and stored in the freezer for 24 hours (Pinckney et al. 1994). After spinning samples at 1400 rpm at 4˚C for 2 minutes, the supernatant was filtered (0.45 µm) into a 2 mL centrifuge tube. Identification and quantification of pigments was done by HPLC with an in-line photodiode array detector (Shimadzu SPD-M6a) (Wright and Jeffrey 1987). Identification of pigment was done by comparing spectra to known standards by Jay Pinckney. Pigment concentrations per gram microbial mat were calculated and ANOVA ($p=0.05$) was performed to test for a difference in community composition between the two sites.

2.2.4. Nutrient Analysis

Water from Salt Pond was collected to analyze phosphate, nitrate, nitrite, and ammonium concentrations using water quality kits (Hach, Loveland, Colorado) and a spectrophotometer (Thermo Multiskan EX Photometric Microplate Absorbance Reader). Bottles for water collection were acid washed (10% HCl) before taking samples. Three

replicate samples of pond water were collected at mid day and mid night and analyzed within 24 hours. Briefly, six standard solutions were prepared for each nutrient to generate a standard curve before measuring the samples. All standards and samples were processed according to the manufactures instruction of the kit and measured at the wavelengths specific to the kits instructions. Average values (n=3) and standard deviations are being reported for all nutrients.

2.2.5. Microsensor Measurements

Oxygen concentrations in the microbial mat were measured with an oxygen microsensor (Unisense, Denmark). The sensor had a tip diameter of 10 µm, a stirring sensitivity of <1.5%, and a 90% response time of 0.2 s. The sensor response was tested by recording the output current in O_2 saturated water (purged with oxygen) and zero oxygen by spurging with N_2, the water was kept at temperature and salinity of the microbial mats. The sensor was mounted and lowered vertically into the mat using a micromanipulator. Three independent O_2 concentrations were determined at 100 µm increments. All measurements were saved in a Microsoft Office Excel (2007) spread sheet. Mean and standard deviation were calculated (n=3) and used for Sigma Plot (11.0) analysis. Light dark shifts were conducted in 200 µm depth (for more information see (Glud et al. 1992) to calculate primary productivity and gross photosynthetic rate.

2.3. Results

2.3.1. Environmental Parameters and Assessment of Mats

Following Hurricane Sandy, where the Pond water had reached high levels and a salinity of 30 g kg^{-1}, at the time of sampling in March (2013) with decreasing water

column the salinity increased to 35 g kg^{-1}. The lowest and highest air temperatures measured for day time were 19˚C and 29.1˚C, respectively, while night time temperatures reached as far down as 17.7˚C. The temperature of the pond water stayed more stable over 24 hours with lowest temperature of 20.7˚C and the highest of 25.5˚C. The lower temperatures and decreased salinities created conditions for increased dissolved oxygen (DO) of the water column. DO over a diel cycle varied between 4.05 to 5.54 $mg*L^{-1}$ depending on the water temperature. Compared to seawater measured across the dune from Salt Pond (DO_{ocean} 6.91±0.39 $mg*L^{-1}$, 25.5˚C), the DO in salt Pond was decreased.

Photosynthetic primary producers, such as Cyanobacteria, generate oxygen in the microbial mats. Using sunlight as their energy source to carry out metabolic functions, photosynthetic active radiation (PAR) as well as microsensor measurements of oxygen in the microbial mats were taken as an indicator of potential phototrophic metabolism (e.g. nitrogen fixation). To compare how much sunlight was reaching the microbial mats near and far shore (site 2, and 1), sun light attenuation in the water column was calculated by measuring PAR at water air surface and on top of the microbial mats. In the far shore site, 79 % of PAR was lost due to turbidity in the water column, whereas the near shore site experienced a 32% loss of PAR (Table 2.3). Far shore mats Near shore mats displayed oxygen maximums of 387.21 ± 34.53 µmol L^{-1} at depth of 1.7 ± 0.1 mm and a relatively broad oxycline of 3 mm depth during mid day photosynthesis (light intensity 556.28 µE m^{-2} s^{-1}). While oxygen penetrated 2.6 mm deep into the far shore mats, the maximum O_2 concentration was approximately 35% lower with a maximum O_2 concentration of 293.2 ± 12.56 µmol L^{-1} at approximately 0.8 mm depth and a shallow oxycline (Figure 2.3). Light-dark shifts were conducted in the mats at both sites to calculate gross and net

primary productivity (Table 2.3). Response time of O_2 production was longer in far shore microbial mats with lower gross O_2 production as compared to near shore mats. Both sides had great standard deviations around the mean (n=3), indicating high variation of O_2 production.

Near shore mats had a grainy green colored uneven surface and more than 10 distinguishable layers of different colors reaching approximately 18 mm deep. The first ~3 mm of the mat were green colored and appeared to have sand grains incorporated into its matrix (Figure 2.1, A). While far shore mats had a brown colored smoother surface (Figure 2.1, B), they had fewer than 4 distinguishable layers reaching to ~5 mm depth. Coloration of far shore mat layers were mostly red-brown and were built on black colored sediment.

2.3.2. Nutrient analysis

Nutrients of pond water can be an important indicator of microbial activity of the water column. Comparison of nutrient concentration at day and night time in the water column showed no significant differences with the exception of Nitrite (NO^{2-}) (T-test, t=-16.971, df = 4, $p<0.05$). Nitrate (NO^{3-}) in the water column had higher concentrations (5077.76 ± 3388.16 µg/L) as compared to the other tested nutrients (nitrite, ammonia, and phosphate) (Figure 2.2). Nitrifying microorganisms in the water column oxidize NH_4^+ to nitrate.

2.3.3. Photosynthetic microbial community comparison

Microbial mat cores from both mat types were collected and photopigments were extracted and analyzed. Overall 12 different photopigments were identified in the mats,

with half of them belonging to the phylum of Cyanobacteria (Table 2.3). Oxygenic prototroph biomass (Chl a) was significantly greater in near shore mats (One way ANOVA: $F_{1,16}$=17.731, p<0.001). Comparing photopigment concentrations at both sites using a multivariate ANOVA ($\alpha = 0.05$) resulted in significantly different community compositions ($p < 0.05$, $n = 12$). The following pigment concentrations were significantly higher (p<0.05) in near shore mats, Scytonemin, Fucoxanthin, Myxoxanthophyll I, Myxoxanthophyll II, Zeaxanthin, Bacteriochlorophyll a, Chla allomer, α carotene, and Echinenone (Figure 2.4.). Bacteriochlorophyll a had the highest concentration of all pigments (p<0.0001). Echinenone, the photopigment indicating the presence of the Cyanobacteria Microccus roseus, was second highest in abundance in near shore mats, while it was the Microalgae Dunaliella salina (β Carotene) in far shore mats.

2.4. Discussion

Microbial mats have been observed to go through growth cycles, after the growth season, the green Cyanobacteria layer was found to die off (STAL, 1995). Due to the lack of a green layer and lower biomass as well as lower abundance of phototrophic primary producers, far shore mats seemed to be at a different step of the growth cycle, possibly at the end of the growth season. While "active" microbial mats trap and bind sediments and particles, such as seen in the first few millimeters of the near shore mats, there is no evidence of that found in far shore mats (Figure 2.1). One possible reason for the appearance of the less active far shore mats could be water turbidity coupled with an increase in grazing pressure at lower salinities (35 g kg^{-1}). Since photosynthetic CO_2 and N_2 fixation is the primary input of organic matter and nutrients, respectively, in this

sediment ecosystem, other microorganism's metabolism and growth are dependent on the abundance and growth of primary producers, thus resulting in a less active microbial mat. Based on the photopigment analysis, purple phototrophic bacteria were the dominant group in both mat types, but Cyanobacteria were more diverse and may be better adapted to changing environmental conditions such as salinity or change in light. The phototrophic community composition based on photopigment analysis indicated two distinct communities between the near and far shore mats, further supporting the claim that there were different types of microbial mats present in Salt Pond.

Table 2.1. Metadata of Salt Pond collected at day and night.

	Dissolved oxygen	pH	Temperature		Salinity
Time	mg * L^{-1}		Air (°C)	Water (°C)	g * kg^{-1}
Day	4.05 ± 0.8	7.4 ± 0.2	26.00	25.50	35
Night	5.04 ± 0.13	7.14 ± 0.1	17.7	20.75	35

Table 2.2. Photosynthetically active radiation (PAR) lost in water column due to turbidity for microbial mat near shore and far shore. Mean values (n = 6) with one standard deviation.

	Site 1 (far shore)	Site 2 (near shore)
% PAR lost in water column	79.47 ± 15.02	32.14 ± 11.11

Table 2.3. O_2 Productivity at 0.2 mm depth. Mean oxygen concentration (n=3) with std. deviations.

	Site 1	Site 2
Gross O_2 production	13.7 ± 10.6	124.9 ± 92.7
Net O_2 production	1.8 ± 13.7	117.3 ± 92.8

Table 2.4: Photopigments found in site 1 and 2 microbial mats, functions and organisms.

Pigments	Function	Organisms	Comment	Reference
Scytonemin	UV-screening pigment, photoprotection molecule	Sheathed cyanobacteria	pigment is known to be synthesized following exposure to high levels of UVA irradiance and to protect cells from those wavelenghts	Dillon et al. (2003), Garcia-Pichel et al. (1991)
Fucoxanthin	carotenoid	Phytoplankton to diatoms, prymnesiophytes, raphidophytes, and crysophytes		Jeffrey & Vesk (1981)
Myxoxanthophyll I	carotenoid glycoside	Cyanobacteria		Mohamed et al. (2005)
Myxoxanthophyll II	common accessory pigment for benthic cyanobacteria	Benthic cyanobacteria	mostly functions in photoprotection by non-photochemical quenching (NPQ)	Hertzberg et al. (1971)
Myxoxanthophyll III	common accessory pigment for benthic cyanobacteria	Benthic cyanobacteria	mostly functions in photoprotection by non-photochemical quenching (NPQ)	Karsten & Garcia-Pichel (1996)
Zeaxanthin	carotenoid	Cyanobacteria		
Bacteriochloroph	Photosynthetic	Purple phototrophic bacteria		Pinckney and Paerl

yll a	pigment		(1997)
Chla Allomer	Degradation product of chl a	Oxygenic phototrophs	
Total Chl a	Essential to release chem. energy	oxygenic phototrophs	Pinckney and Paerl (1997)
α Carotene	UV-sun protection	Microalgae Dunaliella salina	Emeish
β Carotene	UV-sun protection	Microalgae Dunaliella salina	Emeish
Echinenone	carotenoid	Cyanobacteria, microccus roseus	Schwartzel and Cooney (1970)

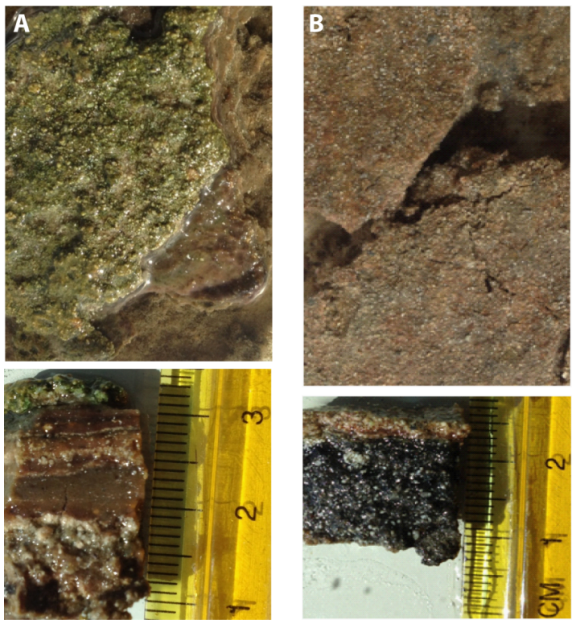

Figure 2.1. Representative surface and cross sections of microbial mats in March 2013 in Salt Pond. **A)** Near shore microbial mat (sample site 2). **B)** Far shore microbial mat (sample site 1). Scale in cm.

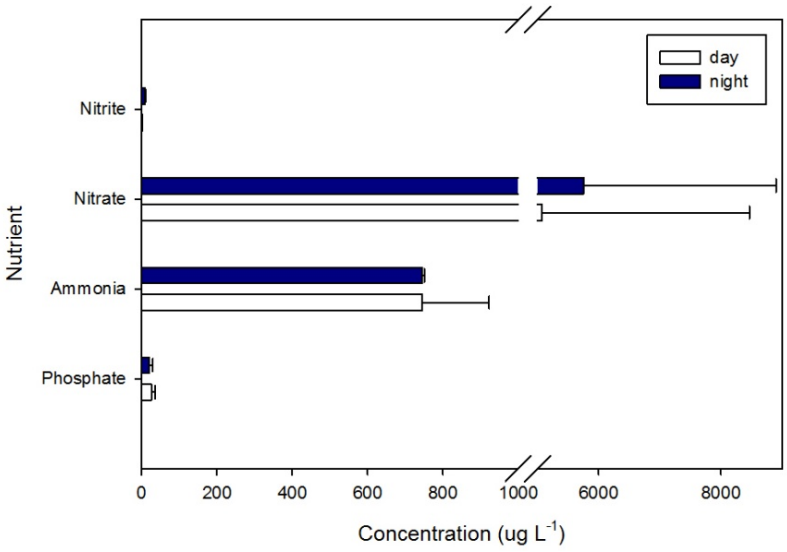

Figure 2.2. Nutrient analysis in Pond water at midday and midnight. Y-axis reports the nutrients tested, nitrite (NO^{2-}), nitrate (NO^{3-}), ammonia (NH_4^+), and phosphate (PO_4). The x-axis shows the concentration of the nutrients tested in µg per liter.

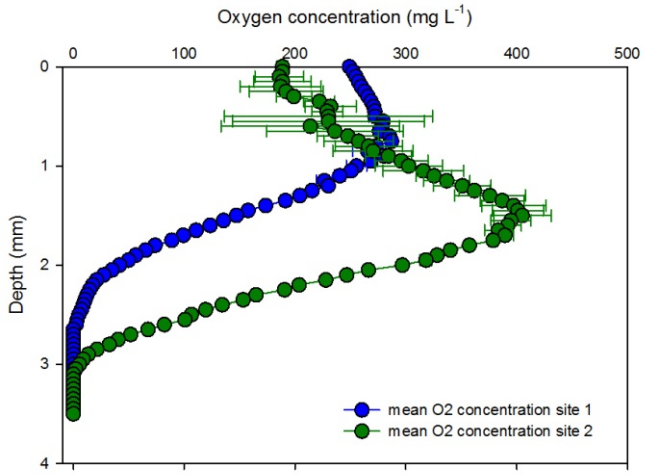

Figure 2.3. Representative oxygen depth profiles taken with microsensor (unisense) of microbial mats on site 1(far shore, blue) and 2 (near shore, green).

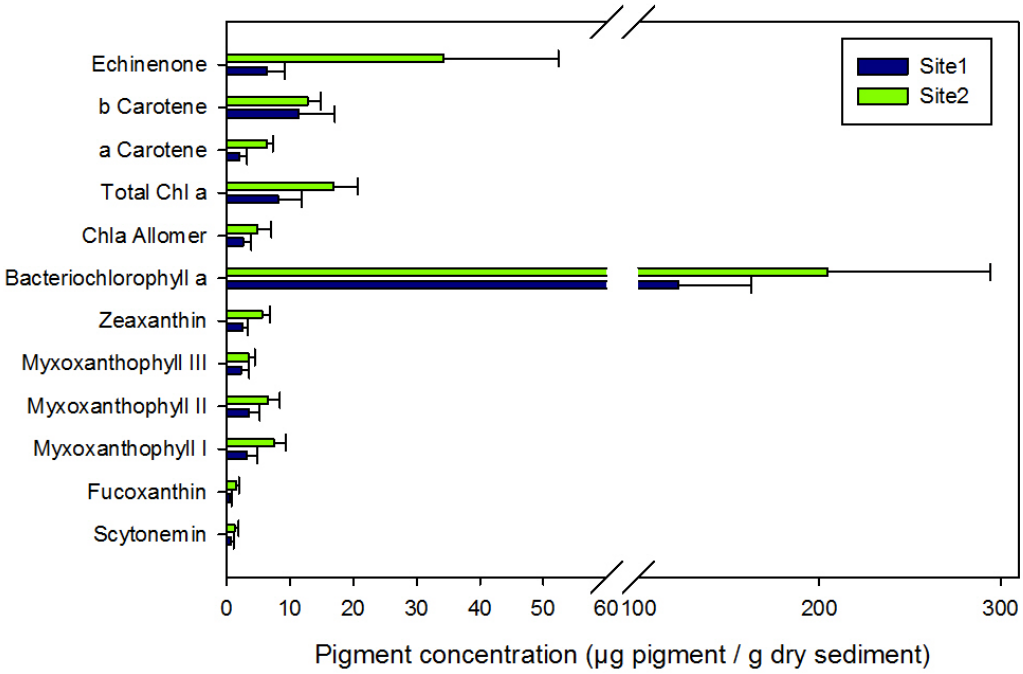

Figure 2.4. Comparison of photopigments detected in Salt Pond microbial mats of sites 1(far shore, blue) and 2 (near shore, green). Photopigment concentrations are in µg pigment per g dry sediment.

CHAPTER 3

MICROBIAL MAT COMPOSITIONAL AND FUNCTIONAL SENSITIVITY TO ENVIRONMENTAL DISTURBANCE

3.1. Introduction

Many ecosystems are in a continuous state of change due to diel, seasonal, and intermittent extreme weather driven fluctuations in abiotic factors (e.g., nutrients, pH, light, temperature, and salinity). The ability of ecosystems to adapt to these changes depends on the duration and intensity of change and the biological diversity of the system (Sousa, 1984; Glasby and Underwood, 1996; Scheffer *et al.*, 2001; Fraterrigo and Rusak, 2008). Significant biological diversity often exists within microbial communities controlling the biogeochemical processes that form the foundation of ecosystems (Falkowski *et al.*, 2008); therefore, understanding the complex links between environmental change and microbial diversity is essential for assessing ecosystem stability (*i.e.* biogeochemical cycling). Studies examining these links within lake (Shade *et al.*, 2011, 2012a), marine sediment (Mohit *et al.*, 2015), soil (Allison and Martiny, 2008), and microbial mat (Boujelben *et al.*, 2012) ecosystems have shown that microbial communities are seasonally variable and often show long-term resilience to larger environmental disturbances. Further insight into the complex dynamics and ecological mechanisms maintaining ecosystems has revealed that while much of the microbial biomass is contained within a few dominant taxa, the greatest genetic diversity and

metabolic potential is maintained within a vast number of low abundance or 'rare' taxa (Sogin *et al.*, 2006). Studies examining the significance of these rare taxa have shown that while some may be active and contribute to important biogeochemical processes (Pester *et al.*, 2010), others are less active and may be providing a genetic reservoir (*i.e.*, seedbank) to maintain ecosystem diversity over time (Jones and Lennon, 2010; Lennon and Jones, 2011). For instance, resuscitation of rare taxa has been suggested to contribute to soil ecosystem functioning (Aanderud *et al.*, 2015). However, the links between shifting environmental parameters and regulation of this dynamic population are unclear and an area of more recent research.

Complex semi-closed organo-sedimentary microbial mat ecosystems contain tightly coupled biogeochemical processes along a narrow vertical chemical gradient often occurring within the first 10 mm of microbial mats (Woebken *et al.*, 2015; Pinckney *et al.*, 1995), allowing them to serve as unique model systems to examine how environmental parameters influence the abundance and potential activity of rare taxa and biogeochemical cycling. While specific responses of the microbial mat rare biosphere to environmental change have yet to be explored, studies have revealed complex community dynamics with taxon-specific responses at different salinities. For instance, Cyanobacteria were shown to be tolerant to a range of salinities (Green *et al.*, 2008), and while oxygenic and anoxygenic phototrophs tolerate a wide range of salinities up to 300 g kg^{-1} (Oren, 1999), in solar salterns, optimal growth of anoxygenic phototrophs has been detected at 100-120 g kg^{-1} and sulfate reducing bacteria are poorly adapted to salinities over 200 g kg^{-1} (Sorensen *et al.*, 2004). With processes within these ecosystems tightly coupled, salinity-driven shifts in community structure will alter biogeochemical cycling

(Ley *et al.*, 2006). For instance, increased salinity decreases nitrogen fixation by Cyanobacteria but increases fixation by Deltaproteobacteria (Severin *et al.*, 2012). While studies have shown that microbial mat communities contain similar phyla with slight biogeographical and salinity-driven compositional differences (Ley *et al.*, 2006; López-López *et al.*, 2013; Schneider *et al.*, 2013; Allen *et al.*, 2009; Dillon *et al.*, 2013), there is little knowledge regarding the complex compositional and functional dynamics occurring within abundant and rare taxa following an environmental disturbance and how these community changes may alter biogeochemical cycling.

This study provides knowledge on microbial mat compositional and functional sensitivity following a pulse disturbance resulting in a large salinity shift. While studies have shown that salinity is one of the most important parameters influencing global patterns of Archaea and Bacteria distribution (Lozupone and Knight, 2007; Auguet *et al.*, 2010; Canfora *et al.*, 2014), these studies often compare communities isolated and adapted to a range of stable salinities. The mat ecosystem investigated here experiences routine seasonal shifts in salinity and extreme disturbances following hurricanes and tropical storms, providing an opportunity to examine the response of a semi-closed microbial community to environmental disturbance. Sequencing of archaeal and bacterial 16S rRNA and rRNA genes showed significant shifts in the day/night protein synthesis potential (PSP) of abundant and rare taxa following the reduction in salinity from 230 to 65 g kg^{-1} that occurred between 2011-2012 following the landfall of Hurricane Irene. Quantitative PCR of genes and transcripts involved in nitrogen and sulfur cycling show concomitant shifts in gene expression indicating a possible change in biogeochemical cycling potential. Together, these data show the compositional and functional sensitivity

of a microbial mat ecosystem to environmental change but also suggest that rare taxa may provide a reservoir of genetic diversity that enhances ecosystem stability following seasonal and extreme environmental disturbances.

3.2. Materials and Methods

3.2.1. Sample Collection and Processing

The mat ecosystem examined in this study is located on San Salvador Island, Bahamas (Figure 3.1). The mat forms well-defined layers and experiences wide ranges in salinity (35 to >305 g kg^{-1}), intense irradiance (>2200 µmol m^{-2} s^{-1}), and high temperatures (>40°C; (Pinckney *et al.*, 1995; Pinckney and Paerl, 1997; Paerl *et al.*, 2003) personal observation).

Mat cores were obtained from similar locations during August 1–2, 2011 (230 g kg^{-1} salinity) and 2012 (65 g kg^{-1} salinity). To focus on the most diverse component of the consolidated microbial mat, samples (0.9–1.5 g) of the top 7 mm of the mat were taken during daytime (10am/5pm) and nighttime (10pm/5am) using a 7-mm Harris Uni-CoreTM device (Ted Pella, Inc, Redding, CA, USA). Five replicate cores were pooled immediately (<1 min) into a 3-ml tube containing 2 ml RNAprotect Bacteria Reagent (Qiagen, Valencia, CA, USA). Triplicate tubes were obtained for each time point, resulting in 6 daytime and 6 nighttime replicates. Samples were homogenized with sterile glass rods and stored at 4°C until further processing. Environmental parameters were measured with an YSI 30 Salinity Meter, a YSI 55 Dissolved Oxygen Meter (YSI, Yellow Springs, OH, USA), a LI-COR LI-250A Light Meter (LI-COR, Lincoln, NE,

USA), and a Mettler Toledo SevenGo Portable pH Meter (Mettler-Toledo, Columbus, OH, USA).

3.2.2. Nucleic Acid Extraction and cDNA Synthesis

Mat samples in RNAprotect Bacteria reagent were centrifuged (8,000 × g for 5 minutes) and RNAprotect discarded. The pellet was resuspended in 7.5 ml RLT Plus buffer (Qiagen) containing 1% 2-mercaptoethanol. Samples were incubated at room temperature for 10 min followed by five freeze/thaw cycles consisting of freezing in liquid nitrogen and thawing at 55°C. Next, silicon carbide beads (DNase- and RNase-free mixture of 0.1 and 1 mm beads) were added and samples vortexed for 10 min and processed using the Allprep DNA/RNA Miniprep Kit (Qiagen) for simultaneous DNA/RNA extraction from each sample. Total RNA and DNA were quantified using a Qubit 2.0 fluorometer (Life technologies, Grand Island, NY, USA). Turbo DNA-free kit (Ambion, ThermoFisher Scientific) was used to remove DNA from total RNA and DNA removal verified through PCR. RNA (100 ng) was reverse transcribed to cDNA using SuperScript III first-strand synthesis (Life Technologies) with random hexamers.

3.2.3. 16S rRNA/rRNA Gene Amplification and Sequencing

The abundance and PSP of archaeal and bacterial communities under different salinities were assessed by sequencing and analysis of 16S rRNA and rRNA genes. For clarity, when comparing 16S rRNA and rRNA gene-based data, these data will be referred to as 16S rRNA and rDNA, respectively. For Bacteria, the V1–V3 hypervariable region was amplified using a combination (1:1 molar ratios) of the 27F forward primer (AGA GTT TGA TCC TGG CTC AG; (Edwards *et al.*, 1989)) and the 27Fd forward primer (AGA GTT TGA TYM TGG CTC AG; (Nercessian *et al.*, 2005)) and the U529

universal reverse primer (ACC GCG GCK GCT GRC; (Marshall *et al.*, 2012)). For Archaea, the V2–V3 hypervariable region was amplified using the forward primer 109F (ACK GCT CAG TAA CAC GT; (Whitehead, 1999)) and the U529 reverse primer. Twelve multiplex identifier (MID) tags were added to reverse primers for sample multiplexing (Table 3.1).

Triplicate 25 µl PCR reactions contained 0.625 units of GoTaq® Hot Start Polymerase (Promega Corp., Madison, WI, USA), 1.5 mM MgCl2, 0.2 mM nucleotide mix, 0.3 µM each primer, and 10 ng template DNA or cDNA. PCR conditions consisted of: initial denaturation: 95° C for 5:00 min; 94° C for 0:45 min, annealing at 62°C for 0:45 min using −0.5°C per cycle, and elongation at 72°C for 0:45 min, for 10 touchdown cycles; (94° C for 0:45 min, 62° C −0.5° C per cycle for 0:45 min, and 72° C for 0:45 min); 25 (for Archaea) or 15 (for Bacteria) additional cycles (94° C for 0:45 min, 57° C for 0:45 min, and 72° C for 0:45 min); final elongation at 72°C for 10:00 min. Amplicons were purified using the QIAquick PCR purification kit (Qiagen) and quantified with a Qubit fluorometer.

For each sample, bacterial and archaeal amplicons with similar MIDs were combined (2:1) and uniquely labeled triplicates for each time point combined (1:1) before Illumina library preparation. Four libraries (2011 rDNA, 2012 rDNA, 2011 rRNA, and 2012 rRNA) were prepared using the NEBNext® DNA Library Prep Master Mix (New England Biolabs, Ipswich, MA, USA). The libraries were combined (1:1) and sequenced on an Illumina MiSeq using the MiSeq Reagent Kit v3 (Illumina, Inc., San Diego, CA, USA). FASTQ formatted paired end reads are located in the GenBank sequence read archive under SRP070186.

3.2.4. Sequence Processing

Sequences were analyzed using mothur [v.1.33.0; (Schloss *et al.*, 2009)] following a modified version of the MiSeq SOP (Kozich *et al.*, 2013). After paired-end reads from all libraries were assembled, sequences not matching quality criteria (maximum ambiguities = 0, ≤8 homopolymers, ambiguous length ≥300 or <650 bp) were culled using the screen.seqs command. Sequences were demultiplexed, MIDs trimmed, and separated into Archaea and Bacteria based on classification (RDPclassifier.trainset9). Non-chimeric sequences were dereplicated and aligned using Silva Archaea and Bacteria databases trimmed to the V1–V3 region. Sequences were assigned to operational taxonomic units (OTUs) with a sequence similarity threshold of 97% identity and classified. For increased stringency, OTUs represented by <20 sequences, across groups (i.e., day and night: 2011 rRNA, 2011 rDNA, 2012 rRNA, and 2012 rDNA) were culled before further analysis. Sequences were rarefied (Bacteria = 27,663 per MID, Archaea = 24,390 per MID) and beta diversity estimated using θYC at a 0.03 distance threshold and visualized using non-metric multidimensional scaling (NMDS). The three dimensions of the NMDS data were plotted in SigmaPlot. Analysis of molecular variance (AMOVA) was performed to test the significance of variation among conditions.

3.2.5. PSP of Rare/Abundant Taxa

Linear discriminant analysis effect size (LEfSe, LDA > 2, and n = 6 per condition) identified statistically significant OTUs among replicates within pre- and post-disturbance salinity conditions (Schloss *et al.*, 2009; Segata *et al.*, 2011). From initial data, 96% of archaeal and 98% of bacterial OTUs were identified as significant among conditions and used for subsequent analysis. The relative abundance (%) of OTUs within

conditions was calculated and classified as "rare" when abundance was <1%, and "abundant" when >1%. Archaeal and bacterial OTU frequencies were square root transformed using SPSS Statistics 22 (IBM Corp., Armonk, NY, USA) to better visualize data distribution. Nonparametric correlations (Kendall's τ and Spearman's ρ) were calculated using transformed data of relative 16S rRNA and rDNA frequencies from 2011 and 2012 samples using SPSS and frequencies plotted with SigmaPlot. The PSP of OTUs was determined by calculating 16S rRNA:rDNA ratios. While this approach may not distinguish between extremely slow- growing and dormant taxa, comparison of the ratio for individual OTUs across salinities is used throughout this study to indicate increased or decreased PSP for given OTUs. Mean (n = 6) PSP for Archaea classes and Bacteria phyla were calculated and reported with its standard error. One-way analysis of variance (ANOVA) was used to determine if there was a significant (p = 0.05) PSP difference between mean PSP values for each condition (Day11, Night11, Day12, and Night12) and a student's t-test for observing significant changes between pre- and post-disturbed conditions using SPSS statistics. Heatmaps were used to visualize mean (n = 6) rRNA:rDNA ratios for OTUs across conditions and constructed within RStudio with the heatmap2 command in gplot (Warnes *et al.*, 2012).

3.2.6. Quantitative PCR

Abundance of genes and transcripts involved in nitrogen and sulfur cycling as well as overall Archaea and Bacteria abundance was measured by quantitative PCR (qPCR). To generate qPCR standard curves, each target gene was initially amplified from either combined 2011/2012 DNA or positive isolate controls. Amplicons were size verified, ligated into pCR2.1-TOPO cloning vectors (Invitrogen), and transformed into

One Shot E. coli DH5α-T1-resistant competent cells according to the manufacturer's instructions. Plasmids from selected clones were extracted using the QIAprep spin mini kit (Qiagen) and target validated by DNA sequencing (Macrogen USA, MA, USA) of the insert and BLASTX comparison against the NCBI NR database. After linearization of plasmids with HindIII endonuclease (New England BioLabs Inc., Ipswich, MA, USA), plasmid concentrations were measured fluorometrically with a Qubit fluorometer (Life technologies) and serially diluted resulting in standards ranging from 103 to 109 copies μl^{-1}. For each target, triplicate qPCR reactions were performed for each standard and biological triplicate in an ABI 7900HT Fast Real-Time PCR system (Applied Biosystems, Carlsbad, CA, USA) with a final volume of 25 µl, including 12.5 µl PerfeCta SYBR Green SuperMix, Rox (Quanta Biosciences, Gaithersburg, MD, USA), 300 nM respective primers (Table 3.2), and 10 ng DNA/RNA (cDNA). Template DNA/RNA consisted of pooled (equal molar) day and night nucleic acids to examine overall day/night biogeochemical cycling and domain distribution during sampling years. The efficiency of each qPCR was calculated and ranged between 90 and 100%. Data were analyzed with SPSS using an independent sample t-test (two-tailed, $p < 0.05$) to detect differences in RNA:DNA ratios between 2011 and 2012, as well as multiple comparison analysis (ANOVA) of 16S rRNA genes to detect differences in Archaea and Bacteria abundances.

3.3. RESULTS

3.3.1. Salt Pond Environmental Conditions

Measurements of the environmental parameters at Salt Pond during August 2011 showed the following day/night pre-disturbance conditions: salinity 230 g kg^{-1}, water

temperature 40/25°C, dissolved oxygen 2.45/1.45 mg/L, and pH 7.6/6.8 (Figure 3.1). The landfall of Hurricane Irene provided a disturbance to the ecosystem, resulting in the following August 2012 post-disturbance day/night conditions: salinity 65 g kg^{-1}, water temperature 35/30°C, dissolved oxygen 3.08/2.30 mg/L, and pH 7.5/7.3. The results outlined below describe the Salt Pond microbial mat community response to this ecosystem disturbance.

3.3.2. Post-disturbance Shifts in Community Diversity

Following the reduction in salinity, qPCR of 16S rRNA genes from replicate day/night samples indicated significant ($p < 0.05$) changes in overall domain prevalence with Archaea decreasing from 57 to 33% and Bacteria increasing from 43 to 67%. To further explore differences in community composition (β-diversity) between salinity conditions, θYC distances were visualized on NMDS plots (Figure 3.2). Distribution of 16S rDNA and rRNA-based distances showed uniform clustering of Archaea and Bacteria day and night samples within respective years, suggesting minimal diel influence on community composition. However, spatial separation was observed between years as 2011 and 2012 samples formed distinct clusters, indicating an overall shift in the archaeal and bacterial communities with decreased salinity. Analysis of molecular variance (AMOVA) further supported the significant difference in community composition between years ($p < 0.0001$). Further comparison between the distribution of rDNA and rRNA-based distances showed uniform clustering for archaeal samples under both salinity conditions, indicating similar rDNA and rRNA-based community structure. However, within the bacterial community, rDNA- and rRNA-based samples formed

unique clusters under the pre-disturbance high saline conditions of 2011 as compared to more even distribution observed after the post-disturbance reduction in salinity.

3.3.3. Post-disturbance Shifts in Archaeal Abundance

To better understand how the archaeal community shifted following the reduction in salinity, the relative abundance of archaeal 16S rRNA genes was compared across years (Figure 3.3A). The relative abundance for each OTU represents the average among six biological replicates and only OTUs that were determined to be significant through LEfSe analysis are displayed. The standard deviation for each OTU is listed in the Table 3.4. Furthermore, due to similarities in day/night abundances, average abundances are discussed for comparison between years. During both pre- and post- disturbance years, approximately 4% of archaeal OTUs had relative sequence abundances >1% and classified as 'abundant' while the majority were <1% and classified as 'conditionally rare'. Although rare OTUs comprised a majority of the community richness, in total they represented only 33 and 39% of overall archaeal 16S rRNA gene abundance in 2011 and 2012, respectively. Following the reduction in salinity, OTU abundance shifted with 4 OTUs remaining abundant across salinities, while 3 shifted from abundant to rare and 11 from rare to abundant. Additionally, 214 OTUs (46%) were detected only in the post-disturbance samples, suggesting greater environmental specialization by taxa than that suggested by the lower-resolution NMDS plots.

Classification of OTUs showed that under the 2011 high salt conditions, the single most abundant class was Halobacteria, representing approximately 45 ± 0.12% of total archaeal 16S rRNA gene abundance (Figure 3.1A, D/N11). While most abundant, the evenness of the Halobacteria community was skewed toward a single OTU belonging

to the family, Halobacteriaceae. While this OTU remained the most abundant in post-disturbance samples, an overall onefold reduction in Halobacteria OTU richness was observed, resulting in a 0.7- fold decrease in Halobacteria relative abundance (Figure 3.3A;

D/N12). The next most abundant classes identified under high salinity were unclassified Euryarchaeota and Thermoplasmata, which showed the highest OTU richness across years but only represented approximately 16.55 ± 0.03 and 29.44 ± 0.10% of overall archaeal 16S rRNA gene abundance, respectively (Figure 3.3A; D/N11). Following salinity reduction, previously abundant Thermoplasmata OTUs decreased while previously rare or not detected OTUs expanded, resulting in a 0.7- fold increase in richness and a 0.5-fold increase in relative abundance (Figure 3.3A; D/N12). Within the archaeal community, the greatest shift in relative abundance was observed for Crenarchaeota, with unclassified and uncultured Crenarchaeota increasing approximately sixfold in post-disturbance samples (Figure 3.3A). While few archaeal OTUs across salinities classified within the Thaumarchaeota phylum, an increase in richness and abundance was observed with the reduction in salinity.

3.3.4. Post-disturbance Shifts in Bacterial Abundance

To examine post-disturbance shifts in the bacterial community, the relative abundance of bacterial 16S rRNA genes was also compared across years (Figure 3.3B). As above, the relative abundance for each OTU represents the average among replicates and only significant OTUs are displayed with standard deviations listed in the Table 3.4. Similar to the archaeal community, during both years, approximately 2% of bacterial OTUs were classified as ‘abundant’ while the remaining were classified as ‘conditionally

rare'. While rare OTUs comprised a majority of the community richness, in total they represented 46 and 65% of relative bacterial 16S rRNA gene abundance in 2011 and 2012, respectively. Following the reduction in salinity, OTU abundance shifted with 2 OTUs remaining abundant across both salinities, while 3 shifted from abundant to rare and 6 from rare to abundant. In addition, 625 OTUs (61%) were only detected in the post-disturbance samples, suggesting environmental specialization by many bacterial taxa.

Classification of bacterial OTUs indicated that Bacteroidetes was the most abundant pre-disturbance phylum with three OTUs classified as Sphingobacteria having the greatest abundance (Figure 3.3B; D/N11). Under post-disturbance conditions, while Bacteroidetes richness remained the same, relative abundance decreased by twofold (Figure 3.3B, D/N12). For the following phyla, Actinobacteria, Chloroflexi, Planctomycetes, and Verrucomicrobia, equal abundance was observed across years, however, some OTUs were only present under one salinity condition. For instance, within the phylum Planctomycetes, one OTU classified as Phycisphaerae was abundant under high salinity and decreased significantly following the shift in salinity. In addition, while all Planctomycetes OTUs belonged to the rare population in 2012, more than half were detected only at lower salinity, resulting in overall increased phylum richness. Cyanobacteria comprised approximately 8% (±1) of the pre- disturbance bacterial 16S rRNA gene abundance and increased by 0.8-fold concomitant with salinity reduction (Figure 3.3B). Within the Cyanobacteria, while most OTUs were classified as conditionally rare, one was abundant under both conditions while two changed from not detected or rare to abundant with salinity reduction. The greatest bacterial community richness across both salinities was contained within the Proteobacteria phylum. Within

this phylum, Alphaproteobacteria was the most abundant class across years, followed by Delta-, Gamma-, and unclassified-Proteobacteria. Furthermore, among the Alphaproteobacteria, four OTUs belonging to the orders Rhizobiales, Rhodobacterales, and unclassified Alphaproteobacteria were the most abundant under high salinity. Following the reduction in salinity, Rhodobacterales OTUs decreased by 0.8-fold, while a single abundant Rhizobiales OTU further increased by one fold, shifting the order to become the most abundant Alphaproteobacteria at lower salinities. While Deltaproteobacteria had the greatest richness among the Proteobacteria, with OTUs spanning nine orders, the Desulfobacterales and unclassified Deltaproteobacteria contained the most OTUs and had the highest abundance within the class. While no change in overall abundance was observed across salinities, OTU distribution among Deltaproteobacteria changed significantly, with half of the OTUs detected only under one condition (Figure 3.3B, non-cross hatched OTUs). The largest shift in proteobacterial abundance across salinities was observed within the Gammaproteobacteria, which increased approximately threefold following the decrease in salinity. This shift in abundance was correlated with an increase in three OTUs classified as Chromatiales and Sedimenticola.

3.3.5. Post-disturbance Shifts in Archaeal 16S rRNA:rDNA Ratios

Correlation analysis was used to test the association between 16S rRNA and rDNA abundance during day and night across conditions (Figure 3.4). A positive correlation between rRNA and rDNA abundance was observed for OTUs during daytime across both years (Figure 3.4A; Kendall's nonparametric $\tau_{day2011} = 0.59$, $p < 0.0001$, $n = 275$; $\tau_{day2012} = 0.59$, $p < 0.0001$, $n = 330$). Similarly, while a positive correlation was

also observed during nighttime, a reduction in the τ coefficient during 2012 suggested a weaker association under the lower salinity nighttime samples (Figure 3.4B; Kendall's nonparametric $\tau night2011 = 0.55$, $p < 0.0001$, $n = 249$; $\tau night2012 = 0.38$, $p < 0.0001$, and $n = 367$). Further analysis showed that most archaeal OTUs had rRNA:rDNA ratios below the 1:1 correlation line under all conditions (Figures 3.4A,B). However, following the salinity reduction in 2012, the total number of abundant and rare OTUs with ratios above the 1:1 line increased by 0.2-fold, indicating an overall increase in archaeal PSP.

To further explore the trends observed in the correlation analysis, archaeal OTUs were classified and 16S rRNA:rDNA ratios compared during day/night across salinity conditions (Figure 3.5). Overall, dynamic shifts in ratios for abundant and rare OTUs within and across classes indicated complex archaeal community environmental adaptation. During the pre-disturbance conditions of 2011, the highest mean rRNA:rDNA ratios were observed within unclassified and uncultured Euryarchaeota, followed by Thermoplasmata, Methanomicrobia, and Thaumarchaeota, (Figure 3.5, D/N11; Table 3.3). Following salinity reduction, a significant ($p < 0.01$) shift in mean rRNA:rDNA ratios was observed concomitant with changes in abundance (Figure 3.3A), which resulted in more even distribution of PSP across classes (Figure 3.3, D12 and N12). For instance, a decrease in mean ratios was observed within unclassified and uncultured Euryarchaeota while ratios increased for unclassified Crenarchaeota, Thermoplasmata, Thaumarchaeota, and miscellaneous crenarchaeotic group. These broad shifts resulted in a significant increase in mean archaeal PSP (Table 3.3).

3.3.6. Post-disturbance Shifts in Bacterial 16S rRNA:rDNA Ratios

As opposed to archaeal OTUs, no significant association between 16S rRNA and rDNA abundance was observed for bacterial OTUs during daytime across both salinity conditions (Figure 3.2C; Kendall's nonparametric $\tau day2011 = 0.05$, $p = 0.15$, and $n = 434$; $\tau day2012 = 0.06$, $p = 0.05$, and $n = 697$). However, a weak positive correlation was observed for nighttime samples across years (Figure 3.4D; Kendall's nonparametric $\tau night2011 = 0.35$, $p < 0.0001$, and $n = 347$; $\tau night2012 = 0.26$, $p < 0.0001$, and $n = 621$). Similar to Archaea, most bacterial OTUs had rRNA:rDNA ratios below the 1:1 correlation line under all conditions (Figures 3.4C, D). However, following the reduction in salinity, daytime rRNA:rDNA profiles shifted, with the number of rare OTUs above the 1:1 line increased by 1.3-fold, indicating greater PSP within this bacterial population. A similar trend was observed in nighttime samples with a 0.9- and 0.3-fold increase in the number of abundant and rare OTUs with higher rRNA:rDNA ratios.

Classification and comparison of rRNA:rDNA ratios for bacterial OTUs across salinity and diel conditions indicated unique PSP profiles across and within phyla (Figure 3.6). Under the high salinity pre-disturbance conditions of 2011, rRNA:rDNA ratios were low for most OTUs with the highest ratios observed for OTUs within the Proteobacteria, Cyanobacteria, and Bacteroidetes phyla (Figure 3.6, D/N11; Table 3.3). Following the reduction in salinity, increased rRNA:rDNA ratios were observed for rare OTUs among all phyla, indicating higher PSP across most phyla and an overall significant ($p < 0.01$) increase in bacterial PSP as determined by the mean day/night ratios for both salinity conditions (Figure 3.6, D/N12; Table 3.3). Examination of diel trends across conditions showed that most phyla didn't show significant differences in average day/night

rRNA:rDNA profiles under the higher salinity conditions of 2011. However, under the lower salinity conditions of 2012, OTUs within most phyla showed decreased rRNA:rDNA ratios at night, resulting in a significant decrease in community mean PSP ($p < 0.01$) as compared to daytime (Table 3.3).

The Proteobacteria phyla was further resolved to better understand how the salinity shift affected rRNA:rDNA profiles of this metabolically diverse group (Figure 3.7). Following salinity reduction, increased rRNA:rDNA ratios were observed for OTUs within and across orders, resulting in a significant increase in mean daytime proteobacterial PSP. The Alphaproteobacteria was most abundant proteobacterial class across conditions (Figure 3.3B) and showed significant increase in mean PSP under lower salinity (Figure 3.7; Table 3.3, Alphaproteobacteria). Among the Alphaproteobacteria, increased rRNA:rDNA ratios were observed for OTUs classified within the nitrogen fixing Rhizobiales and the purple non-sulfur bacteria, Rhodobacterales and Rhodospirillales. The Deltaproteobacteria had the highest OTU richness among proteobacterial classes (Figure 3.3B) and showed the greatest mean PSP in daytime 2012, with OTUs among all orders increasing rRNA:rDNA ratios following salinity reduction (Figure 3.7; Table 3.3, Deltaproteobacteria). The Gammaproteobacteria had the greatest increase in abundance following salinity reduction due to the expansion of three OTUs contained within the Chromatiales and Sedimenticola orders (Figure 3.3B) which showed concomitant increases in rRNA:rDNA ratios (Figure 3.7, Gammaproteobacteria).

3.3.7. Biogeochemical Cycling

3.3.7.1. Nitrogen Fixation

The dinitrogenase reductase gene (*nifH*) abundance was measured to examine community nitrogen fixation potential (Figure 3.8). Across both pre- and post-disturbance conditions, no significant difference ($p > 0.05$) was observed in *nifH* DNA gene copy numbers per gram of microbial mat during day [2011: $(3.8 \pm 0.7) \times 10^8$; 2012: $(1.6 \pm 1.4) \times 10^8$] or night [2011: $(3.4 \pm 0.8) \times 10^8$; 2012: $(2.4 \pm 0.7) \times 10^8$], suggesting overall community genetic potential for nitrogen fixation remains similar across salinities (Figure 3.8, *nifH* D/N11 vs. D/N12). However, using the RNA/DNA ratio as a measure of potential *nifH* gene expression, an increase in daytime expression from below detection to 33% was observed following the reduction in salinity (Figure 3.8, *nifH* D11 vs D12 shaded bar). Nighttime *nifH* expression was below detection under both salinities.

3.3.7.2. Nitrification

Bacterial and archaeal ammonia monooxygenase genes (*amoA*) were analyzed to investigate the potential contribution of nitrification among ammonia-oxidizing Archaea (AOA) relative to ammonia-oxidizing Bacteria (AOB). Attempts to amplify bacterial *amoA* genes from pre- and post-disturbance conditions were unsuccessful and typical AOB taxa were not identified in Proteobacteria 16S rRNA or rRNA genes. However, archaeal *amoA* genes were identified in DNA at similar copy numbers with no significant difference ($p > 0.05$) across years [2011: day $(3.8 \pm 3.2) \times 10^7$; night $(3.0 \pm 0.9) \times 10^7$] and [2012: day $(2.7 \pm 2.5) \times 10^7$); night $(5.9 \pm 6.7) \times 10^7$] (Figure 3.8, *amoA* D/N11 vs. D/N12). Analysis of *amoA* gene expression during day and night showed average

RNA/DNA ratios of 35% and 13% under high salinity conditions and increased to 63% and 20% following the 2012 post-disturbance salinity reduction.

3.3.7.3. Denitrification

The denitrification potential of the community was estimated through analysis of the *nirK*/*nirS* (nitrite reductase) and *nosZ* (nitrous oxide reductase) genes. Amplification of nitrite reductase genes from the Salt Pond microbial mat under both salinity conditions only identified *nirS* genes. Similar ($p > 0.05$) gene abundance for *nirS* and *nosZ* were observed during day [2011: *nirS* $(1.2 \pm 0.03) \times 10^9$, *nosZ* $(2.8 \pm 0.7) \times 10^8$; and 2012: *nirS* $(1.1 \pm 0.6) \times 10^9$, and *nosZ* $(3.5 \pm 2.8) \times 10^7$) and night (2011: *nirS* $(9.5 \pm 2.8) \times 10^8$, *nosZ* $(1.9 \pm 0.6) \times 10^8$; and 2012: *nirS* $(1.6 \pm 0.2) \times 10^9$, and *nosZ* $(9.7 \pm 3.4) \times 10^7$) under both salinity conditions (Figure 3.8). However, comparison of *nirS* to *nosZ* across both years indicated that the abundance of *nirS* was greater than *nosZ*. In addition, while *nirS* and *nosZ* gene abundances remained similar across years, significant increases ($p < 0.001$) in daytime RNA/DNA ratios for both genes were observed during 2012 (Figure 3.8, *nirS*, *nosZ*: D11 and D12). When examining potential differences in diel expression, *nirS* transcripts were below detection at night in both years while *nosZ* showed minimal (2.2%) nighttime expression during 2011 and below detection in 2012. Anaerobic ammonia oxidation (anammox) was also investigated and while taxa affiliated with the Plantomycetes phylum were identified, attempts to amplify the hydrazine oxidoreductase (*hzo*) genes were unsuccessful.

3.3.7.4. Sulfate Reduction

In this study, the dissimilatory sulfite reductase (*dsrA*) gene was analyzed as a marker for pre- and post-disturbance SRB (Wagner *et al.*, 2005) potential and the

expression of *dsrA* genes by the Salt Pond microbial mat community (Figure 3.8). There were no significant differences ($p > 0.05$) in *dsrA* gene abundance in day/night DNA during both years [day11: $(8.2 \pm 2.0) \times 10^9$, night11: $(6.4 \pm 1.1) \times 10^9$; day12: $(1.7 \pm 1.4) \times 10^9$), night12: $(6.2 \pm 2.7) \times 10^9$]. While gene abundance was equal across conditions, RNA/DNA ratios indicated low-level *dsrA* expression (≤7%) under all conditions except in the 2012 lower salinity day samples. Under the 2012 daytime condition, the average RNA/DNA ratio increased to 81% representing a significant increase (, $p < 0.001$) in expression. When examining day/night differences in 2012, RNA/DNA ratios indicate that *dsrA* expression was greatest during the day and suppressed at night.

3.3.7.5. Sulfide Oxidation

In this study, we measured the abundance of the *soxB* gene to determine the microbial community sulfide oxidizing potential and activity by the Salt Pond community during day and night under high and low salinity. There were no significant differences in *soxB* gene abundance extracted from day [2011: $(5.7 \pm 0.7) \times 10^8$; 2012: $(4.0 \pm 1.6) \times 10^8$] and night [(2011: $3.1 \pm 2.2) \times 10^8$; 2012: $(1.8 \pm 1.1) \times 10^8$] samples across years, suggesting the potential for sulfide oxidation exists under both salinity conditions (Figure 3.8). However, no *soxB* genes were detected in RNA isolated from the same samples (other biogeochemical gene were amplified from these samples).

3.4. Discussion

3.4.1. Microbial Mat Compositional Sensitivity to Environmental Disturbance

We used a coastal hypersaline microbial mat ecosystem to examine the sensitivity of a semi-closed community to a pulse disturbance, and to examine the extent to which overall community shifts altered biogeochemical potentials. Community sensitivity was

examined through comparative 16S rDNA and rRNA analysis to determine shifts in archaeal and bacterial abundance and metabolic potential. Studies have previously used 16S rRNA:rDNA ratios to infer metabolic activity; however, a number of caveats could potentially confound data interpretation (Blazewicz *et al.*, 2013; Denef *et al.*, 2016). Given the considerations outlined in the aforementioned studies, we used rRNA:rDNA ratios to conservatively estimate the metabolic potential (PSP) of the community. Domain-level sensitivity was first observed, with Bacteria becoming more abundant than Archaea following the post-disturbance reduction in salinity. Differences in beta diversity observed across conditions suggest significant changes in community structure, which further supports studies that have identified salinity as a main determining factor in controlling microbial diversity (Benlloch *et al.*, 2002; Rietz and Haynes, 2003; Tripathi *et al.*, 2005; Lozupone and Knight, 2007; Canfora *et al.*, 2014; Webster *et al.*, 2015; Aanderud *et al.*, 2016). In addition, uniform clustering of rDNA and rRNA distances was observed for all conditions except for the bacterial community at high salinity. These data suggest that the archaeal community may contain habitat generalists with a wide range of osmotic tolerance while the bacterial community consists of more habitat specialists that are selected under different environmental conditions. These results support a previous study that observed selection of bacterial specialists within isolated ecosystems that have adapted to salinity extremes (Logares *et al.*, 2013). OTU-level analysis across conditions was used to further resolve changes in community structure and showed dynamic shifts in rare/abundant OTUs throughout both archaeal and bacterial communities. In addition to increased abundance of large numbers of previously rare OTUs, approximately 46% and 61% of archaeal and bacterial post-disturbance OTUs were detected only under the lower

salinity conditions. These data suggest that the microbial mat rare biosphere played a significant role in the post-hurricane adaptation of the ecosystem and further supports other studies suggesting that the rare biosphere provides functional flexibility to ecosystems during periods environmental disturbance (Jones and Lennon, 2010; Lennon and Jones, 2011; Shade *et al.*, 2012b; Aanderud *et al.*, 2015; Coveley *et al.*, 2015). Classification of OTUs indicated that rare/abundant shifts occurred broadly across archaeal and bacterial taxonomic ranks, often coinciding with shifts in 16S rRNA:rDNA ratios.

Within the archaeal community, post-disturbance trends were observed wherein richness and abundance significantly decreased for Halobacteria and increased for Thermoplasmata, Crenarchaeota, and Thaumarchaeota following the salinity shift. The decrease in Halobacteria abundance is not surprising as taxa within this class are known to thrive in environments with salinities over 100 g kg^{-1} (Ochsenreiter *et al.*, 2002; Sorensen *et al.*, 2005; Maturrano *et al.*, 2006; Oren, 2008; Youssef *et al.*, 2012; Sorokin *et al.*, 2014; Williams *et al.*, 2014; Najjari *et al.*, 2015). However, while Halobacteria decreased in total abundance, some OTUs shifted from rare to abundant concomitant with increased rRNA:rDNA ratios. Similar to a previous study (Najjari *et al.*, 2015), these shifts suggest salinity-driven succession within the halobacterial community. The increased abundance and PSP of Crenarchaeota in post- disturbance samples suggests that high salinity provided an environmental constraint to OTUs within this taxon. This is consistent with a study that found Crenarchaeota to be dominant in lake sediments of intermediate salinity while Halobacteria became more abundant in lakes with higher salinity (Liu *et al.*, 2016). Thermoplasmata and Thaumarchaeota were observed under

pre-disturbance conditions but increased in abundance and PSP following the salinity shift, suggesting greater adaptation to lower salinity. Overall, data show that the pulse disturbance generated dynamic shifts in archaeal OTU abundance and rRNA:rDNA ratios, resulting in numerous rare/abundant shifts and an increase in total archaeal PSP. Some taxa within these groups are thought to be involved in methanogenesis (Paul *et al.*, 2012) and ammonia-oxidation (Brochier-Armanet *et al.*, 2008; Pester *et al.*, 2011), suggesting that post-disturbance conditions may increase archaeal biogeochemical cycling potential within the microbial mat.

Dynamic shifts in abundance and rRNA:rDNA ratios were also observed across bacterial phyla, with Bacteroidetes abundance decreasing while Cyanobacteria and Proteobacteria increased following the reduction in salinity. The shift in Bacteroidetes occurred as a result of the abundant to rare transition of three OTUs classified within the Sphingobacteria, suggesting they represent halophilic taxa similar to those observed in other hypersaline systems (Trigui *et al.*, 2011). Cyanobacteria are considered pioneer species in many microbial mats and show a range of salt tolerance, resulting in salinity-driven specialization and distribution (Braithwaite and Whitton, 1987; Dubinin *et al.*, 1992; Franks and Stolz, 2009). A range of salt tolerance was also suggested for Cyanobacteria in the current study with one OTU remaining abundant across conditions and others increasing from rare to abundant following the post- disturbance salinity reduction. This is consistent with another study that also identified a shift in cyanobacterial taxa within a microbial mat following environmental disturbance (Yannarell *et al.*, 2007). Within the Proteobacteria, OTUs classified within the Chromatiales order and as Sedimenticola shifted from rare to abundant following

ecosystem disturbance, resulting in a significant increase in the abundance of Gammaproteobacteria. Taxa within Chromatiales have been identified in ecosystems ranging from freshwater to hypersaline (Caumette *et al.*, 1988; Mesbah *et al.*, 2007; Gomes *et al.*, 2010) but appear to be suppressed at the extreme high salinity found in the pre- disturbance conditions of this study. In addition, Sedimenticola are potential denitrifiers using sulfide as electron donor (Russ *et al.*, 2014) and have been previously described in ocean sediments, indicating possible tolerance toward lower salinities. These results are consistent with a previous study showing decreased bacterial diversity under high salinity conditions (Benlloch *et al.*, 2002) and suggest that the reduced salinity occurring after Hurricane Irene provided more favorable environmental conditions which resulted in a significant increase in overall bacterial PSP. Post-disturbance diel trends showed that the increase in PSP was significantly higher during daytime compared to nighttime. Primary productivity has been shown to be suppressed under high salinity, resulting in a breakdown of typical microbial mat redox gradients (Pinckney *et al.*, 1995). The differences in diel PSP observed here was likely explained by the re-establishment of redox gradients and biogeochemical cycles within the mat ecosystem following the reduction in salinity.

3.4.2. Microbial Mat Functional Sensitivity to Disturbance

Microbial mats are often considered natural bioreactors due to the close microbial metabolic coupling occurring within a millimeter scale and resulting in enhanced biogeochemical cycling (Visscher and Stolz, 2005). For example, the microbial mat investigated in this study grows in an oligotrophic ecosystem requiring community production and recycling of nitrogen and sulfur compounds. The shift in salinity

experienced by the mat ecosystem investigated in this study following Hurricane Irene resulted in dynamic changes in the abundance and PSP of archaeal and bacterial taxa. Many of these taxa likely play a role in biogeochemical processes; therefore, we next examined how the post-disturbance community shifts affected expression of nitrogen and sulfur cycling genes. Quantitative PCR was used to determine the abundance of genes and transcripts as a measure of genetic potential and expression, respectively. Other studies have used a similar approach to identify nitrogen and sulfur cycling potential and expression and have observed a correlation between gene expression and process rates (Church *et al.*, 2005; Philippot and Hallin, 2005; Bernhard *et al.*, 2010; Akob *et al.*, 2012; Turk-Kubo *et al.*, 2012; Headd and Engel, 2013; Bowen *et al.*, 2014). However, it should be noted that potential post-transcriptional modifications and temporal decoupling (Chen *et al.*, 1998; Kim *et al.*, 1999; Nogales *et al.*, 2002; van de Leemput *et al.*, 2011) may confound the link between gene expression and process rates and is therefore used in this study as a comparative measure to assess how the pulse disturbance influenced the biogeochemical potential within the microbial mat ecosystem.

3.4.3. Nitrogen Cycling

To assess how the microbial mat potential for nitrogen fixation shifted across conditions, *nifH* genes and transcripts were examined and RNA:DNA ratios compared. While *nifH* genes were observed under all conditions, expression was repressed under pre-disturbance conditions and significantly increased following the salinity reduction. These results are consistent with a study observing suppression of N_2 fixation in microbial mats at salinities over 90 g kg^{-1} (Paerl *et al.*, 1993; Pinckney *et al.*, 1995, 2011). In addition, studies of N_2 fixation have also observed complex diel regulation of

nifH expression within different ecosystems(Pinckney *et al.*, 1995; Colón-López *et al.*, 1997; Church *et al.*, 2005; Steunou *et al.*, 2008; Severin and Stal, 2010; Woebken *et al.*, 2015). Within the microbial mat community, *nifH* expression was observed only during daytime, suggesting that N_2 fixation may be coupled to phototrophy through direct (i.e., heterocystous Cyanobacteria) or indirect (i.e., photosynthate utilization by noncyanobacterial diazotrophs) pathways. While the contribution of individual taxa to *nifH* expression was not established in this study, many OTUs within Classes/Orders known to contain diazotrophic members, such as Methanobacteria, Rhizobiales, and Desulfobacterales, demonstrated increased abundance and PSP in daytime samples following the post-disturbance reduction in salinity.

Nitrification was examined through comparative analysis of *amoA* genes and transcripts. Within the microbial mat, no bacterial *amoA* genes were detected; however, amplification of archaeal *amoA* genes across conditions suggests a dominant role of the archaeal community in nitrification within this ecosystem. While *amoA* transcripts were detected in both day and night samples during the high salinity conditions, the transcript abundance increased following the salinity reduction, suggesting increased expression and higher nitrification potential. As discussed earlier, while taxa within Thaumarchaeota showed high PSP at day and night under both salinities, OTU abundance, richness, and PSP shifted under the lower salinity condition and may have played a role in the increased *amoA* expression. Diel trends showed that *amoA* expression was always higher in daytime samples. Given that AOA require molecular oxygen and show possible pH sensitivity (Beman *et al.*, 2011; Gubry-Rangin *et al.*, 2015), the observed differences in diel expression may result from partial physiological constraints as the photosynthetically

driven mat shifts from daytime oxic-alkaline conditions to nighttime anoxic–acidic conditions (Revsbech *et al.*, 1983). For instance, one Thaumarchaeota OTU further classified within the Nitrososphaeria class had increased activity during day versus night. Members of this class have been shown to have a preference to alkaline conditions (Gubry-Rangin *et al.*, 2015), suggesting shifts in pH may regulate the activity of this OTU. While archaeal *amoA* genes have been identified in a range of ecosystems (Francis *et al.*, 2005; Stahl and de la Torre, 2012; Yang *et al.*, 2013), the expression observed under the high salinity condition in this study expands the known range of salinity tolerance.

The process of denitrification, reduction of nitrate or nitrite to nitrous oxide or dinitrogen, is the major mechanism by which fixed nitrogen returns to the atmosphere from soil and water. While both *nirK* and *nirS* nitrite reductase genes have been identified in microbial mats across a range of salinities (Desnues *et al.*, 2007; Fan *et al.*, 2015), only *nirS* was identified in the mat ecosystem examined in this study. This supports other studies suggesting possible environmentally driven differences in the ecological distribution of *nirK*/*nirS* genes (Oakley *et al.*, 2007; Smith and Ogram, 2008; Jones and Hallin, 2010). Across both years, the abundance of *nirS* and *nosZ* (nitrous oxide reductase) genes remained similar, suggesting the overall denitrification potential of the community was maintained in both pre- and post-disturbance conditions. Similar to another study that observed decreased gene abundance along the denitrification pathway (Bru *et al.*, 2011), we also observed greater abundance of *nirS* compared to *nosZ*. This difference in abundance is likely linked to the sequential reduction in energy gained by each step (Koike and Hattori, 1975). While gene abundance remained similar across

conditions, increased RNA:DNA ratios observed in post-disturbance samples suggest increased gene expression and potential for denitrification with reduced salinity. While rates of denitrification are regulated by many variables (e.g., oxygen concentration, pH, temperature, and salinity), the greatest influence is often considered to be carbon and nitrogen availability (Hallin *et al.*, 2009; Jones and Hallin, 2010; Babbin and Ward, 2013). Extreme salinities have been shown to reduce microbial mat photosynthetic carbon fixation and nitrogen fixation; therefore, the post- disturbance reduction in salinity likely increased carbon and nitrogen availability and enhanced denitrification. The low nighttime expression of these genes suggests that denitrification might be coupled to anoxygenic photosynthetic bacteria as has been observed in lake sediments (Shen and Hirayama, 1991) or that the routine diel changes in pH, oxygen, and carbon availability provide an environmental constraint that limits denitrification to daytime. Post-disturbance community profiles showed that OTUs classified as Halobacteriaceae, Rhodospirllales, and Rhodobacterales significantly increased PSP following the reduction in salinity. Denitrification has been shown by some taxa within these groups (Tomlinson *et al.*, 1986; Yoshimatsu *et al.*, 2000; Hattori *et al.*, 2016), suggesting a possible increasing contribution of these taxa to denitrification within the microbial mat ecosystem.

3.4.4. Sulfur Cycling

Microbial mats typically have high rates of primary productivity resulting in the production and excretion of photosynthates into surrounding sediments (Bateson and Ward, 1988). Within marine hypersaline systems, these organic compounds are mineralized, in large part, by microbes using anaerobic respiration coupled to sulfate

reduction (Baumgartner *et al.*, 2006; Brocke *et al.*, 2015). During both years, no difference in *dsrA* gene abundance was observed, suggesting that the community contains similar sulfate reduction potential across conditions. While genetic potential remained similar, significant increases in RNA:DNA ratios were observed under the lower salinity daytime condition. This result indicates that the high salinity conditions constrained potential community sulfate reduction while lower salinity conditions enhanced potential reduction. Others have also observed decreased sulfate reduction at salt saturation (Oren, 1999; Kulp *et al.*, 2007; Gu *et al.*, 2012). While the exact mechanism of suppression is unclear, it has been hypothesized that sulfate reduction may not supply enough energy for osmoadaptation (Oren, 1999, 2011) or that increased borate concentration occurring at salt saturation may act as a specific inhibitor of this metabolism (Kulp *et al.*, 2007). In addition, 2012 diel trends indicate that *dsrA* expression was greatest during the day and suppressed at night. While sulfate reduction is considered to be a strict anaerobic process, oxygen tolerance has been observed (Cypionka, 1995) and provides a selective advantage by increasing accessibility to carbon derived from photosynthetic processes. This finding is in agreement with other studies that observed high rates of sulfate reduction in the upper layers of microbial mats coupled to carbon fixation by the phototrophic community (Teske *et al.*, 1998). The ability to use sulfur species as an electron acceptor has been identified in a taxonomically diverse group of Archaea and Bacteria. For instance, within the Archaea, all known sulfate-reducing taxa are considered hyperthermophiles and have been classified within the Crenarchaeota, Thermoplasmata, and Methanobacteria (Liu *et al.*, 2012). Within Bacteria, sulfate- reducing taxa are mostly located within the Deltaproteobacteria and Epsilonproteobacteria and have been identified in a wide range

of ecosystems, including microbial mats (Muyzer and Stams, 2008). Under the 2011 high salinity condition, while all potential sulfate-reducing groups were active, taxa within the Thermoplasmata had the highest OTU richness and abundance, suggesting these taxa may play a greater role in maintaining the sulfur cycle under extreme salinity (Figures 3.3, 3.5, and 3.7). Following the post-disturbance reduction in salinity, OTU richness, abundance, and activity increased for all groups concomitant with significant increases in *dsrA* expression. However, OTUs within the Deltaproteobacteria showed the greatest increase in richness and activity during daytime, suggesting a possible shift in the predominant sulfate- reducing group. Overall, it is likely that within this microbial mat ecosystem, salinity influences the major sulfate-reducing taxa with archaeal Thermoplasmata taxa playing a greater role under higher salinities and bacterial Deltaproteobacteria playing a greater role in lower salinity conditions.

Within microbial mat ecosystems, sulfate reduction is closely coupled to the oxidation of reduced sulfur compounds by chemolithotrophic and anoxygenic phototrophic microorganisms utilizing the Sox enzymatic system (Headd and Engel, 2013). Among the Sox system, the *soxB* gene, encoding the periplasmic thiosulfate-oxidizing Sox enzyme, is often used as a marker of microbial community sulfide oxidation potential (Headd and Engel, 2013). In this study, *soxB* genes were detected in all samples while transcripts were undetected. These results suggest that while sulfide oxidation potential exists, the gene is suppressed under all analyzed conditions. The mechanism of this suppression is unclear and is the focus of future studies. However, it is possible that, while sulfide oxidation is thermodynamically favorable for osmoadaptation, increased levels of salinity or other environmental factors may have suppressed the

activity of the sulfide oxidizing community. Evidence for a possible salinity-driven suppression of sulfide oxidation was observed in a study examining the sulfur cycle along a salinity gradient from freshwater into the Dead Sea (Häusler *et al.*, 2014). This study observed that increasing salinity selected for different sulfide oxidizing communities with the highest salinity restricting growth to only halotolerant or halophilic taxa. Similarly, while OTUs affiliated with possible sulfide oxidizing groups were detected in Salt Pond samples, their PSP was low across both salinity conditions. Therefore, the sulfide oxidizing community within this ecosystem may be composed of taxa adapted to lower salinity conditions resulting in the suppression of *soxB* expression.

Table 3.1. MID sequences added to the U529 reverse primer.

ID	MID Sequence	Library 1 2012 rDNA	Library 2 2011 rDNA	Library 3 2012 rRNA	Library 4 2011 rRNA
MID1	ACG AGT GCG T	Bac/Arc 10 am 1	Bac/Arc 10 am 1	Bac/Arc 10 am 1	Bac/Arc 10 am 1
MID2	ACG CTC GAC A	Bac/Arc 10 am 2	Bac/Arc 10 am 2	Bac/Arc 10 am 2	Bac/Arc 10 am 2
MID3	AGA CGC ACT C	Bac/Arc 10 am 3	Bac/Arc 10 am 3	Bac/Arc 10 am 3	Bac/Arc 10 am 3
MID4	AGC ACT GTA G	Bac/Arc 5 pm 1	Bac/Arc 5 pm 1	Bac/Arc 5 pm 1	Bac/Arc 5 pm 1
MID5	ATC AGA CAC G	Bac/Arc 5 pm 2	Bac/Arc 5 pm 2	Bac/Arc 5 pm 2	Bac/Arc 5 pm 2
MID6	ATA TCG CGA G	Bac/Arc 5 pm 3	Bac/Arc 5 pm 3	Bac/Arc 5 pm 3	Bac/Arc 5 pm 3
MID7	CGT GTC TCT A	Bac/Arc 10 pm 1	Bac/Arc 10 pm 1	Bac/Arc 10 pm 1	Bac/Arc 10 pm 1
MID8	CTC GCG TGT C	Bac/Arc 10 pm 2	Bac/Arc 10 pm 2	Bac/Arc 10 pm 2	Bac/Arc 10 pm 2
MID9	CAT AGT AGT G	Bac/Arc 10 pm 3	Bac/Arc 10 pm 3	Bac/Arc 10 pm 3	Bac/Arc 10 pm 3
MID10	TCT CTA TGC G	Bac/Arc 5 am 1	Bac/Arc 5 am 1	Bac/Arc 5 am 1	Bac/Arc 5 am 1
MID11	TGA TAC GTC T	Bac/Arc 5 am 2	Bac/Arc 5 am 2	Bac/Arc 5 am 2	Bac/Arc 5 am 2
MID12	TAC TGA GCT A	Bac/Arc 5 am 3	Bac/Arc 5 am 3	Bac/Arc 5 am 3	Bac/Arc 5 am 3

Table 3.2. Quantitative PCR Primers for genes involved in biogeochemical processes and taxa used in this study.

Target group / process	Primer set	Amplicon size (bp)	Annealing T_a (°C)	Annealing time (min)	Reference
N_2 fixation	*nifH*1 F, *nifH*6 R	341	51	1:00	(Marusina *et al.*, 2001)
Nitrification	arch-*amoA*F, arch-*amoA*R	664	53	1:00	(Francis *et al.*, 2005)
	amoA-1F, *amoA*-2R	491	60	1:30	(Rotthauwe and Witzel, 1997)(Avrahami *et al.*, 2003)
Anaerobic ammonium oxidation	*hzo*QPCR1F, *hzo*QPCR1R	224	53	0:45	(Long *et al.*, 2013)
Denitrification	*nirS*Cd3aF, *nirS*R3cd	325	60	1:00	(Throbäck *et al.*, 2004)
	*nosZ*1F, *nosZ*1R	179	60	1:00	(Henry *et al.*, 2006)
	nirK876, *nirK1040*	165	63	0:30	(Henry *et al.*, 2004)
Sulfate reduction	*dsr*1F, *dsr*4R	780	54	1:00	(Wagner *et al.*, 1998)
Sulfide oxidation	*soxB*693, *soxB*1446	765	55.6	0:30	(Petri *et al.*, 2001)
Archaea	arc109F, U529R	420	62	0:45	(Whitehead, 1999)
Bacteria	27F, U529R	502	62	0:45	(Edwards *et al.*, 1989)

Table 3.3. Comparison of pre- and post-disturbance mean PSP (rRNA/rDNA ratios) of Archaea classes and Bacteria phyla. One-way analysis of variance (ANOVA) (p=0.05) was used to test the differences of mean PSP among conditions. Student's t-test was used to test total mean PSP between 2011 and 2012.

Archaea		mean PSP				
Class	OTUs	Day 2011	Night 2011	Day 2012	Night 2012	significance
Thaumarchaeota unclassified	20	0.81 ± 0.27 [a]	1.30 ± 0.42 [a]	3.70 ± 0.75 [ab]	5.20 ± 0.48 [b]	0.003
MCG	8	0.19 ± 0.10 [a]	1.17 ± 1.16 [a]	1.06 ± 0.23 [a]	2.92 ± 0.66 [b]	0.041
Crenarchaeota unclassified	17	0.22 ± 0.1 [a]	0.71 ± 0.58 [a]	5.82 ± 2.08 [ab]	14.52 ± 4.90 [b]	<0.001
Halobacteria	17	0.78 ± 0.10	0.85 ± 0.13	3.00 ± 1.30	2.30 ± 0.83	>0.05
Methanomicrobia	2	1.12 ± 0.62	0.45 ± 0.39	2.12 ± 0.51	2.96 ± 1.65	>0.05
Thermoplasmata	122	1.28 ± 0.19 [a]	0.91 ± 0.18 [a]	0.95 ± 0.08 [a]	3.32 ± 0.83 [b]	<0.001
Euryarchaeota unclassified	90	2.80 ± 0.60 [a]	1.76 ± 0.25 [ab]	0.60 ± 0.12 [b]	0.52 ± 0.21 [b]	<0.001
Euryarchaeota uncultured	15	2.48 ± 0.64 [a]	1.38 ± 0.34 [ab]	0.53 ± 0.19 [b]	0.39 ± 0.18 [b]	<0.001
total mean PSP	291	1.66 ± 0.21 [a]	1.21 ± 0.12 [a]	1.42 ± 0.16 [a]	3.01 ± 0.48 [b]	<0.001
total mean PSP 2011 vs 2012		1.43 ± 0.12 [a]		2.22 ± 0.25 [b]		0.005

Bacteria		mean PSP				
Phylum	OTUs	Day 2011	Night 2011	Day 2012	Night 2012	significance
Acidobacteria	6	0.21 ± 0.08 [a]	0.14 ± 0.07 [a]	2.57 ± 0.90 [b]	1.04 ± 0.24 [b]	0.001
Actinobacteria	6	0.66 ± 0.19	0.58 ± 0.23	6.05 ± 3.16	0.40 ± 0.19	> 0.05
Bacteroidetes	62	1.35 ± 0.39[ab]	0.77 ± 0.22 [a]	3.88 ± 1.37 [b]	1.30 ± 0.17 [ab]	<0.001
Chloroflexi	3	0.07 ± 0.05	0.04 ± 0.02	0.91 ± 0.38	0.62 ± 0.29	>0.05
Cyanobacteria	32	2.44 ± 0.41 [a]	2.13 ± 0.25 [ab]	0.85 ± 0.26 [b]	1.74 ± 0.45 [ab]	0.01
Deferribacteres	3	0.00 ± 0.00 [a]	0.00 ± 0.00 [a]	5.53 ± 2.58 [b]	2.27 ± 0.96 [ab]	0.01
Deinococcus-Thermus	2	1.39 ± 0.57	1.09 ± 0.37	3.20 ± 2.10	0.16 ± 0.07	>0.05
Firmicutes	1	0.00 ± 0.00 [a]	0.00 ± 0.00 [a]	0.26 ± 0.16 [a]	5.27 ± 2.38 [b]	0.01
Lentisphaerae	5	1.13 ± 0.51	0.55 ± 0.24	2.90 ± 0.97	2.09 ± 1.27	>0.05
Planctomycetes	37	0.42 ± 0.08 [a]	0.41 ± 0.07 [a]	3.28 ± 0.46 [b]	1.79 ± 0.31 [c]	<0.001
Proteobacteria	146	0.97 ± 0.10 [a]	1.29 ± 0.16 [a]	2.76 ± 0.31 [b]	1.39 ± 0.16 [a]	< 0.001
Alphaproteobacteria	50	0.85 ± 0.13 [a]	1.34 ± 0.35 [ab]	2.37 ± 0.41 [bc]	1.02 ± 0.16 [bd]	0.01
Deltaproteobacteria	75	0.98 ± 0.16 [a]	1.15 ± 0.15 [a]	3.33 ± 0.52 [b]	1.65 ± 0.28 [a]	<0.001
Gammaproteobacteria	12	0.82 ± 0.22	0.93 ± 0.28	1.91 ± 0.57	1.13 ± 0.40	>0.05
Unclassified	9	1.65 ± 0.51	2.61 ± 0.89	1.27 ± 0.30	1.70 ± 0.54	>0.05
Spirochaetes	25	0.94 ± 0.43 [a]	0.86 ± 0.31 [a]	2.22 ± 0.37 [b]	0.56 ± 0.16 [a]	0.002
unclassified	49	0.14 ± 0.04 [a]	0.16 ± 0.67 [a]	4.70 ± 0.74 [b]	1.28 ± 0.24 [a]	<0.001
Verrucomicrobia	3	0.00 ± 0.00 [a]	0.00 ± 0.00 [a]	7.53 ± 3.71 [b]	2.55 ± 0.78 [ab]	0.02
total mean PSP	380	0.90 ± 0.08 [a]	1.10 ± 0.08 [a]	3.09 ± 0.26 [b]	1.33 ± 0.08 [a]	<0.001
total mean PSP 2011 vs 2012		0.98 ± 0.06 [a]		2.13 ± 0.13 [b]		<0.001

Table 3.4. Archaea class summary shows summed 16S rRNA gene abundances of OTUs based on class level taxonomic classification with standard deviations.

Phylum	Class	DNA day11	DNA night11	DNA day12	DNA night12
Thaumarchaeota	unclassified	0.92±0.01	0.01±0.2	0.2±0	0±3.38
Crenarchaeota	MCG	0.04±0	0	0	0±0.98
	unclassified	0.1±0	0	0	0±4.35
	uncucltured	0.04±0	0	0	0±1.37
Euryarchaeota	Halobacteria	40.73±0.11	0.11±50.69	50.69±0.12	0.12±29.9

Methanomicrobia	0.02±0	0±0.02	0.02±0	0±0.2
Thermoplasmata	30.59±0.06	0.06±28.3	28.3±0.09	0.09±46.36
unclassified	19.02±0.03	0.03±14.08	14.08±0.04	0.04±8.29
uncucltured	4.32±0.02	0.02±1.99	1.99±0.01	0.01±0.62

Table 3.5. Bacteria phyla and class summary shows summed 16S rRNA gene abundances of OTUs based on class level taxonomic classification with standard deviations.

Phylum	DNA Day2011	DNA Night 2011	DNA Day 2012	DNA Night 2012
Acidobacteria	0.2±0.06	0.06±0.19	0.19±0.08	0.08±1.69
Actinobacteria	1.33±0.33	0.33±1.22	1.22±0.53	0.53±1.81
Bacteroidetes	32.75±3.58	3.58±33.57	33.57±3.31	3.31±7.57
Candidate_division_BRC1	0.28±0.15	0.15±0.15	0.15±0.05	0.05±1.66
Chloroflexi	9.66±1.22	1.22±9.83	9.83±0.92	0.92±9.66
Cyanobacteria	7.66±0.95	0.95±7.64	7.64±1.25	1.25±13.76
Deferribacteres	0.06±0.06	0.06±0.05	0.05±0.04	0.04±0.28
Deinococcus-Thermus	0.14±0.09	0.09±0.14	0.14±0.06	0.06±0.44
Firmicutes	0	0	0	0
Gemmatimonadetes	0	0	0.04±0.02	0.02
Lentisphaerae	0.11±0.05	0.05±0.09	0.09±0.05	0.05±0.51
Planctomycetes	5.57±0.53	0.53±5.24	5.24±0.68	0.68±5.05
Alphaproteobacteria	20.12±1.53	1.53±20.74	20.74±1.87	1.87±21.45
Deltaproteobacteria	10.72±0.96	0.96±9.55	9.55±0.89	0.89±11.08
Gammaproteobacteria	2.58±0.46	0.46±2.56	2.56±0.49	0.49±8.6
Proteobacteria	0.98±0.21	0.21±1.04	1.04±0.2	0.2±3.85
Spirochaetes	5.31±0.72	0.72±5.77	5.77±0.57	0.57±3.56
unclassified	1.3±0.55	0.55±1.22	1.22±0.46	0.46±6.12
Verrucomicrobia	0.58±0.2	0.2±0.49	0.49±0.15	0.15±0.58

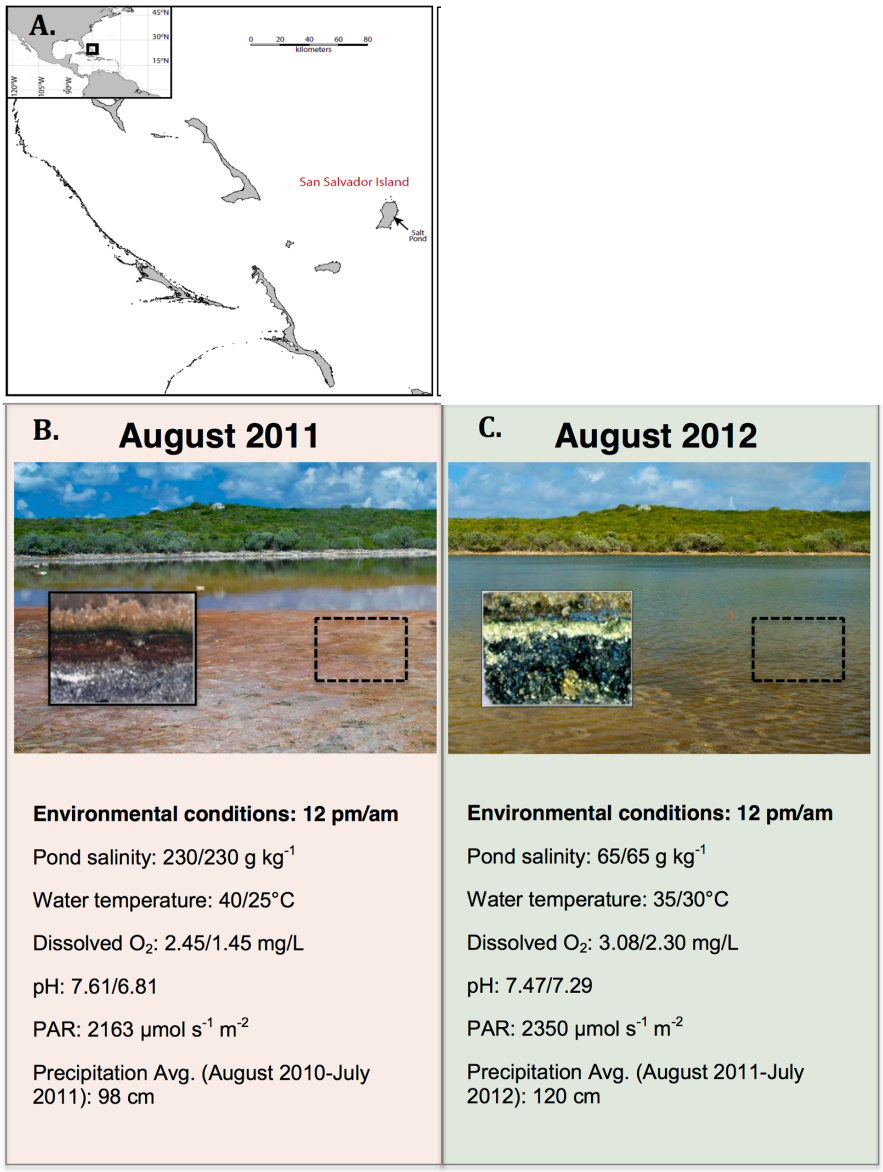

Figure 3.1. Overview of Sample Site. (**A**) Map of the Salt Pond sample site on San Salvador Island, The Bahamas. (**B** and **C**) Photographs of Salt Pond in August 2011 and August 2012 with sampling area indicated by the dashed box. Insets show an approximately 2.5 cm microbial mat crosssection. Day and night environmental conditions of Salt Pond in August 2011 and August 2012 are listed below the photographs.

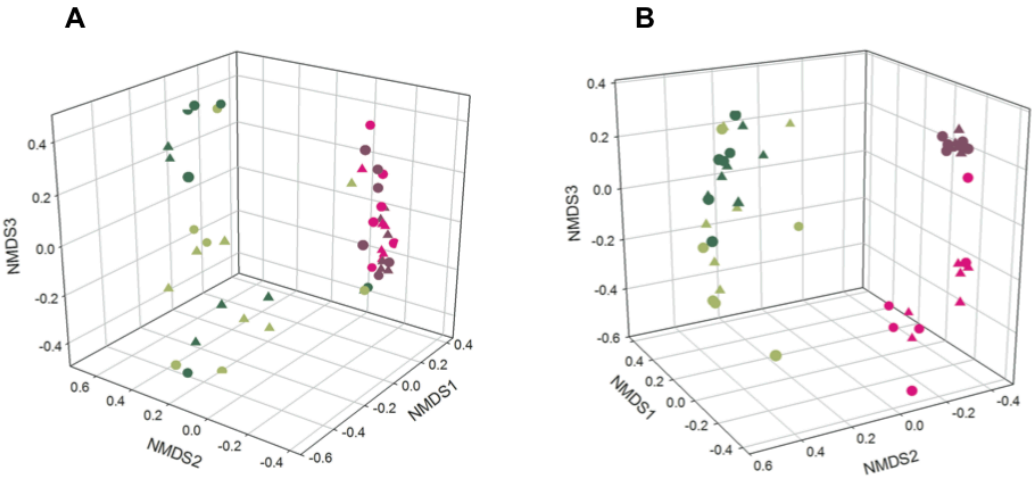

Figure 3.2. Non-parametric multidimensional scaling (NMDS) plots showing salinity-driven spatial separation of **A**) Archaea and **B**) Bacteria day (n_{day}= 6) and night (n_{night}=6) samples from 2011 and 2012. Purple: 2011 16S rRNA genes, pink: 2011 16S rRNA. Dark green: 2012 16S rRNA genes, light green: 2012 16S rRNA. Circles: day samples; triangle: night samples.

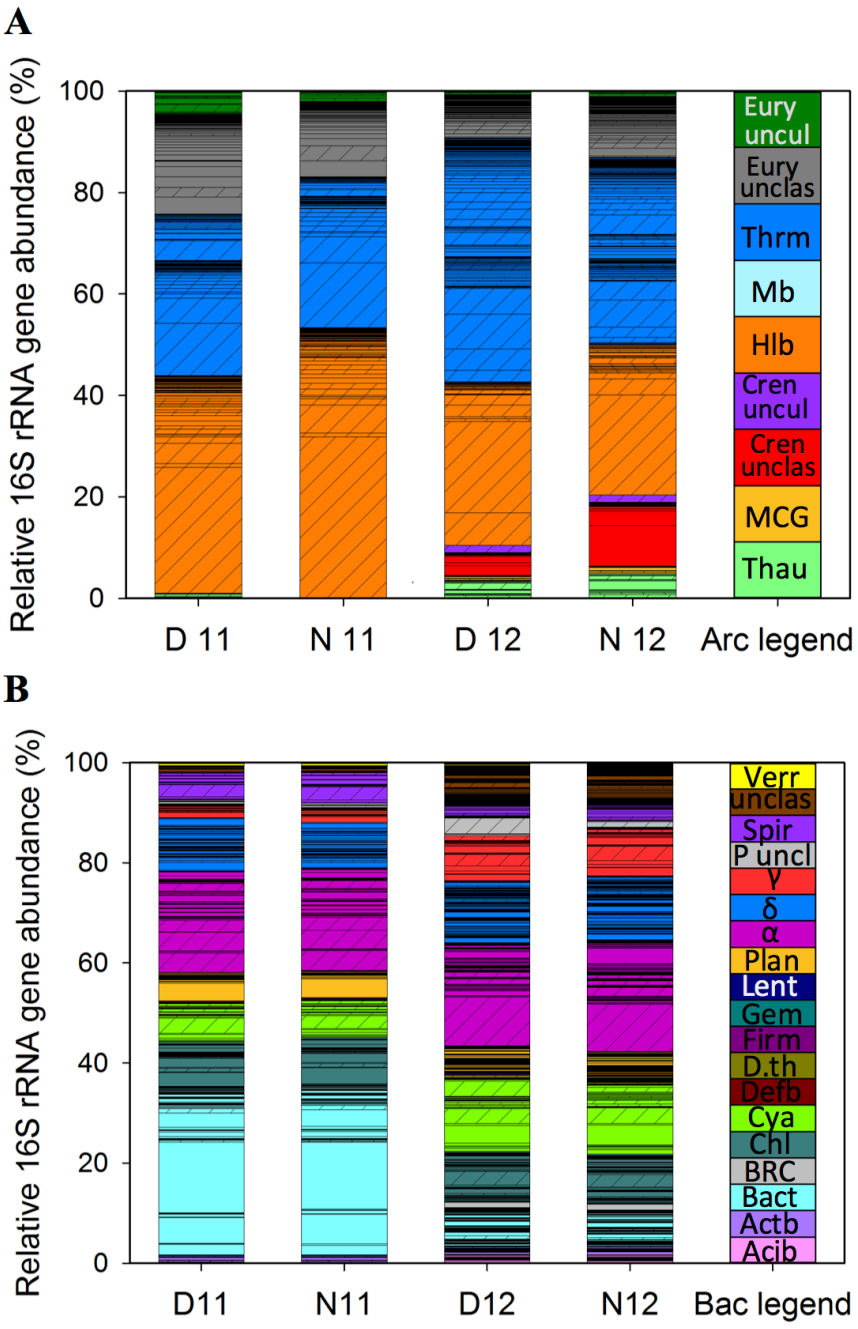

Figure 3.3. Stacked bar charts of microbial mat community profiles for Archaea (**A**) and Bacteria (**B**) based on relative 16S rRNA gene abundance of operational taxonomic units (OTUs) sorted by phylogenetic classification during day and night under high (2011) and lower salinity (2012). Bars represent the average (n = 6) relative 16S rRNA gene abundance of each OTU under the following conditions: D11, day 2011; N11, night 2011; D12, day 2012; N12, night 2012. Standard deviations for OTUs based on class level taxonomic classification are located in the Table 4 and 5. Cross hatched bars represent OTUs present under both salinities. Phylogenetic classification was made with

Silva archaea or bacteria reference files using the 16S rRNA gene MiSeq sequencing data. (**A**): Thau, Thaumarchaeota; MCG, Miscellaneous Crenarchaeotic Group; Cren unclas, Crenarchaeota unclassified; Halo, Halobacteria; Mb, Methanobacteria; Thrm, Thermoplasmata; Eury unclas, Euryarchaeota unclassified; Eury uncul, Euryarchaeota uncultured. (**B**): Acib, Acidobacteria; Actb, Actinobacteria; Bact, Bacteroidetes; BRC1, Bacteria Candidate division BRC1; Chl, Chloroflexi; Cya, Cyanobacteria; Defb, Deferribacteria; D.th, Deinococcus Thermus, Firm, Firmicutes; Gem, Gemmatimonadetes, Lent, Lentisphaerae; Plan, Planctomycetales; α, Alphaproteobacteria, δ, Deltaproteobacteria; γ, Gammaproteobacteria; P uncl, Proteobacteria unclassified; Spiro., Spirochaetales; unclas, Bacteria unclassified; Verr, Verrucomicrobia.

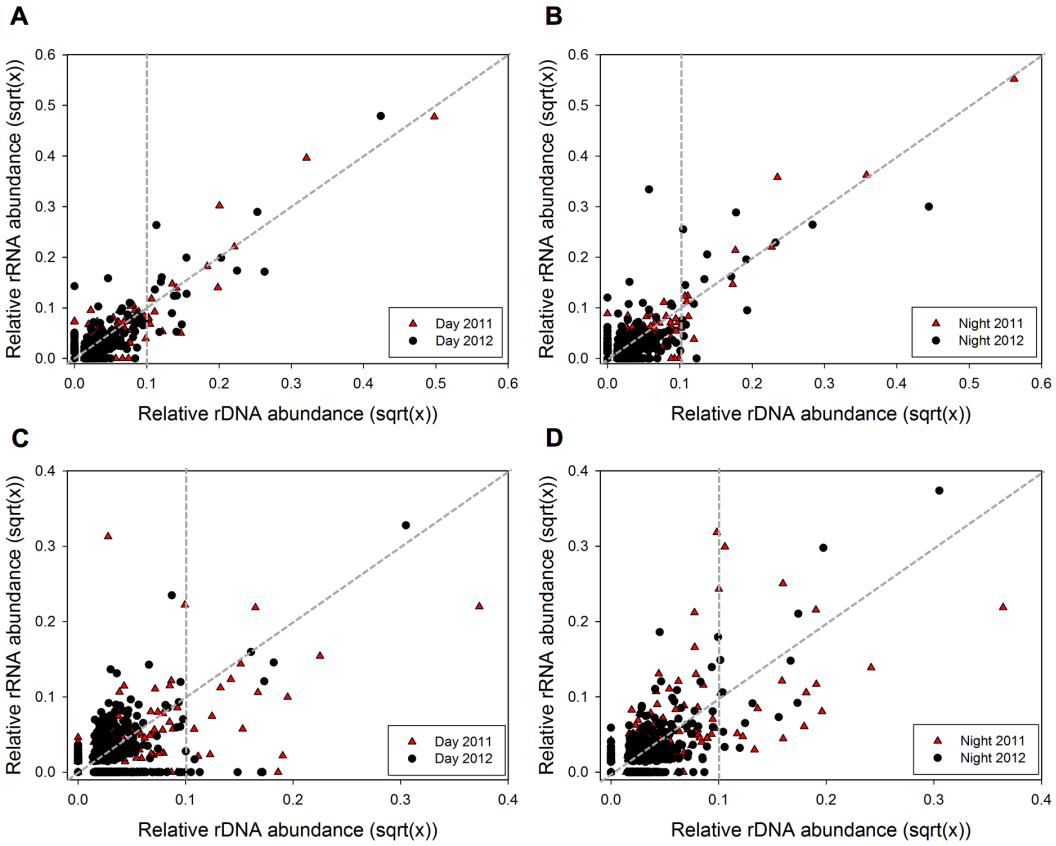

Figure 3.4. Relationship between rRNA and rDNA abundance for each OTU defined by 16S rRNA and 16S rRNA gene MiSeq sequencing dataset for subsampled communities comparing 2011 (black) and 2012 (red). Archaeal (**A**) day ($n_{day}2011$= 277, $n_{day}2012$= 330) and (**B**) night ($n_{night}2011$= 249, $n_{night}2012$= 367); and bacterial (**C**) day ($n_{day}2011$= 372, $n_{day}2012$= 697), and (**D**) night ($n_{night}2011$= 347, $n_{night}2012$= 621). Data points in graph are square root transformed paired relative rRNA and rDNA abundances for each OTU. Vertical gray dashed line differentiates between rare and abundant OTUs (rare <

0.1%, abundant > 0.1% rDNA abundance). Data points above and below the 1:1 line represent OTUs with higher and lower PSP, respectively.

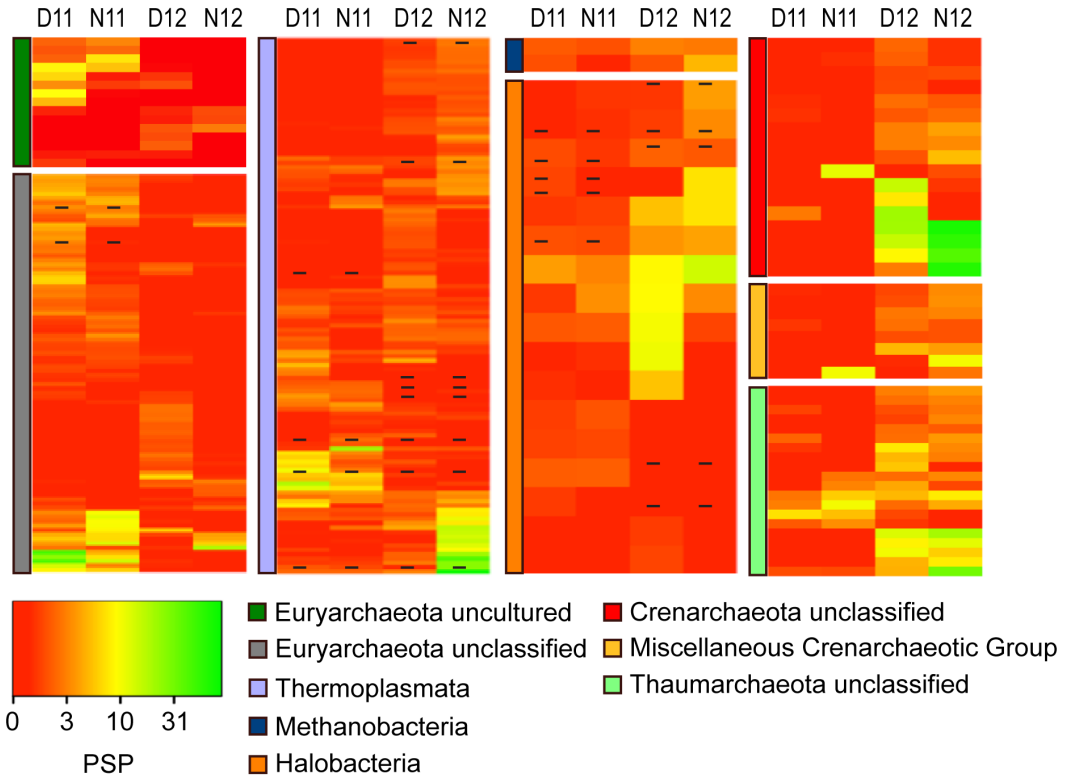

Figure 3.5. Heatmap analysis of OTU PSP for each archaeal class for day and night samples across years (D11, Day 2011; N11, Night 2011, D12, Day 2012; N12, Night 2012). The heatmap color represents the extent of protein synthesis potential (PSP) as measured by rRNA: rDNA ratio for each OTU. Square colors shifted toward brighter green indicate higher PSP of that OTU. Dash within squares indicates abundant OTUs. Standard deviations are located in Table 3.

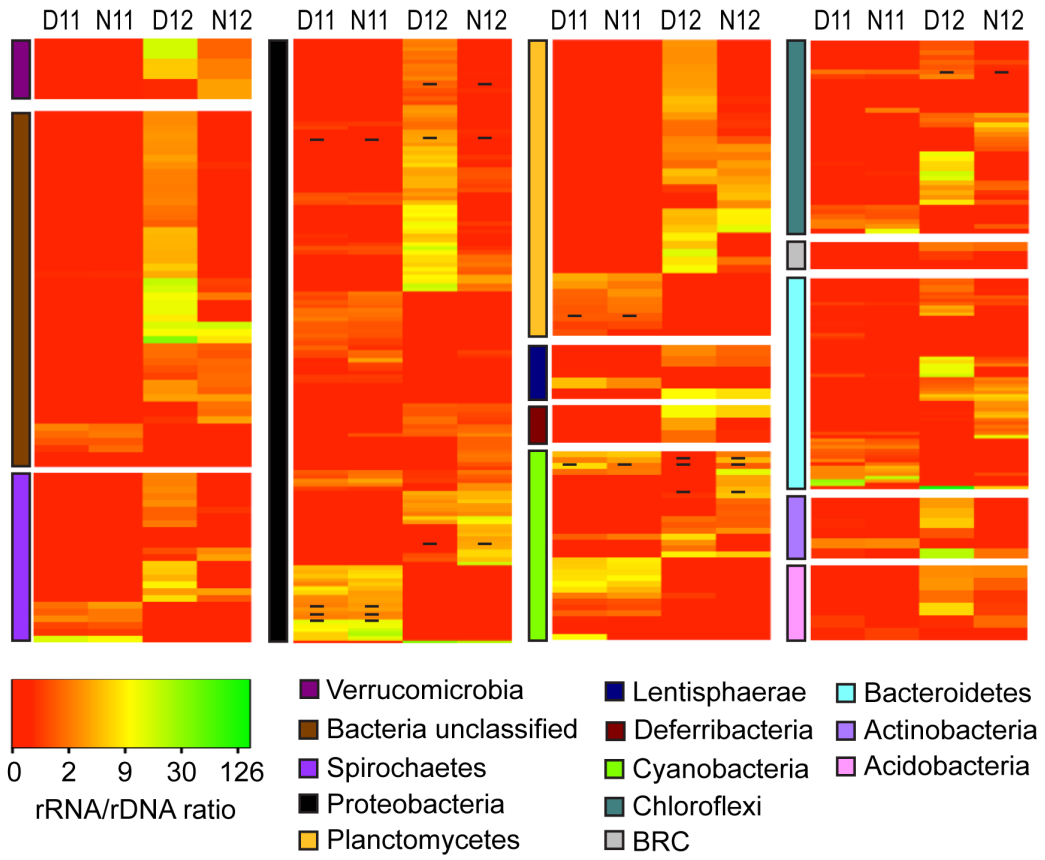

Figure 3.6. Heatmap analysis of OTU PSP for each bacterial phylum for day and night samples across salinities (D11, Day 2011; N11, Night 2011; D12, Day 2012; N12 Night 2012). The heatmap color represents the extent of PSP as measured by rRNA:rDNA ratio within each OTU. Square colors shifted toward brighter green indicate higher PSP of that OTU. Dash within squares indicates abundant OTUs. Standard deviations are located in Table 3.

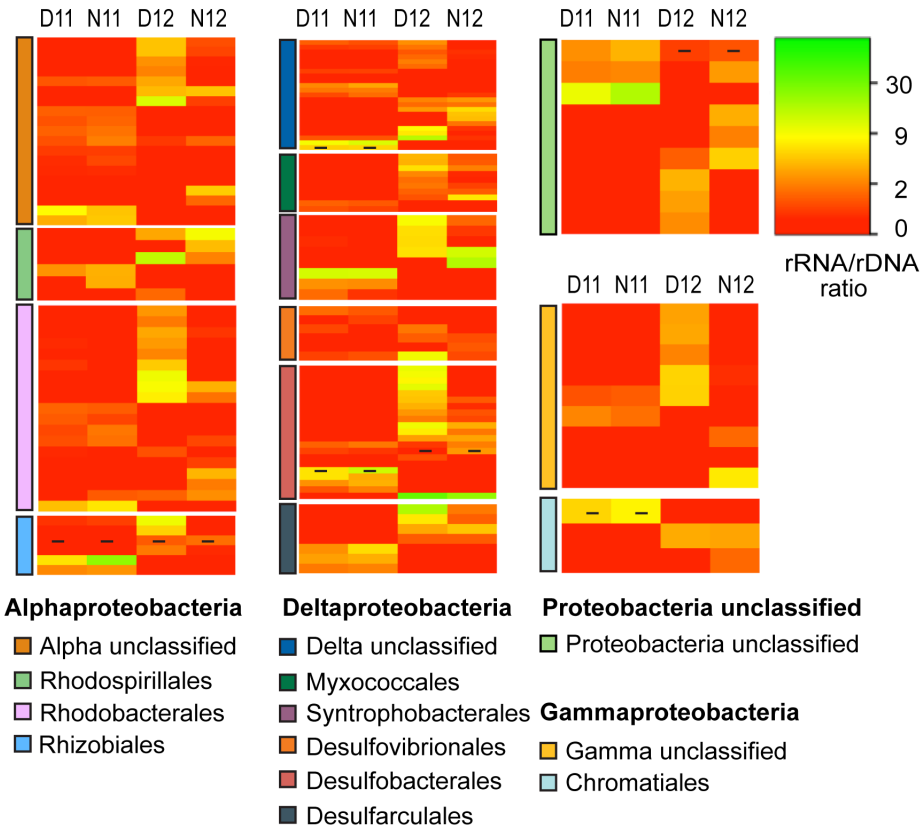

Figure 3.7. Heatmap analysis of OTU PSP for each proteobacterial order for day and night samples across salinities (D11, Day 2011; N11, Night 2011; D12, Day 2012; N12 Night 2012). The heatmap color represents the extent of PSP as measured by rRNA: rDNA ratio within each OTU. Square colors shifted toward brighter green indicate higher PSP of that OTU. Dash within squares indicates abundant OTUs. Standard deviations are located in Table 3.

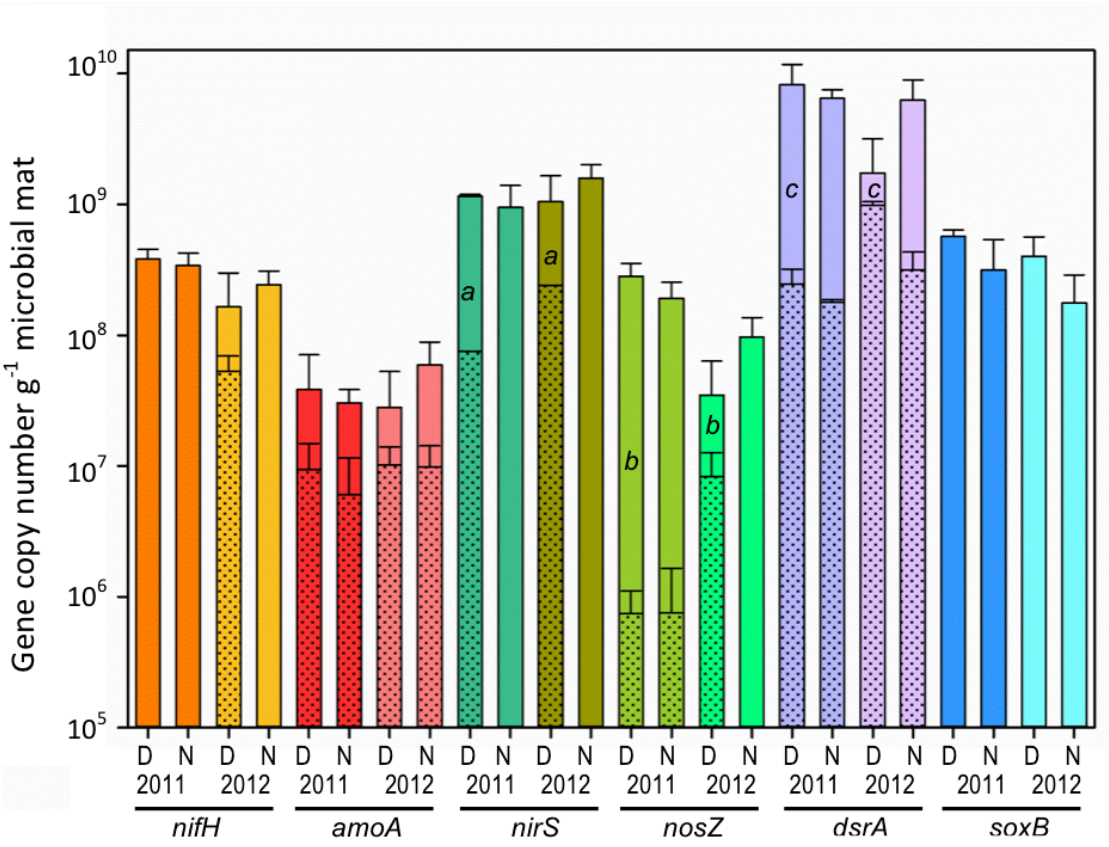

Figure 3.8. Microbial mat community potential for biogeochemical cycling as determined by qPCR amplification of genes (DNA) and transcripts (cDNA) involved in nitrogen and sulfur cycling for day (D) and night (N) samples during 2011 (11) and 2012 (12) (n = 6). Nitrogen cycling genes/transcripts analyzed: nitrogen fixation (*nifH*), archaeal nitrification (*amoA*), and denitrification (*nosZ*, and *nirS*). Sulfur cycling genes/transcripts analyzed: sulfate reduction (*dsrA*) and sulfide oxidation (*soxB*). Shaded areas within solid bars represent transcript abundance (no shade indicates that transcripts were not detected). Different lower case letters indicate significantly different cDNA/DNA ratios across years (independent t-test, $p < 0.05$).

CHAPTER 4

LONG-TERM RESILIENCE OF A MICROBIAL MAT ECOSYSTEM TO SEASONAL AND PULSE-DISTURBANCES

4.1. Introduction

Ecosystem disturbances have been shown to directly change microbial community structure and composition (Shade *et al.*, 2012a; Preisner *et al.*, 2016). Understanding microbial community traits and their behavior in disturbed environments or after disturbance events is crucial, as they are the foundation of ecosystems and impact the sustainability of food webs. Gradual (press) and sudden (pulse) changes in natural conditions as well as the character of disturbance (e.g. fire, storm, etc.), affect microbial communities in different ways (Berga *et al.*, 2012). Microbial communities displayed some form of resistance, as measured by the unchanged composition of sediment microbial communities, to an artificially induced disturbance event (Bowen *et al.*, 2011). Other microbial communities showed resilience in their community composition to a disturbance event, by which a lake water column was artificially mixed (Shade *et al.*, 2012b). The effects of natural disturbances, such as fires (Cutler *et al.*, 2017; Lee *et al.*, 2017) or hurricanes (Yannarell *et al.*, 2007; Amaral-Zettler *et al.*, 2008; Balmonte *et al.*, 2016; Preisner *et al.*, 2016) on microbial communities have been studied in different ecosystems. Results from these studies point out that microbial communities are sensitive and have low resistance to natural disturbances, as indicated by relatively quick change

in community composition. The altered microbial community may subsequently lead to temporal changes in ecosystem function. Studies including ecosystem function when assessing disturbances showed that there were more types of responses as when just studying compositional changes (Marxsen *et al.*, 2010; Reed and Martiny, 2007). Depending on the type of microbial ecosystem, its function can be measured by assessing the rate of respiration when interested in mineral cycling (Prosser, 1997), or measuring the abundance of targeted functional genes (Bowen *et al.*, 2014; Preisner *et al.*, 2016). Some studies showed that ecosystem function is not concomitantly shifting with microbial community composition after disturbance, so the community may be functionally redundant where there is a replacement of microbial taxa with new species that are carrying out the same function (Müller *et al.*, 2002; Wertz *et al.*, 2007). In some instances the microbial community may remain the same but ecosystem functions change after the disturbance and may return to its original state or remain altered (Agrawal, 2001). This complex community composition – function relationship does not follow a pattern and depends on the level of the studied function and ecosystem type (Comte and del Giorgio, 2009; Severin *et al.*, 2014). The rate at which an ecosystem then returns to its pre-disturbed state, the ecosystem resilience (Pimm, 1984), is difficult to measure in natural ecosystems and most often requires long-term studies in natural ecosystems (Allison and Martiny, 2008). Our current understanding of how large-scale disturbances such as hurricanes or tropical storms affect microbial ecosystems is still limited and requires more research. A few studies that have investigated typhoon, hurricane and larger storm disturbance event showed varying types of responses in the microbial ecosystem. After typhoon events Jones (Jones *et al.*, 2008) found that the microbial lake

community was resilient to the disturbance and consistently returned to its pre-disturbed composition. Another study found that after a large storm event, the coastal bacterioplankton community composition only differed in four out of thirteen sites, suggesting resistance to the disturbance (Yeo *et al.*, 2013). Studies investigating the microbial community of floodwaters found a distinct and highly diverse microbial community after two hurricanes (Sinigalliano *et al.*, 2007; Amaral-Zettler *et al.*, 2008). In a riverine ecosystem, disturbance signatures of previously undetected taxa of diverse origins were detected after impacted by Hurricane Irene, and suggests that ecosystem functioning was enhanced post hurricane (Balmonte *et al.*, 2016). Similar findings were revealed in a complex microbial mat ecosystem post hurricane disturbance, where community composition shifted and ecosystem functioning and protein synthesis potential were significantly enhanced (Preisner *et al.*, 2016). Although these studies provide insight into community response to a disturbance, more investigations are necessary to understand microbial ecosystem resistance, stability, functioning and resilience to large-scale disturbances over time.

In this study we monitored a hypersaline lagoon ecosystem that harbors complex microbial mat communities through seasonal and pulse disturbances over the course of four years to better understand community resistance, stability, function, and resilience in a natural ecosystem. Changes in salinity caused by precipitation or evaporation of the water column of hypersaline lagoons act as a natural disturbance to microbial communities in microbial mats because it changes the complex ecosystem including chemical gradients of the water column, turbidity, and predatory pressure, all factors known to shape those microbial communities (Pinckney *et al.*, 1995; Canfora *et al.*,

2014). Salinity has been shown to directly influence the size and activity of the microbial community, due to changes in nutrient and water availability for the ecosystem, thus impacting biogeochemical cycling in the ecosystem (Steppe *et al.*, 2001; Rietz and Haynes, 2003; Tripathi *et al.*, 2005; Pinckney *et al.*, 2011). In addition to altering the salinity, hurricanes or stronger tropical storms also have the potential to deposit sand from the dunes on the microbial mat surface resulting in a disturbance to the ecosystem. Since microbial mats contain tightly coupled biogeochemical processes along a narrow vertical chemical gradient often occurring within the first 10 mm of microbial mats (Pinckney *et al.*, 1995; Woebken *et al.*, 2015) they provide a unique system to study the complex community dynamics that follow disturbances. Due to the vertical chemical gradient within the mat we examined perturbation-induced changes to the microbial mat community diversity and relative abundance at vertical millimeter scale using a metagenomic approach. By targeting functional genes, involved in biogeochemical cycling of the ecosystem (nitrogen and sulfur cycling) the change of ecosystem functioning was assessed through seasonal and pulse disturbances. Together with correlation analysis of metadata and vertical elemental composition of the microbial mat over time, this combination of methods provides a robust assessment of the microbial community response (resistance and stability), ecosystem functioning, and resilience to perturbation.

4.2. Materials and Methods

4.2.1. Sample and Metadata Collection

Microbial mat samples were collected over the course of four years from 2013-2016 (see Table 4.1 for details), with at least one sampling point within the yearly wet-

and one sampling point within the dry season. Microbial mat samples were taken at noon and at midnight at each time point, together with measurements of temperature (air and water), salinity, pH, and dissolved oxygen (DO) in pond water, as well as photosynthetic active radiation (PAR) in the water column and on the surface of the microbial mats, and the PAR diffuse attenuation coefficient for downward irradiance was calculated using the Beer-Lambert Law equation. Microbial mat cores with a small core device (diameter 1 cm), the first 4 millimeters (referring to layers 1-4) of the core were then sliced with a razor blade into 1 mm slices, while the deeper layer 5 contained 3 mm of the mat core. Mat slices were then transferred into separate cryogenic vials filled with 2 ml of RNAProtect Bacteria Reagent (QIAGEN). A total of eight slices were pooled for each layer (~ 1 g, surface area of 39.5 cm^2), and four replicates were collected. Samples in RNA protect were homogenized with a sterile RNase-free glass rod. For elemental analysis, three replicates of sectioned microbial mat (layer 1-5) were collected as described above and stored in cryogenic vials and stored at -80˚C until further processing. For water quality analysis, three replicates of approximately 50 ml of pore and pond water were collected in 50 ml syringes and filtered through a 0.22 µm EMD Millipore Sterivex Sterile Pressure-Driven Devices (Fisher Scientific) into acid washed and muffled amber vials (15 ml) and subsequently acidified with a 10N HCl to reach a pH <3, for dissolved carbon analysis.

4.2.2. Elemental Analysis of Microbial Mat

For elemental analysis (P, S, Al^{27}, As^{75}, Ba^{138}, Be^{9}, Ca^{43}, Cd^{111}, Co^{59}, Cr^{52}, Cu^{63}, Fe^{56}, Fe^{57}, K^{39}, Mg^{24}, Mn^{55}, Mo^{88}, Na^{23}, Ni^{60}, Pb^{208}, V^{51}, Zn^{66}), microbial mat samples were first freeze dried overnight, then 100 ± 0.05 mg of microbial mat were added to an

acid washed 15 ml polypropylene centrifuge tube (VWR) and digested overnight in a mixture of 2 ml nitric acid (OPTIMA grade, Fisher Scientific) and 0.5 ml hydrogen peroxide (OPTIMA grade, Fisher Scientific). Samples were filtered through an acid washed 0.2 µm Teflon syringe filter (17 mm, National Scientific) and diluted with ultrapure water to 1.144 mg ml^{-1}. An aliquot of 0.1% (10 ppb) internal standard mix (PerkinElmer pure plus Atomic Spectroscopy standard, PerkinElmer Life and Analytical Sciences, Connecticut) was added to each sample. Ultrapure water blank was prepared and processed in the same manner as the samples. A PerkinElmer NexION® 350D inductively coupled mass spectroscopy (ICP-MS) was used, equipped with the Syngistix™ Nano Application Software Module for the following elements Al^{27}, As^{75}, Ba^{138}, Be^{9}, Ca^{43}, Cd^{111}, Co^{59}, Cr^{52}, Cu^{63}, Fe^{56}, Fe^{57}, K^{39}, Mg^{24}, Mn^{55}, Mo^{88}, Na^{23}, Ni^{60}, Pb^{208}, V^{51}, Zn^{66}, and an ICP optical emission spectrometry (ICP-OES) for analyzing S and P.

4.2.3. Metagenomic library preparation, sequencing, and quality assessment

For preparation of shotgun sequencing libraries, all DNA samples were first quantified with a Qubit 2.0 fluorometer (Life technologies, Grand Island, NY, USA) and day and night samples were combined in a 1:1 concentration ratio. An aliquot containing 250 ng of each sample was sheared to approximately 400 bp using a CovarisTM under the following parameters: Methods, Frequency sweeping, and 11 cycles of 10% duty cycle, level 4 intensity, and 200 cycles per bursts. Successful shearing was monitored using the High Sensitivity DNA Analysis Kit on the Agilent 2100 Bioanalyzer (Agilent Technologies, Santa Clara, CA, USA). The library preparation protocol followed that

described in the NEBNext® UltraTM DNA Library Prep Kit for Illumina® (New England BioLabs Inc., Ipswich, MA, USA) including a left and right side size selection around 400bp after the adapter ligation step using the SPRIselect beads (Beckman Coulter, Brea, CA, USA). The PCR enrichment step was done using the NEBNext Index Primers for Illumina, and a second right side size selection step was done with the SPRIselect beads targeting a size of 400 bp. A subsequent High Sensitivity DNA Analysis Chip was run on the Agilent 2100 Bioanalyzer and after smear analysis, the average size and concentration of the sample peak was determined. An aliquot of 15 $ng*ul^{-1}$ of each sample was combined for an Illumina MiSeq sequencing run. Following the dilutions recommended in Protocol A of the MiSeq System Denature and Dilute Libraries Guide (Illumina) the library was diluted to 4 nM. After denaturation of the 4 nM library with 0.2N NaOH the library was diluted to 17 pM and an additional heat denaturation step at 97˚C was done in a heat block after which the samples were immediately transferred onto ice. Before loading onto the sequencer all libraries were spiked with 1% Illumina PhiX control.

4.2.3. Metagenomic and statistical analysis

For an overview of the metagenomic workflow see Figure 4.1. Raw Illumina MiSeq sequence reads were imported into CLC genomics workbench 7.0.4 (QIAGEN). Illumina sequencing adapters were trimmed off and paired end and single end files were created. Using bbmap v36.85 (Bushnell, 2015) paired end and single end files were trimmed (ktrim=r, k=23, mink=11, hdist=1, tpe, tpo, qtrim=r, trimq=20, maq=20, entropy=0.8, minlen=100) and any sequences matching the phiX internal standard were removed from sequence files (k=31, hdist=1). Fastq files were converted to fasta format

using the FASTX-Toolkit v0.14 (http://hannonlab.cshl.edu/fastx_toolkit/) and information of the number of sequences in each file was obtained. To maximize time efforts, fasta files were split into files containing no more than 99,000 sequences and each individual file was searched against the 16S SILVA database (Quast *et al.*, 2013) using BLASTn (States and Gish, 1994). Those sequences matching the 16S SILVA database with a bit score greater than 50 were parsed from all non-hit sequences, and the split files were merged to contain only sequences with hits to the 16S SILVA database. Single-end and paired-end hit files of one sample were merged. Relative abundance of Archaea and Bacteria phyla was calculated for each sample. For the implementation of statistical analyses various packages in R (R Development Core Team, 2015) were used. Alpha diversity index, Shannon-Weaver, and species richness were calculated for each time point using the vegan package (Dixon, 2003) in R. A one-way Analysis of Variance (ANOVA, $p<0.05$) and Tukey's post hoc test was used to calculate significant ($p<0.05$) differences between alpha diversity and species richness of the different layers. Significant changes in phyla abundance were calculated between the layers (ANOVA and Tukey's post hoc test, $p<0.05$). Bray-Curtis distances were used to construct the dissimilarity matrices for microbial community composition of each layer. Permutational multivariate analysis of variance (Adonis function) was conducted to test the statistical significance of difference between the eight time points for each individual layer (vegan 2.3-0). The metaMDS function for the calculated Bray-Curtis dissimilarities was used and plotted (see Figure 4.5). In R, a one-way ANOVA ($p<0.05$) was conducted for each individual layer to compare the mean abundance of each phylum across time points. Tukey's post hoc test was used to calculate significant ($p<0.05$) differences between the

time points with 95% confidence intervals. For the phyla of Euryarchaeota and Proteobacteria abundance for class level were calculated.

For de novo reference assembly, overall metagenomic reads (from all samples) were assembled using MEGAHIT (Li *et al.*, 2015) with the meta-sensitive setting (k-mer values 21 ,31 ,41 ,51 ,61 ,71 ,81 ,91 ,99). Evaluation of assembly quality was done with MetaQuast (Mikheenko *et al.*, 2016) and genes were predicted using Prodigal (Hyatt *et al.*, 2010). For further check of quality of assembly, Bbmap (Bushnell, 2015) was used to map sequences from each time point to the overall assembly. To analyze significant changes in abundance (2 fold, FDR $p<0.05$) of genes of the different layers over time, the exact test in EdgeR Bioconductor package in CLC Genomics was used. The reads per kilobase million (normalizes for sequencing depth and length of the gene) for each prodigal called gene was used for analysis. The contigs from the overall metagenome were searched against the NR using BLASTn and subsequently parsed based on classification of the lineage (Archaea, Bacteria, Eukaryotes, Virus) for an overview of the relative percentage of bases belonging to each lineage of the overall metagenome and visualized using Krona plots (Ondov *et al.*, 2013).

To identify Archaea and Bacteria genes and their functions, reads were functionally annotated using the eggNOG-mapper (EggNOG 4.5.1) with the DIAMOND mapping mode against the Clusters of Orthologous Groups (COG) protein database. COG category counts were converted into percent and visualized in Krona plots (Ondov *et al.*, 2013) to depict different COG group levels in concentric circles. To gain insights into the different functional capacity of the archaeal metagenomes over time, Statistical Analysis of Metagenomic Profiles (STAMP, version 2.1.3 (Parks *et al.*, 2014)) was used to

compare abundances (based on RPKM values of each gene, n=3) of COG categories between the samples. Significant differences in abundance were identified using the multiple group statistic test (ANOVA, $p<0.01$) and post-hoc test (Tukey-Kramer) with effect size (eta-squared) and subsequently visualized using Box plots to provide a more concise summary of the distribution of proportions within a group.

4.3. Results

4.3.1. Sampling site monitoring and metadata analysis over the time period of the study

Over the course of four years (August 2013 – July 2016) Salt Pond was studied over eight time points (Figure 4.2A), with water levels of the Pond varying (Table 4.1) from no water covering the sampling site to 69 cm overlaying water post Hurricane event (December 2015). During the two time points (July 2014 and September 2015) where no water covered the microbial mat, the mat itself was not desiccated and pore water was extractable from the mat. Sampling time points were chosen based on the season (dry and wet season in Spring and Summer, respectively) with one pulse disturbance event where sampling was carried out before Hurricane Joaquin (September 2015) and three months post Hurricane (December 2015) when the infrastructure on the Island was rebuild and the research station opened. Regardless of the season, salinity of the pond water varied from as low as 46 g kg^{-1} in August 2013 up to 305 g kg^{-1} in September 2015. Three wet season time points (July - September) showed salinities above 100 g kg^{-1}, and three dry season time points (December – April) had salinities close to 50 g kg^{-1}. August 2013 and

April 2015 were exceptions, with August 2013 being closer to 50 g kg^{-1} and April 2015 showing salinities over 100 g kg^{-1}.

Air temperatures in the wet season (July - September sampling points) were on average 4.67°C higher as compared to the dry season (December – April time points), while pond water temperature was an average of 9°C higher in the wet season (Table 4.1).

According to Wetzel (Wetzel, 2001) dissolved oxygen, the amount of unbounded O_2 molecules in the water column is directly depended on the temperature and salinity of the water as well as the overlaying atmospheric pressure. Over the course of the study, we found that dissolved oxygen directly measured above the microbial mat was strongly negative correlated with both, salinity and temperature of the water column (Pearsons correlation, $p<0.01$; salinity cor= -0.89; temperature cor = -0.82). Increased temperature and salinity decreased the dissolved oxygen concentrations in the pond water (Figure 4.2). Light penetration and availability in the water column of the pond have great importance for the microbial mat photosynthetic community. Photosynthetic active radiation (PAR) measurements were used to calculate the attenuation coefficient (K_d) to estimate water turbidity and the amount of PAR reaching the mat (Table 4.1). K_d was found to vary significantly between the time points. The highest K_d values were obtained when the water column was relatively shallow (12 and 19 cm for April 2015 and July 2016, respectively) but had high salinities.

When comparing pore and pond water dissolved organic carbon (DOC), we found that pore water DOC was higher than pond water DOC, however, at salinities >150 g kg^{-1}, pond water DOC increased and was significantly higher ($p<0.01$) than concentrations

in pore water (Figure 4.4). For the time point of March 2016, where the salinity remained the same as compared to previous time point, pore water DOC was significantly lower ($p<0.01$) than pond water DOC, however there was an overall linear increase in pore water DOC post Hurricane – July 2016. Other pore and pond water comparisons (see Table 4.1) included pH, which was always significantly higher ($p<0.01$) in pond water as compared to pore water, except for the highest salinity time point of September 2015, where there was no significant difference between the two values. When comparing the nutrients (Figure 4.5) between pore and pond water, we found that concentrations of all three nutrients tested (Phosphorous, Ammonia, and Nitrate) were significantly elevated in pore water, suggesting that cycling of nutrients occur at higher rates within the mats and do not diffuse into the pond water. Ammonia concentrations in pore water were positively correlated with pond water salinity up until September 2015, after the hurricane event in December 2015 and March 2016 ammonia concentrations were twice as high as compared to the pre- hurricane time point (Figure 4.5). Concentrations of phosphate in pore water were lower at lower salinities (46 and 52 g kg^{-1}) and increased with higher salinities (>100 g kg^{-1}).

4.3.2. Assessing the chemical microenvironment over time

Elemental analysis of the five layers of each time point was undertaken using ICP-MS and OES, hence concentrations or presence of chemical elements may be linked to biological activities and specific taxonomic microbial groups. The most abundant elements in the mat throughout the years were Calcium (range: from 9020.20 ppm in September 2015 up to 13731.63 ppm in March 2014), Sodium (range: from 2854.35 ppm

in December 2015 up to 8656.26 ppm in July 2016), Magnesium (range: from 1702.89 ppm in December 2015 up to 2530. 81 ppm in March 2014), and Molybdenum (range: from 252.45 ppm in December 2015 up to 2282.77 ppm in March 2014). Analysis of elemental abundance within the different layers of the microbial mat revealed that out of the 18 elements detected, 10 and 14 elements showed significant enrichment in the deeper layers of the mat (layer 3, 4, and 5) for the time points of April and September 2015, respectively. While in April the higher abundances of the following elements Al, Be, Co, Cr, e, Mn, Mo, Ni, Pb, and V were found, in September 2015, the deeper layers of the mat were enriched by Al, As, Ca, Ba, Be, Co, Cr, Cu, Fe, Mn, Mo, Ni, Pb, and V. Abundance of elements did not significantly differ within depth of the mat of March 2014 for all elements except Be which was enriched in the lower layers of the mat. For the contextual data collected we analyzed whether any of those elements regardless of layer were correlated with pond water salinity. We found that out of all elements measured, 9 showed weak correlations ($p<0.05$) to pond water salinity. Only sodium and potassium had weak positive correlations with salinity (Kendall's roh: Na 0.32, $p=0.02$; K 0.34, $p=0.014$), while the other elements, Co, Cd, Ca, Cu, Mo, Ni, and V had weak negative correlations with pond water salinity. Sulfur and potassium were strongly positive correlated to sodium concentrations in the microbial mat regardless of depth (Sulfur 0.63, $p<0.01$; K 0.77, $p<0.001$).

4.3.3. Microbial mat community compositional changes

4.3.3.1 Changes in community diversity

Based on taxonomic annotation of the metagenome, genes classified as archaeal or bacterial 16S rRNA genes were used for community diversity estimates. Species richness and alpha diversity (Shannon and Weaver) were calculated based on the phylum level of each sample. The number of different phyla observed over the eight different time points ranged from as low as 11 up to 39 phyla. Species richness between the layers (1-5) remained the same ($p>0.05$) for August 2013, March 2014, and July 2014 time points (Table 4.3). For the following five time points a significant trend was observed wherein the first layer always showed a significantly lower number of phyla ($p<0.05$) as compared to the deeper layers (3, 4, and 5) (Table 4.3). During the highest salinity conditions observed during the study, September 2015, layers 1 and 2 showed the lowest mean number of phyla (~11 phyla), however right after the salinity drop due to the Hurricane mean phyla richness increased to ~24 in layer 1 and remained unchanged for the following time points. Similar to phyla richness, alpha diversity did not significantly change between the layers for August 2013 and March 2014. A significant increase ($p<0.05$) in species richness was observed from layer 4 to layer 5 during the July 2014 time point. There was a significant increase ($p<0.05$) in alpha diversity with depth for the time point of April 2015. All remaining time points did not show significant changes in alpha diversity between the layers (Table 4.3). When examining abundance change of phyla within depth of the microbial mat, we observed that in the lower salinity time points (August 2013, March 2014, December 2015, and March 2016) there were fewer phyla that significantly (one-way ANOVA, $p<0.05$) changed in abundance between the

layers as compared to the higher salinity time points. For August 2013 and the following time point of March 2014, there was a significant change in mean abundance within the layers for only two and one phyla, respectively, while the time points of December 2015 and March 2016 both had 5 phyla that changed significantly in mean abundance (Table 4.2). For July 2014 and September 2015, 11 phyla changed significantly in mean abundance within depth, while April 2015 had the most phyla (12) and 9 phyla changed in July 2016. The phylum of Cyanobacteria was always significantly higher in layer 1 from April 2015 to July 2016. During the high salinity time points of July 2014, April 2015, and September 2015, Thaumarchaeota mean abundance was significantly higher in the deepest layer 5 as compared to the upper layers, while abundance was significantly elevated in layer 3 as compared to layer 1 in the other high salinity time point of July 2016. Euryarchaeota mean abundance increased towards the deeper layers of the microbial mat and layer 5 was significantly different than layer 1 and 2 in August 2013, while in July 2014 Euryarchaeota mean abundance of layer 5 was significantly higher than all other layers. The same trend was observed for April and September of 2015, where the upper layers (1 and 2) had significantly lower abundance of Euryarchaeota. The uncultured archaeon was only found to be significantly higher in mean abundance in layer 5 of July 2014. During the time points of July 2014, September 2014, March and July 2016, Acidobacteria mean abundance was significantly higher in the middle layers (2, 3, and 4) as compared to layer 1 and 5. Actinobacteria only showed significant changes within depth for the time point of July 2016 where layer 2 and 5 were highest in mean abundance. Bacteroidetes mean abundance was significantly elevated in the first layer of the April and September 2015 time points, while in July 2016 layer 3 had a

significantly higher abundance as compared to layer 1. While mean abundance for Chloroflexi significantly increased in the lower layers (3, 4, and 5) during July 2014, April 2015, and March 2016, layer 1 showed the highest mean abundance in July 2016. For Firmicutes significant changes for the layers were only found in July 2014 and December 2015 where the first layer had higher mean abundance as the lower layers (3, 4, and 5). In July 2014, mean abundance for Lentisphaerae and Deferribacteres phyla was significantly elevated in the lower layers as compared to layer 1, and in September 2015 Deferribacteres abundance was found to be highest in layer 3. The phyla of Spirochaetea and Verruchomicrobia were both found to be significantly different between the layers in April 2015 and July 2016. Both phyla were higher in abundance in the deeper layers in April 2015, but while Spirochaetea followed the same trend in July 2016, Verruchomicrobia mean abundance was found to be higher in layer 1 as compared to layer 5. Proteobacteria mean abundance was significantly different within the microbial mat depth profile for the following three time points, March and July 2014, and September 2015. While for the first of the three time points layer 1 had significantly higher abundance than layer 4, in July 2014 layer 4 had higher mean abundance than layer 5, and in September 2015 layer three had the highest mean abundance as compared to first and last layer. The only other phyla that showed significant changes within depth in August 2013 was Candidate division OP3, where it was found to be significantly higher in mean abundance in lower layers. This trend was also observed for the time points of July 2014 and April 2015. While Candidate division OD1 was significantly higher in the first layer in July 2014, layer 5 was significantly enhanced in mean abundance during December 2015. In April 2015, three more members of the Candidate

division (BRC1, OP8, and OP11) were found to be significantly different in mean abundance between the layers. While BRC1 was more abundant in layer 2 as compared to layer 4, OP8 was most abundant in the deeper layers of the mat, and OP11 was found to have greater abundance in the upper layers. OP8 was also found to have significant changes in abundance in the following time point, September 2015, where it was highest in the deeper layer of the mat. OP11 had the highest abundance in the lowest layer in December 2015 and July 2016. The high salinity time point of September 2015 showed also significant changes in mean abundance for the following phyla, Candidate division WS6, Chlamydiae and TM6. WS6 was most abundant in the first layer, while Chlamydiae phyla were highest in layer 3, and TM6 was most abundant in layer 5. SHA-109 was found to have significant shifts in abundance between the layers during the lower salinity time points of December 2015 and March 2016. However, while it was most abundant in layer 5 in December, layer 3 had the greatest abundance in March 2016. The phylum BD1-5 was in lower abundance across all layers in April 2015, but was significantly elevated in the lower layers. In April 2015, the phylum NPL-UPA2 was significantly enhanced in layer 5.

Next, we examined how the whole community of the different layers changed over time based on Bray-Curtis community dissimilarities (Figure 4.6, 4.7, and 4.8). Community composition of layer 1 changed significantly (Adonis, $p<0.05$), with the initial August community only being least dissimilar ($p>0.05$) to the April 2015 time point (Figure 4.6, Figure 4.7 A). The March 2014 community of layer 1 was not significantly dissimilar ($p<0.05$) from the community composition of September 2015, March 2016, and July 2016 time points. The microbial community composition of July

2014 was not significantly dissimilar from the April 2015, December 2015, March 2016, and July 2016 time points. Overall, as salinity of Salt Pond fluctuated the whole community composition of layer 1 underwent significant changes, but seemed not to be related to salinity or season. The Hurricane event between the sampling points of September and December 2015 did not significantly change the composition of layer 1, which might be due to the high variation in community composition between replicates pre Hurricane event (Figure 4.6, Figure 4.6 A). Out of the total 44 phyla detected for layer 1, 18 of them changed significantly in abundance (ANOVA, $p<0.01$) between the time points. The initial community of August 2013 had 8 phyla (Acidobacteria, Candidate division OP3, Candidate division OP8, Chloroflexi, Euryarchaeota, NPL-UPA2, Spirochaetae, and Thaumarchaeota) that were significantly higher in abundance as compared to other time points (Figure 4.6). For instance, Acidobacteria (Figure 4.5, red) were significantly higher in abundance compared to all other time points but March 2014. Euryarchaeota (Figure 4.6, sky blue) were significantly higher in abundance in August 2013 as compared to the following time point of March 2014, and the highest salinity time point of September 2015. Spirochaetae (Figure 4.6, navy blue) were significantly higher in abundance in August 2013, July 2014, and April 2015, as compared to the other time points.

Other changes in abundance from August 2013 were seen for Bacteroidetes that were significantly lower in abundance in August 2013 as compared to April and September 2015. Planctomycetes fluctuated in abundance but were significantly enhanced in March 2014, September 2015, as well as March and July of 2016. While Proteobacteria (Figure 4.6, teal) fluctuated in abundance, significant differences were

only found between the initial time point of August 2013 and the following time point, March 2014. Cyanobacteria (Figure 4.6, green) changed significantly in abundance after the Hurricane event (time point, December 2015) and remained significantly higher in the following time point of March 2016.

Comparison of the community of layer 2 over time also showed significant changes (Adonis, $p<0.05$). It appeared that the initial community of August 2013 was only most dissimilar to the community of March 2014, December 2015, and March 2016. Even though the August 2013 time point had a lower salinity (46 g kg^{-1}), it was most dissimilar in community composition to the other lower salinity time points (Figure 4.6, Figure 4.7 B). In agreement to layer 1, the high salinity time point of September 2015 also showed a greater community variation between replicate samples, as clustering of the sample points show (Figure 7 B, pink dots). Out of the 28 phyla detected in layer 2, half of them changed significantly in abundance throughout the time points. Acidobacteria (Figure 4.6, red), for instance, were significantly higher in abundance in the last time point of July 2016, as compared to the other two highest salinity time points of July 2014, and September 2015. Bacteroidetes (Figure 4.6, light blue) fluctuated in abundance, where the initial abundance of August 2013, dropped significantly to the next time point, and then significantly increased again in July 2014, followed by a stable abundance through April 2015, but significantly decreased and stayed lower at the following time points. The phylum BD1-5 (Gracilibacterium) (Figure 4.6 B, white) appeared in lower abundances from August 2013 to December 2015 and significantly increased in March and July 2016. The mean abundance of Candidate division BRC1 (Figure 4.6, black) was found to be significantly higher at the initial time point (August

2013). The Chlorobi (Figure 4.6, dark blue) phylum abundance of April 2015 was significantly higher than all the other time points. Chloroflexi abundance was lowest at the two highest salinity time points (July 2014, and September 2015) and didn't change significantly in abundance between the others (Figure 4.6, cream). During the high salinity time points of July 2014 and September 2015, Cyanobacteria abundance was significantly enhanced as compared all other time points but December 2015. While Deferribacteres abundance was significantly greater at the initial time point, it decreased over the next two time points and peaked again in April 2015. While for Archaea phyla of Euryarchaeota and Thaumarchaeota (Figure 4.6, blue and purple) mean abundance significantly changed over time, it was highest for Euryarchaeota in August 2013 and April 2015, and significantly increased for Thaumarchaeota in August 2013 over the March 2014, September 2015, and July 2016 time points. The mean abundance of Firmicutes (Figure 4.6, mustard) fluctuated over time, and was significantly enhanced in March 2014. Lentisphaerae (Figure 4.5, sky blue) mean abundance peaked in August 2013 and in the time point after the pulse disturbance (December 2015). While Planctomycetes (Figure 4.6, dark grey) mean abundance fluctuated over time it was found to be significantly higher in March 2014.

Similar to layer 1, Spirochaetae abundance (Figure 4.6, navy blue) was significantly enhanced in August 2013, July 2014, and April 2015, as compared to the other time points. The other 14 phyla where the change in mean abundance was not found to be significant included Proteobacteria, Actinobacteria, and other lower abundance phyla.

The trend of variation of the September 2015 replicates that was found in the previous layers was not found in deeper layers of the mat (layer 3-5) and must therefore be only limited to the surface layers (Figure 4.7 C, pink dots).

The communities of the time points in layer 3 cluster closer together on the NMDS plots (Figure 4.7 C), however there were significant dissimilarities between them (Adonis, $p<0.05$) (Figure 4.6). It stood out that the high salinity, September 2015, time point was different from previous time points, but remained similar after the Hurricane event up until March 2016. Out of the 44 detected phyla for layer 3, only 14 changed significantly in mean abundance between the time points. Acidobacteria significantly decreased in mean abundance at high salinities of July 2014, April and September 2015 as compared to the lower salinity time points. In July 2014, the mean Bacteroidetes abundance was significantly increased over the previous time point (March 2014) and compared to March 2016. The phylum of Candidate division BD1-5 peaked at the July 2016 time point as compared to August 2013, September and December 2015. Candidate division OD1 (Parcubacteria) (Figure 4.6, grey) significantly increased in September 2015, while Candidate division OP3 (Omnitrophica, provisional name) was only significantly increased in August 2013. During September 2015, the mean abundance for Chalmydiae (Figure 4.6, pink) was significantly elevated as compared to all other time points, while Chloroflexi mean abundance was significantly lower as compared to April 2015. While Cyanobacteria phylum abundance was lowest for August and March 2014 it significantly increase in July 2014, after which it decreased again. During the time point of March 2014, Firmicutes, Planctomycetes, and Spirochaetae mean abundance was significantly elevated. While Archaea phylum abundance of Thaumarchaeota was

significantly elevated in the initial time point, the abundance of uncultured archaeon was highest in April 2015. Even though Proteobacteria and Actinobacteria mean abundance fluctuated over time there was no significant change between the time points.

In layer 4 the initial community of August 2013 changed and was significantly dissimilar to all the other time points ($p<0.05$). While all other time points clustered together on the NMDS plots (Figure 4.7 D) and were not significantly different from each other, the April 2015 community was. For layer 4, 47 phyla were detected and more than half (24 phyla) showed significant changes in mean abundance over time. August 2013 had the most phyla (Candidate division KD1, OP3, OP8, as well as Thaumarchaeota, uncultured archaeon, Fusobacteria, and TA06) with a significantly higher mean abundance compared to the other time points. Actinobacteria (Figure 4.6, plum) showed the highest mean abundance in March 2014, and the lowest after pulse disturbance in December 2015. March 2014 also had the highest mean abundance for Firmicutes, and Planctomycetes, while Proteobacteria were significantly lower than the other time points. For Proteobacteria, there was a significant shift in abundance from one time point to the next, following a trend of down and up. The July 2014 and April 2015 time points showed significant increases in mean abundance for Candidate division SR1 and Hyd-24, respectively. The highest salinity sampling point of September 2015 increased the mean abundance of Chalmydiae, Candidacte division OD1, and OP11 significantly as compared to the other time points. After the Hurricane disturbance, two phyla (JL-ETNP-Z39, and Nitrospirae) showed a significant increase in mean abundance over the other time points. Bacteroidetes mean abundance fluctuated over time, with highest mean abundance in August 2013, July 2014, and December 2015. Similar to layer 4,

Acidobacteria mean abundance significantly decreased and was lowest at the high salinity time points of April and September 2015. Cyanobacteria mean abundance was significantly lower during the first two as compared to following time points.

In layer 5, the August 2013 and April 2015 communities were not significantly different ($p>0.05$) from each other, however the August time point was significantly dissimilar to all the other communities, while April clustered with most of the other ones on the NMDS plot (Figure 4.7 E), and did not show significant dissimilarities to the communities of July 2014, September 2015, and December 2015. A total of 48 different phyla were detected for layer 5, from which 22 showed significant differences in mean abundance over time. There were four phyla (Euryarchaeota, Candidate division JS1, Deferribacteres, and Candidate division OP3) that did not show significant differences in mean abundance between August 2013 and April 2015. In August 2013 mean abundance of eight phyla was significantly different as compared to the other time points. With six phyla (Thaumarchaeota, uncultured archaeon, Fusobacteria, Candidate division OP8 and WS3, as well as NPL-UPA2) having a higher mean abundance, while the other two (Actinobacteria and Candidate division OP11) were significantly lower compared to the other time points (Figure 4.6). For Bacteroidetes, the lowest mean abundance was observed during the two time points of 2014 (March and July). While Cyanobacteria were lowest in mean abundance in March 2014, their highest abundance was observed in the following time point of July 2014. The phyla Gemmatimonadetes and Lentisphaerae were significantly higher in March 2014 and July 2014, respectively. Spirochaetaes mean abundance was elevated in August 2013 and July 2014 as compared to the lower abundance of the other time points. In an opposite trend to Spirochaetaes, Planctomycetes

mean abundance significantly fluctuated from August 2013 up to March 2014, and decreased in the following time point, after which mean abundance did not change significantly over time. Proteobacteria mean abundance was lowest at the high salinity time point of September 2015, and significantly increased in the following time points being most abundant in July 2016.

Out of all phyla of the microbial mat the phylum of Proteobacteria showed the highest abundance but mean abundance within the microbial mat depth profile was only significantly different for three time points (March and July 2014, and September 2015). We resolved the phylum further into class level to investigate significant changes within the Proteobacteria classes (Alpha-, Beta-, Delta-, Epsilon-, Gamma-, and Zetapoteobacteria, as well as the class Proteobacteria Incertae Sedis). Alpha-, Delta-, and Gammaproteobacteria were always more abundant in all layers and time points.
For August 2013, Delta- and Gammaproteobacteria dominated all layers followed by Alphaproteobacteria. The following trend was observed for Alphaproteobacteria, for the time points before the Hurricane (from March 2014 – April 2015), they were significantly higher in the first layer, while at the highest salinity time point of September 2015, the class dominated all layers, and post Hurricane event, was found to dominate the deepest layer 5.

4.3.4. Metagenome assembly

The overall reference assembly created by assembling sequence reads from all time points had a total length of 4,554,991,043 bp, including 4,529,340 contigs, with the largest contig being 164,517 bp long (Table 4.10). The average GC content of the assembly was 59.21% and had a N50 value of 1013. From the overall assembly

7,526,810 genes were called. Approximately 68% of reads from each time point mapped back to the overall assembly (Table 4.11).

The overall metagenome assembled from all eight-time points was visualized with the Krona chart (Figure 4.9). The overall assembly consisted of 92.52% genes annotated as Bacteria, 4.14 % of genes belonged to the linage of Eukaryota, 2.27% genes were classified as Archaea, and 0.55% of genes belonged to Viruses. Only 0.48% of genes were not classified and 0.02% of genes were not found in the database (Table 4.2, Figure 4.9). Within Archaea, genes belonged to 19 different phyla, while the majority 32. 58% and 30.99% were classified to belong to the phyla of Methanomicrobia and Halobacteria, respectively (Table 4.3, Figure 4.10). Genes of the linage Bacteria belonged to 39 different phyla (Table 4.4). While the majority of genes (41.21%) were classified as Proteobacteria, followed by Planctomyctes (13.84%), Actinobacteria (10.93%), Chlorofelxi (8.90%), Bacteroidetes (5.54%), Cyanobacteria (4.79%), and Firmicutes (4.18%), Acidobacteria (2.03), and environmental samples (2.05), the other 29 phyla made up 1% or less (Table 4.4). Genes belonging to Eukaryota were mainly represented by the phyla of Opisthokonta (64.66%) and Viridiplantae (20.65%) (Table 4.5). The lineage Virus had 13 subdivisions and 58.86% of genes were classified as dsDNA viruses, environmental samples (20.53%), and unclassified bacterial viruses (16.41%) (Table 4.6).

Since the majority of assembled genes classified as Proteobacteria, the phylum was further separated into class division to evaluate which class had the most genes (Table 4.7, Figure 14.1). Seven classes of Proteobacteria were found of which Deltaproteobacteria had the highest percentage of genes included in the assembly

(38.93%), followed by Alphaproteobacter (24.49%), Gammaproteobacteria (24.29%), and Betaproteobacteria (12.17%), while the other three classes were below 0.1%.

4.3.5. Functional Annotation by Protein Family Classification of Archaeal and Bacterial Metagenomes

In order to characterize the functional profile of the archaeal and bacterial communities, contigs from the overall archaeal and bacterial assembly were mapped to the EggNOG (Huerta-Cepas *et al.*, 2016) database for finding of non-supervised orthologs groups of proteins. Functionally annotated metagenomic proteins mapped to four different groups. For Archaea, the majority, 40.39% of genes, belonged to the metabolism group, while 27.24% mapped to the poorly characterized group, 16.01% belonged to the group of cellular processes and signaling, and 15.46% were classified as information storage and processing (Figure 4.12, inner circle). Within the metabolism group, genes carrying out energy production and conversion were the most abundant (C, 12%), followed by aminoacid transport and metabolism (E, 8%), inorganic ion transport and metabolism (P, 6%), and carbohydrate transport and metabolism (G, 5%) (Figure 4.12). Genes involved in cellular processes and signaling mostly carried out the following functions; cell wall / membrane / envelope biogenesis (M, 4%), posttranslational modification, protein turnover, chaperones (O, 4 %), signal transduction mechanisms (T, 4%), and defense mechanisms (V, 3%). In the group of information storage and processing, replication, recombination and repair were the most abundant genes (L, 6%), followed by translation, ribosomal structure and biogenesis (J, 6%), and transcription (K, 3%). Similar to the Archaea functional annotation, for the bacterial metagenome the majority of genes mapped to the Metabolism group (36%), followed by genes annotated

as Poorly characterized proteins (26%) and Cellular Processes and Signaling (25%) and only 14% of the genome was classified to belong to functional group of Information Storage and Processing (Figure 4.13, inner circle). Similar to the Archaea Metabolism group, genes carrying out the function of Energy Production and Conversion (C) were most abundant (8%), followed by Amino acid transport and metabolism (E, 7%), Carbohydrate transport and metabolism (G, 6%), and Inorganic ion transport and metabolism (P, 5%). The distribution of genes involved in Cellular processes and signaling differed from Archaea. The following functions were mostly carried out in this group were Cell wall / membrane / envelope biogenesis (M, 6%), Intracellular trafficking secretion, and vesicular transport (U, 6%), and Signal transduction metabolism (T, 6%). Posttranslational modification, protein turnover, chaperones (O, 4 %) and defense mechanisms (V, 2%) had fewer genes. In the group of information storage and processing, replication, recombination and repair were the most abundant genes (L, 6%), followed by translation, ribosomal structure and biogenesis (J, 4%), and transcription (K, 3%)

4.3.6. Comparison of Functional Annotation of Archaeal Metagenomes over Time

From a total of 123,234 ORFs in the Archaea metagenome, only 23% (for time points of August 2013 and July 2014) and 27% (for all other 6 time points) of ORFs, could not be assigned to functional groups in the COGs database. To identify where the time point metagenomes differed in their apparent functional capacity, a quantitative comparison of 23 COG functional categories was performed. The functional characteristics of the 23 COG categories were compared between the time points and revealed distinct clustering of the first three time points (August 2013 – July 2014) from

all other time points (Figure 4.14), suggesting that they are more dissimilar in their functionality than the other time points. Some September 2015 component pairs in the PCA analyses clustered with samples from April 2015, December 2015, March and July 2016, while April 2015 formed one cluster with samples from December 2015 and July 2016, suggesting that the metagenomes of these time points had similar functional groups (Figure 4.14).

A closer view at the specific functional description showed similar distributions of genes between the 4 different groups (Cellular processes and signaling, Information storage and processing, Metabolism, and Poorly characterized) as it was found for the overall assembly (Figure 4.12, 4.15). The majority of genes were annotated and assigned to the Metabolism group, followed by the groups of Poorly characterized, Cellular processing and signaling and Information storage and processing (Figure 4.15 A-D). Significant differences between the eight metagenomes were observed in many categories (Figure 4.15). The results of the PCA analysis indicated that the first three time points were significantly different from all other time points in their functional capacity. A comparison of the time points within the 4 distinct functional groups showed that August 2013 had significantly more contigs (~49% of August 2013 contigs mapped to Metabolism group) in the Metabolism group as compared to all other time points (Figure 4.15 C) and significantly fewer genes in the group "Information storage and processing" as compared to time points 3-8 (Figure 4.15 B). The March 2014 time point had significantly ($p<0.001$) fewer contigs assigned to the groups of Cellular processing and signaling (~11% of contigs, Figure 4.15 A) and Information storage and processing (~5% of contigs, Figure 4.15 B), while significantly more genes were "Poorly characterized"

(~27% of contigs, Figure 4.15 D), as compared to all other time points. The July 2014 time point had more contigs belonging to the Poorly characterized group (~25% of contigs, Figure 4.15 D) as compared to the following time points.

The significant higher proportion of genes assigned to Metabolism of the August 2013 time point can be explained by the significantly higher mean RPKM values in the category "Secondary metabolites biosynthesis, transport, and catabolism" (Q, effect size $\eta^2 = 0.99$, $p<0.0001$, Figure 4.16).

The significant lower proportion of Archaea genes assigned to Cellular processing and signaling of the March 2014 time point can be explained by a decrease in mean RPKM value of contigs belonging to signal transduction mechanism (T, effect size $\eta^2 = 0.7$, $p<0.001$), Defense mechanisms (V, effect size $\eta^2 = 0.7$, $p<0.001$), and Intracellular trafficking secretion and vesicular transport (U, effect size $\eta^2 = 0.65$, $p<0.001$) (see Figure 4.14). While the significant decrease in March 2014 of contigs belonging to Information storage and processing is attributed to the significantly lower mean abundance of contigs involved in transcription (K, effect size $\eta^2 = 0.99$, $p<0.0001$) (Figure 4.15), the significant increase of contigs in the group of Poorly characterized genes can equally be explained by the increase in mean RPKM value of contigs functionally assigned to categories "General function prediction only" and "Function unknown" (R, effect size $\eta^2 = 0.99$, $p<0.0001$; S, effect size $\eta^2 = 0.99$, $p<0.0001$; see Figure 4.16).

To examine possible distinct genetic capacities between the layers of each time point, an analysis of significant changes in abundance (≥ 2 fold, $p<0.05$) of archaea genes within depth of each time point was conducted. As visible from Figure 4.16, there was no

significant change in mean RPKM value between most layers of each time point. Of all archaeal contigs (123,234) a total of only 10, 23, 16, and 45 changed between the layers of the first 4 time points, while September 2015 had a total of 1739 genes significantly changing in abundance, in December 2015 only 138 genes changed, and in the following 2 time points 31 and 376 genes significantly changed in abundance. Throughout most time points the majority of genes were found to be significantly different to the deepest layer 5. For 4 time points (August 2013, September 2015, March 2016, and July 2016) more tan half of significantly changing genes increased in abundance, while for the remaining time points more than half decreased significantly in abundance. Only in August 2013 belonged the majority of significantly changing genes to the COG group Cellular Processes and Signaling", all remaining time points had either increases or decreases in abundance in the Metabolism group.

4.3.7. Comparison of Functional Annotation of Bacterial Metagenomes over Time

For the Bacterial metagenome a total of 3,444,865 ORFs were found. ORFs that were not assigned to functional groups in the COG database ranged from ~10% (for time points of August 2013 and July 2016) to ~13% (for all other 6 time points). The same approach that was used to compare the functional annotation of Archaea was applied to the bacterial metagenome. When comparing the functional characteristics of the four different groups (Cellular processes and signaling, Information storage and processing, Metabolism, and Poorly characterized) between the time points, there was no distinct clustering of any time points in the PCA analysis, suggesting that all time points are similar in their overall functionality (Figure 4.17) and a great variation between individual time point layers.

When assessing the specific functional description there was a similar distribution pattern of genes between the 4 different groups (Cellular processes and signaling, Information storage and processing, Metabolism, and Poorly characterized) to the bacterial overall assembly of COG classified genes (Figure 4.13, 4.18). The majority of genes were annotated and assigned to the Metabolism group (~36%), followed by the groups of Poorly characterized (~29%), Cellular processing and signaling (~21%) and Information storage and processing (~14%) (Figure 4.19 A-D).

Comparing the functional categories of the eight metagenomes indicated that there were significant differences. The results of the PCA analysis showed that there was no distinct clustering of the time points based on their functional capacity (Figure 4.17) and when comparing each of the 4 different groups (Cellular processes and signaling, Information storage and processing, Metabolism, and Poorly characterized) over time there were no significant differences in Cellular processing and signaling ($p=0.442$), as well as Information storage and processing ($p=0.132$) (Figure 4.18). For the other two groups (Metabolism and Poorly characterized) there were significant changes ($p<0.05$) between the time points. Contigs belonging to the metabolism group were significantly increased in August 2013 and July 2014, while contigs of the Poorly characterized group significantly decreased for the months of August 2013 and July 2014 (Figure 4.18).

Analysis of variance showed a high variation in Bacteria contig abundance between the five layers that might explain the overall few changes within the four COG groups over time. The four groups were broken down into their respective sub-categories and contig abundance was compared on a depth profile (layer 1-5). The comparison showed that there were significant changes within each of the four groups (Cellular

processes and signaling, Information storage and processing, Metabolism, and Poorly characterized) (Table 4.12). The first two millimeters (layer 1 and 2) as well as the deepest layer (layer 5) showed that Bacteria contig abundance significantly changed over time in most of the 22 sub-groups (layer 1 ~86%, layer 2 ~73%, and layer 5 ~91%), while in layer 3 and 4 only ~4.5% and ~9%, respectively, changed significantly in Bacteria contig abundance over time. Within the group of Cellular processes bacterial genes assigned to the sub-group of Cytoskeleton (Z) were in lowest abundance of all time points and did not change significantly over time in any of the layers (Table 4.12). The sub-group L (replication, recombination and repair) followed a seasonal trend in first two millimeter (layer 1 and 2), where it had significantly higher abundance of genes in the warmer wet season as compared to the cooler dry season (Figure 4.19). The deeper layer 3 and 4 did not show any significant differences in gene abundance over time, but the deepest layer 5 changed significantly in gene abundance and a trend between season and gene abundance was apparent for the first four time points (Figure 4.19).

When examining significant changes in bacterial gene abundance within the COG sub-categories pre and post hurricane, there was a significant increase in genes belonging to the sub-category A (RNA processing and modification) in all layers but layer 4 (Figure 4.19). In the first millimeter of the mat (layer 1) nine out of the 22 sub-categories significantly decreased in abundance in the post hurricane time point of December 2015. Out of the nine sub-categories, five belonged the metabolism group (E, F, H, I, and Q), three were in the information storage and processing group (J, K, and L,), and one was assigned to the sub-group O within the cellular processes COG group. While there were mainly significant decreases in gene abundance post hurricane in layer 1, there were more

(seven out of the 22 sub-groups) significant increases in gene abundance in layer 2 and layer 5. While four of the seven sub-groups in layer 2 were within the metabolism group (C, E, F, and P), layer five showed more significant changes in the cellular processes group (D, V, T, and O). Assessing the sub-groups of each of the four COG groups over time to investigate if there were any trends in gene abundance changes in each layer showed that for layer 1-4 there were no apparent trends (Figure 19). However, within layer 5, all sub-groups of the COG category of metabolism showed the same trend in gene abundance over time, while the sub-groups of Information storage and processing and Cellular processes did not show the same trends. In the metabolism group, the August 2013 and July 2014 time points were always elevated in gene abundance as compared to all other time points.

4.4. Discussion

4.4.1. Sampling site monitoring and metadata analysis over the time period of the study

The study site is located in a sub-tropical region, where the amount of rainfall received in the wet season (summer-fall) is almost twice as much as in the dry season (winter-spring) (Sealey, 2017). However, the salinity of Salt Pond water did not follow that expected seasonal pattern where lower pond water salinities would be assumed in the wet season (summer and fall) and higher salinities in the dry season (winter and spring). On the contrary, we observed three wet season time points with salinities above 100 g kg^{-1} and three dry season time points with salinities around 50 g kg^{-1}. With an average of 4.67°C higher air temperatures measured in the wet season time points and increased

winds, evaporation rates in the wet season exceed the ones found in the dry season so that the shallow lagoon may promptly return to higher salinities even after a rainfall event. In addition, the winter months have cold fronts arrive as often as twice a week creating conditions for lower evaporation rates, whereas in the summer months, developments of lower pressure systems create warm winds (Sealey, 2017). The different salinities reflected changes in chemical gradients of the water column, such as dissolved oxygen, dissolved organic carbon, and pH. We observed that an increase in water temperature and salinity resulted in a decrease of dissolved oxygen in the water column, but dissolved organic carbon had a strong positive correlated with salinity (Pearson's, r 0.84, $p<0.01$). Evaporation events concentrate dissolved organic matter in the water column and increased DOC has been shown to turn the water column darker (brownish tint) (Worrall and Burt, 2010) and thus reducing light penetration. Our findings support that increased DOC, decreases light attenuation as measured by an increase in the attenuation coefficient (K_d). With the high salinity time points (low water column depth) showing the highest K_d values. Another chemical parameter analyzed was pH of the pond and pore water (Table 4.1). Neither pond nor pore water pH was correlated with salinity, however, pond water pH was always significantly higher than pore water pH indicating that pore and pond water were chemically different at all time points. Using chemical test of pond and pore water and subsequent analysis, by comparing concentrations of nutrients (phosphorous, ammonia, and nitrate), resulted in significant differences of pond and pore water chemistry. All three nutrients tested were significantly elevated in pore water, suggesting that the microbial mat is the main producer of the nutrients and that there is little diffusion into the overlaying water and the nutrients are being cycled in the mat.

Exopolysaccharides (EPS) (as seen in Figure 4.2B) that are part of the mat matrix act as a laminar diffusion barrier (Decho, 1990), hence aiding the nutrients to cycle in the mat. In pore water, ammonia concentrations were positively correlated with pond water salinity up until September 2015, after the hurricane event in December 2015 and March 2016 ammonia concentrations were twice as high as compared to the pre- hurricane time point (Figure 4.5) suggesting that the conditions during the highest pond water salinity time point (September 2015, 305 g kg^{-1}) significantly reduced ammonia concentrations indicating ammonia was being cycled in the mat, but post-hurricane disturbance conditions aided ammonia increase in the mat, as it was possibly not cycled and accumulated. Within the pore water, phosphate concentrations were generally lower at lower salinities (around 50 g kg^{-1}) and increased with increased salinities (>100 g kg^{-1}), suggesting that increased salinities enhance phosphate production in the mat.

4.4.2. Assessing the chemical microenvironment over time

The steep biogeochemical gradient found in microbial mats suggests that metabolic exchange occurs at a micrometer scale (van Gemerden, 1993; Jørgensen and Revsbech, 1985). To understand the function of the microbial mat community and how it changes, the chemical microenvironment (elemental composition of each layer) was studied using ICP-MS and OES. The overall composition of the most abundant elements (Ca, Na, and Mg) of the microbial mat in Salt Pond was similar to microbial mats in hypersaline environments such as Shark Bay, Australia (Wong *et al.*, 2015). Calcium, sodium, and magnesium accumulation in hypersaline lagoons are derived from the input of seawater and its evaporation (Oren, 2013). The relatively high concentrations of calcium in the mat can be explained by the microbial mediated precipitation of calcium

carbonates and the calcification of the mat itself and the trapping of calcium ions from the water column by EPS (Dupraz and Visscher, 2005). Sodium and potassium showed positive correlations, while calcium had a negative correlation with pond water salinity. EPS production is stimulated under increased salinities (~ 90 g kg^{-1}) for some photosynthetic species (Liu and Buskey, 2000) and may negatively impact the diffusion of calcium ions in the mat (Kawaguchi and Decho, 2002). Sulfur and potassium concentrations in the mat were positively correlated to sodium concentrations in the mat. The accumulation of sulfur suggests a reduction in sulfur cycling. Comparing changes in distribution of the elements within a vertical gradient did not reveal any patterns but for two time points (April and September 2015) where there was a significant enrichment of some elements in the deeper layers of the mat, suggesting that the chemical microenvironment remains relatively homogeneous.

4.4.3. Microbial mat community compositional changes

Changes in community richness, diversity, and abundance of phyla along the vertical scale of the mat for each time point were used as a starting point for determining underlying ecological causes and consequences. Archaeal and bacterial community richness was found to remain unchanged for the first three time points but decreases significantly for the first layer from April 2015 until July 2016. Unlike other hypersaline microbial mats where diversity increased with depth (Wong *et al.*, 2015), Salt Pond microbial mats alpha diversity did not change over the course of the study.

During the high salinity time points there were more phyla that significantly shifted in abundance between the layers as compared to the lower salinity time points, however analysis of phyla abundance revealed phylogenetic stratification of the mat for all time

points. Depending on how much PAR reaches the surface of the mat, subsequent penetration of light through the mat may be limited and the abundance of photosynthetic primary producers like Cyanobacteria may be enriched in one layer. For the first three time points that had high amounts of PAR reaching the mat surface, Cyanobacteria abundance was not significantly different within a vertical gradient (first 7 mm of mat), suggesting that light was penetrating deeper layers. The other time points (April 2015 – July 2016) had enrichment of Cyanobacteria in the surface layer (layer 1) with a significant decrease with depth, suggesting that less PAR penetrated through the mat.

Results from the microbial mat community composition analysis showed that the community significantly changed in each layer over time but did not reveal any pattern related to salinity, season, or disturbance event on phyla level. The upper most layers (layer 1 and 2) showed a high variation between replicates pre disturbance event and explain why they were not significantly different to the post disturbed time point. For all layers but layer 4, the initial community of August 2013 was most similar to the April 2015 time point. Examining changes in different phyla revealed that Cyanobacteria in the surface layer significantly increased in abundance post hurricane event and showed a higher abundance in layer two pre-hurricane event. Similar to other studies investigating hypersaline sediments, soils and waters, we found that the metabolic diverse phylum of Proteobacteria dominated all layers in abundance (Mouné *et al.*, 2003; Lefebvre *et al.*, 2006; Mesbah *et al.*, 2007; Hollister *et al.*, 2010) and fluctuated between time points. When further resolved to class level, Alphaproteobacteria were found to be enriched in the surface layer for the first four time points, while they vertically even distributed pre-hurricane event (September 2015), and then dominated the deepest layer 5 for the

following three post hurricane time points. Other hypersaline mats, Guerrero Negro (Harris *et al.*, 2013) and Solar Lake mats (Sorensen *et al.*, 2005) showed higher abundances Alphaproteobacteria at the surface but non-lithifying mats of Shark Bay showed enrichment in the deeper layers (Wong *et al.*, 2015). The relatively low abundance of Cyanobacteria in the surface layer for the first four time points might have opened a niche for Alphaproteobacteria since this class contains photosynthetic members (Rhodobacterales). Cyanobacteria perform oxygenic photosynthesis thus increasing oxygen concentrations in the mat, their lower abundance at the surface layer together with oxygen consumption rates might have created conditions of lower oxygen tensions and allowing members of the purple non-sulfur photosynthetic Alphaproteobacteria to increase in abundance. With an increase in Cyanobacteria abundance post hurricane time points, Alphaproteobacteria decreased in the surface layer and became most abundant in the deepest layer, suggesting that the microenvironment of the surface layer had changed and was no longer conducive to Alphaproteobacteria growth.

Since phyla level resolution did not show significant differences in community composition between the pre and post pulse disturbance event, we further analyzed pre and post hurricane time point communities on class level. Beta diversity dissimilarity analysis showed that the communities of September 2015 (pre hurricane) and December 2015 (post hurricane) were significantly different (Adonis, $p<0.05$), but the composition did not further change to the March 2016 time point. The microbial community of July 2016 did not return to its original composition suggesting that the overall community did not show resilience for the time frame measured. However, compositional analysis along a vertical gradient revealed, that the deepest layer 5 did not significantly change after the

hurricane event and remained the same throughout July 2016, suggesting that the deepest layer was resistant to pulse disturbance.

4.4.4. Comparison of functionality of Archaeal and Bacterial metagenomes

The majority of genes of the overall metagenomic assembly were annotated as bacterial genes (92.5%), followed by eukaryotic genes (4.1%), and archaeal genes (2.3%), indicating that Salt Pond microbial mats are, like other microbial mats (Robertson *et al.*, 2009), dominated by Bacteria but that contributions of Eukaryota and Archaea to metabolic activities of the mat may be significant. Similar to other hypersaline microbial mats (López-López *et al.*, 2010) the majority of archaeal genes belonged to the phyla of Methanomicrobia and Halobacteria. In agreement to other four hypersaline mats (Schneider *et al.*, 2013; López-López *et al.*, 2010; Ley *et al.*, 2006; Kirk Harris *et al.*, 2012) the majority of bacterial genes belonged to phylum of Proteobacteria (41.2%), while there were fewer genes belonging to Cyanobacteria (4.8%). Within the phylum of Proteobacteria, most genes were assigned to Deltaproteobacteria, a highly diverse class known to thrive under aerobic and anaerobic conditions.

To identify functions encoded by the archaeal and bacterial metagenomes, genes belonging to different eggNOG clusters were analyzed. Archaeal and bacterial metagenomes recruited to four different groups in approximately the same ratios. Most genes mapped to the metabolism group and genes carrying out the function of energy production and conversion were most abundant. To the subcategory energy production and conversion belong processes such as photosynthesis, certain steps of biogeochemical cycling, and ATP production. While the approach of protein classification of the metagenome does not give direct insights into the community function, it is useful by

detecting enrichment of functions that might suggests that these functions are important to some aspect of the dynamic interaction between the community and its environment. The relatively high number of genes belonging to the COG functional group of Poorly characterized reflects the existing poor understanding of the resident microbiota in this system.

4.4.5. Comparison of functionality of Archaeal metagenomes over time

To identify where the time point archaeal metagenomes differed in their apparent functional capacity, 23 COG functional categories were quantitatively compared. Results of this comparison revealed distinct clustering of the first three time points (August 2013 – July 2014) from all other time points, suggesting that they were more dissimilar in their functionality than the other time points. August 2013 had significantly more genes belonging to the metabolism sub group of secondary metabolites biosynthesis, transport, and catabolism. Those proteins of are not involved in growth, development, or reproduction of an organism but are a defense mechanisms (e.g. antibiotics) and are usually formed during the late growth phase (Ruiz *et al.*, 2010). Those results suggesting that the some aspects of the community-environment interactions caused the community to shift to this type of metabolism.

The time point of September 2015 showed a higher variation in functionality between samples and did not cluster closely together with the post disturbance time point of December 2015, suggesting different functionality of the metagenome.

Comparing shifts in abundance of genes on vertical scale for each time point showed that all time points but September 2015 had relatively few genes (~0.02%) that changed significantly in abundance within depth, suggesting that the genetic structure of

the mat was more homogeneous. The September 2015 time point had more genes (1.4%) significantly shifting in abundance between layers indicating a more stratified structure.

4.4.6. Comparison of functionality of Bacterial metagenomes over time

The comparison of 22 COG functional categories was used to identify where each time point bacterial metagenomes differed in their apparent functional capacity. Analysis of this comparison showed that there was no distinct clustering for any of the time points and that time points did not closely cluster together, suggesting that all time points were more similar in their overall functional potential. When assessing the four COG groups (Cellular processes, Information storage and processing, Metabolism, and Poorly characterized) over time, there were no significant differences between any of the time points for Cellular processes as well as Information storage and processing, however, significant differences were observed within the metabolism group and the poorly characterized group. Those few significant differences can be explained by the large variation within each time point, as for this analysis the gene abundance of the layers was combined.

The four COG groups were then broken down into 22 COG functional categories and analyzed on a vertical scale (separation by layer) with statistically significant over-representation or under-representation providing clues about the functional traits characteristic of each of the time points. This analysis showed significant changes in gene abundance for 21 COG functional categories, where most changes occurred in layer 1, 2, and 5. The lower gene abundance category of Cytoskeleton (Z) within the COG group Cellular processes did not change in abundance over time.

Interestingly, layer the middle layers 3 and 4 did not change significantly in gene abundance over time for most of the 22 COG functional categories and might explain the few overall changes for the four COG groups that were apparent from the PCA analysis (Figure 4.17) and boxplot graph (Figure 4.18). The changes in gene abundance for the first two millimeters of the microbial mat were expected, as they are immediately exposed to the abiotic (physical and chemical) changes occurring in the environment, as well as disturbances such as depositional events, storm over wash, and heavy rainfall in Salt Pond. The deeper layers 3 and 4 were more stable in gene abundance within most of the 22 COG functional categories, suggesting that gene abundance within these layers were resistant to seasonal and pulse disturbance. When assessing the 22 functional categories for seasonal disturbances, layer 1, 2, and 5 significantly changed in gene abundance within the replication, recombination, and repair category (L). The significant increase in gene abundance in this category for the warmer wet season suggests adaptation to different environmental stress such as increased UV radiation and temperature that may cause significant damage to DNA (Jiménez *et al.*, 2012). When assessing changes in gene abundance for the 22 COG functional categories pre and post hurricane, there was an increase in the low abundant group of RNA processing and modification in layer 1-4. In layer 1 the increase in genes assigned to the signal transduction (T) group might help microorganisms to cope with changing environmental conditions (Eloe *et al.*, 2011). Within layer 2, genes assigned to the energy generation group (C) significantly increased in abundance post disturbance event and might suggest adaptation to sub-normal, or extreme conditions (Tyson *et al.*, 2004; Chen *et al.*, 2015), such as a disturbance event, as genes in this group are associated with a fundamental

phenomenon for microbes to drive physiologically significant mechanisms for their survival.

While it was not possible to make a direct link from the results of the archaeal and bacterial comparison of the functional annotations to ecosystem function, there were significant shifts in functional capacity over time on a vertical scale, future research will identify how particularly archaeal and bacterial genes involved in biogeochemical cycling (N- and S-cycling) respond to the disturbance event and investigate if there is functional resilience of the ecosystem.

Table 4.1. Metadata collected at each time point from Salt Pond sampling site.

Sampling Event	Year	2013	2014	2014	2015	2015	2015	2016	2016
	Month	Aug	Mar	Jul	Apr	Sept	Dec	Mar	Jul
Salinity	(g kg-1)	46	52	166	130	305	54	54	115
Water column	(cm)	30	35	0	12	0	69	68	19
Temperature (˚C)	Water	33	29.5	42.1	32.2	42	26.5	26.5	33.5
	Air	29.7	25.8	32	27.4	31.2	26.4	25.3	30.6
PAR (µE m-2 s-1)	Water surface	832.9	1344.4		1875.5		1772.5	1799.0	2004.6
	Mat surface	602.4	701.1	2092.0	686.7	2038.8	163.7	334.3	738.5
	Kd value	0.01	0.02	0	0.08	0	0.04	0.03	0.05
pH	Pond water	7.64	7.67	8.02	8.2	7.25	8.11	7.76	8.14
	Pore water	7	6.97	7	7.64	7.5	7.3	7	7.4

Table 4.2. Alpha-diversity measure between the different layers of the microbial mat over the course of the study.

Shannon-Weaver Diversity Index						
Time point	**Layer 1**	**Layer 2**	**Layer 3**	**Layer 4**	**Layer 5**	**P**
Aug 2013	2.55± 0.04	2.50± 0.04	2.51± 0.13	2.51± 0.10	2.67± 0.07	0.16
Mar 2014	1.91± 0.21	2.03± 0.13	2.18± 0.13	2.15± 0.19	2.43± 0.04	0.05
Jul 2014	2.23± 0.06	2.23± 0.08	2.26± 0.06	2.22± 0.10 [a]	2.40± 0.03 [b]	0.04*
Apr 2015	2.15± 0.07 [a]	2.37± 0.14	2.54± 0.07 [b]	2.51± 0.06 [b]	2.51± 0.05 [b]	<0.01*
Sep 2015	1.93± 0.13	1.81± 0.40	2.19± 0.13	2.18± 0.08	2.25± 0.09	0.11
Dec 2015	2.18± 0.09	2.32± 0.06	2.17± 0.19	2.20± 0.02	2.32± 0.17	0.39
Mar 2016	2.19± 0.01	2.33± 0.03	2.32± 0.07	2.31± 0.07	2.23± 0.10	0.09
Jul 2016	2.22± 0.17	2.40± 0.02	2.39± 0.09	2.33± 0.03	2.25± 0.09	0.15

Table 4.3. Species Richness of microbial mat layer by layer over the course of the study.

Species Richness						
Time point	**Layer 1**	**Layer 2**	**Layer 3**	**Layer 4**	**Layer 5**	**P**
Aug 2013	33.00± 5.30	32.33± 3.21	36.33± 10.02	34.67± 5.13	39.00± 6.93	0.73
Mar 2014	15.67± 3.21	16.67± 3.06	18.00± 1.00	17.33± 4.93	24.50± 2.12	0.11
Jul 2014	31.33± 2.08	31.00± 1.00	34.00± 7.21	35.67± 2.08	35.00± 1.00	0.42
Apr 2015	25.00± 3.00 [a]	31.33± 5.51	36.33± 2.08 [b]	35.67± 5.13 [b]	35.33± 3.06	0.03*
Sep 2015	11.33± 3.21 [a]	11.33± 9.29 [a]	28.00± 6.08 [b]	28.33± 3.06 [b]	27.67± 4.04 [b]	0.01*
Dec 2015	24.33± 1.53 [a]	30.33± 0.58 [b]	29.00± 4.00	30.33± 0.58 [b]	27.00± 1.00	0.02*
Mar 2016	20.33± 7.64 [a]	27.33± 2.08	30.00± 3.61	32.33± 3.06 [b]	23.00± 2.65	0.04*
Jul 2016	19.67± 4.93 [a]	32.33± 0.58 [b]	32.33± 3.06 [b]	34.00± 1.73 [b]	27.67± 3.51	0.01*

Table 4.4. Metagenome assembly of all time points of the study classified by lineage.

Lineage	Number of sequences	Number of sequences (%)	Size (kb)	Size (%)
Archaea	70196	2.52	72776.436	2.27
Bacteria	2554129	91.86	2962981.727	92.52
Eukaryota	129488	4.66	132485.083	4.14
Virus	14526	0.52	17720.121	0.55
Unclassified	11195	0.40	15473.124	0.48
Other sequences	519	0.02	577.794	0.02
Not found	531	0.02	534.315	0.02
Total sequences	2780584	100.00	3202548.6	100.00

Table 4.5. Metagenome assembly of all time points of the study: Archaea phyla.

Archaea phyla	Number of sequences	Number of sequences (%)	Size (kb)	Size (%)
Can. Micrarchaeota	1	<0.01	1.057	<0.01
Can. Nanohaloarchaeota	62	0.09	46.174	0.06
Nanoarchaeota	77	0.11	74.299	0.10
Environmental samples	4941	7.04	4995.799	6.86
Archaeoglobi	1639	2.33	1696.225	2.33
Eury. environmental samples	1659	2.36	1844.101	2.53
Halobacteria	23259	33.13	22551.097	30.99
Methanobacteria	2819	4.02	2769.927	3.81
Methanococci	1555	2.22	1483.631	2.04
Methanomicrobia	21099	30.06	23710.869	32.58
Methanopyri	476	0.68	611.849	0.84
Thermococci	4118	5.87	4454.551	6.12
Thermoplasmata	1269	1.81	1183.976	1.63
Unclassified Euryarchaeota	751	1.07	752.431	1.03
Can. Bathyarchaeota	158	0.23	188.596	0.26
Can. Korarchaeota	138	0.20	155.783	0.21
Crenarchaeota	2755	3.92	2984.9	4.10
Thaumarchaeota	2455	3.50	2336.169	3.21
Unclassified Archaea	965	1.37	935.002	1.28
Total	70196	100	72776.436	100

Can. Candidatus

Eury. Euryarchaeota

Table 4.6. Metagenome assembly of all time points of the study: Bacteria phyla.

Bacteria phyla	Number of sequences	Number of sequences (%)	Size (kb)	Size (%)
Acidobacteria	48511	1.90	60265.909	2.03
Actinobacteria	305832	11.97	323926.655	10.93
Aquificae	1829	0.07	2272.936	0.08
Armatimonadetes	3548	0.14	4142.054	0.14
Bacteroidetes/Chlorobi gr.	151098	5.92	164296.671	5.54
Caldiserica	227	0.01	240.93	0.01
Calditrichaeota	8406	0.33	8857.054	0.30
Can. division Zixibacteria	5	0.00	3.326	<0.01
Can. Cloacimonetes	323	0.01	275.09	0.01
Can. Latescibacteria	182	0.01	194.249	0.01
Can. Marinimicrobia	3	0.00	2.175	<0.01
Can. Omnitrophica	4	0.00	4.55	0.0002
Chlamydiae	6615	0.26	8847.812	0.30
Chloroflexi	178450	6.99	263704.487	8.90
Chrysiogenetes	860	0.03	914.634	0.03
Cyanobacteria	109467	4.29	141937.889	4.79
Deferribacteres	1264	0.05	1464.788	0.05
Deinococcus-Thermus	26986	1.06	31402.736	1.06
Dictyoglomi	565	0.02	758.646	0.03
Elusimicrobia	399	0.02	412.622	0.01
Environmental samples	51901	2.03	60853.899	2.05
Fibrobacteres	164	0.01	151.312	0.01
Firmicutes	111424	4.36	123809.717	4.18
Fusobacteria	2024	0.08	2000.436	0.07
Gemmatimonadetes	13914	0.54	15580.358	0.53
Kiritimatiellaeota	15612	0.61	17607.046	0.59
Lentisphaerae	1	0.00	0.611	<0.01
Nitrospinae	34	0.00	35.425	<0.01
Nitrospirae	8460	0.33	9394.204	0.32
Planctomycetes	305468	11.96	410097.648	13.84
Proteobacteria	1118226	43.78	1220989.061	41.21
Spirochaetes	24351	0.95	23719.379	0.80
Synergistetes	4236	0.17	4744.035	0.16
Tenericutes	1056	0.04	1108.917	0.04
Thermodesulfobacteria	1165	0.05	1319.147	0.04
Thermotogae	4191	0.16	4368.349	0.15
Unclass. Bacteria	14334	0.56	16037.725	0.54

Unclass. Terrabacteria gr.	2283	0.09	3152.813	0.11
Verrucomicrobia	30711	1.20	34086.432	1.15
total	2554129	100.00	2962981.727	100.00

Table 4.7. Metagenome assembly of all time points of the study: Eukaryota phyla.

Eukaryota phyla	Number of sequences	Number of sequences (%)	Size (kb)	Size (%)
Alveolata	5264	4.07	5702.63	4.30
Amoebozoa	2084	1.61	2220.44	1.68
Apusozoa	862	0.67	928.64	0.70
Centroheliozoa	1	0.00	0.51	0.00
Cryptophyta	362	0.28	386.73	0.29
Environ. samples	40	0.03	41.63	0.03
Euglenozoa	932	0.72	913.75	0.69
Fornicata	35	0.03	31.55	0.02
Glaucocystophyceae	17	0.01	19.16	0.01
Haptophyceae	2109	1.63	2075.43	1.57
Heterolobosea	106	0.08	121.95	0.09
Jakobida	26	0.02	40.06	0.03
Malawimonadidae	10	0.01	31.52	0.02
Metazoa	2	0.00	1.54	0.00
Opisthokonta	83903	64.80	85659.69	64.66
Oxymonadida	3	0.00	2.10	0.00
Parabasalia	145	0.11	148.04	0.11
Rhizaria	37	0.03	40.59	0.03
Rhodophyta	579	0.45	655.89	0.50
Stramenopiles	5997	4.63	6059.67	4.57
Unclass. eukaryotes	23	0.02	38.96	0.03
Viridiplantae	26951	20.81	27364.63	20.65
Total	129488	100.00	132485.08	100.00

Table 4.8. Metagenome assembly of all time points of the study: Virus phyla.

Virus phyla	Number of Sequences	Number of sequences (%)	Size (kb)	Size (%)
dsDNA viruses, no RNA	8316	57.25	10429.80	58.86

stage				
dsRNA viruses	5	0.03	5.12	0.03
environmental samples	3139	21.61	3638.13	20.53
Retro-transcribing viruses	30	0.21	30.52	0.17
Satellites	2	0.01	1.29	0.01
ssDNA viruses	14	0.10	15.31	0.09
ssRNA viruses	32	0.22	37.33	0.21
unassigned viruses	17	0.12	13.81	0.08
unclassified archaeal viruses	3	0.02	15.23	0.09
unclassified bacterial viruses	2677	18.43	2907.67	16.41
unclassified virophages	4	0.03	10.81	0.06
unclassified viruses	280	1.93	609.51	3.44
Virus families not assigned to an order	7	0.05	5.61	0.03
Total	14526	100	17720121	100

Table 4.9. Metagenome assembly of all time points of the study: Proteobacteria class.

Proteobacteria class	Number of Sequences	Number of Sequences (%)	Size (b)	Size (%)
Acidithiobacillia	1180	0.11	1150.985	0.094
Alphaproteobacteria	294246	26.31	299055.62	24.49
Betaproteobacteria	141222	12.63	148593.55	12.17
delta/epsilon subdivisions	409297	36.60	475380.58	38.93
environmental samples	89	0.01	122.93	0.01
Gammaproteobacteria	272070	24.33	296578.35	24.29
unclassified Proteobacteria	122	0.01	107.04	0.01
total	1118226	100	1220989.06	100

Table 4.10. Quality of overall reference assembly based on Quast report.

		Overall reference assembly
Quast	# contigs (>= 0 bp)	4,529,340
	# contigs (>= 1000 bp)	1,141,285
	# contigs (>= 5000 bp)	51208
	# contigs (>= 10000 bp)	12536
	# contigs (>= 25000 bp)	1388
	# contigs (>= 50000 bp)	168

	Total length (>= 0 bp)	4,554,991,043
	Total length (>= 1000 bp)	2306713248
	Total length (>= 5000 bp)	468255501
	Total length (>= 10000 bp)	208998890
	Total length (>= 25000 bp)	51294101
	Total length (>= 50000 bp)	11361596
	# contigs	4,529,340
	Largest contig	164517
	Total length	4,554,991,043
	GC (%)	59.21
	N50	1013
	N75	665
	L50	1112246
	L75	2531477
	# N's per 100 kbp	0
Prodigal	Number of genes	7,526,810

Table 4.11. Summary of Bbmap quality report.

Read mapping	Mapped Reads	% of reads mapped to Assembly
All reads	258926676	67.99
Aug 2013	35084344	59.62
Mar 2014	29922943	69.98
Jul 2014	33689307	66.18
Apr 2015	34198506	65.24
Sep 2015	31264536	78.73
Dec 2015	33054050	71.78
Mar 2016	30640202	69.91
Jul 2016	31072788	67.11

Table 4.12 ANOVA comparison of RPKM values between time points based on their COG sub-categories.

COG groups	COG sub-categories	Layer 1	2	3	4	5
Cellular Processes	D	*	*	not sig	not sig	*
	V	*	*	not sig	not sig	*
	T	*	not sig	not sig	not sig	*
	M	*	*	not sig	not sig	*
	N	*	*	not sig	*	not sig
	Z	not sig	not sig	not sig	not sig	not sig
	U	*	not sig	not sig	not sig	*
	O	*	*	not sig	not sig	*
Information Storage	J	*	*	not sig	not sig	*
	A	*	*	*	not sig	*
	K	*	*	not sig	not sig	*
	L	*	*	not sig	not sig	*
Metabolism	B	not sig	not sig	*	not sig	*
	C	*	*	not sig	not sig	*
	G	not sig	*	not sig	not sig	*
	E	*	*	not sig	not sig	*
	F	*	*	not sig	not sig	*
	H	*	not sig	not sig	not sig	*
	I	*	*	not sig	not sig	*
	P	*	*	not sig	not sig	*
	Q	*	not sig	not sig	not sig	*
Poorly Characterized	S	*	*	not sig	not sig	*

* significant at $p<0.05$

D Cell cycle control, cell division, chromosome partitioning; **V** Defense mechanism; **T** Signal transduction mechanisms; **M** Cell wall/membrane/envelope biogenesis; **N** Cell motility; **Z** Cytoskeleton; **U** Intracellular trafficking, secretion, and vesicular transport; **O** Posttranslational modification, protein turnover, chaperones; **J** Translation, ribosomal structure and biogenesis; **A** RNA processing and modification; **K** Transcription; **L** Replication, recombination and repair; **B** Chromatin structure and dynamics; **C** Energy production and conversion; **G** Carbohydrate transport and metabolism; **E** Amino acid transport and metabolism; **F** Nucleotide transport and metabolism; **H** Coenzyme transport and metabolism; **I** Lipid transport and metabolism; **P** Inorganic ion transport and metabolism; **Q** Secondary metabolites biosynthesis, transport and catabolism; **S** Function unknown.

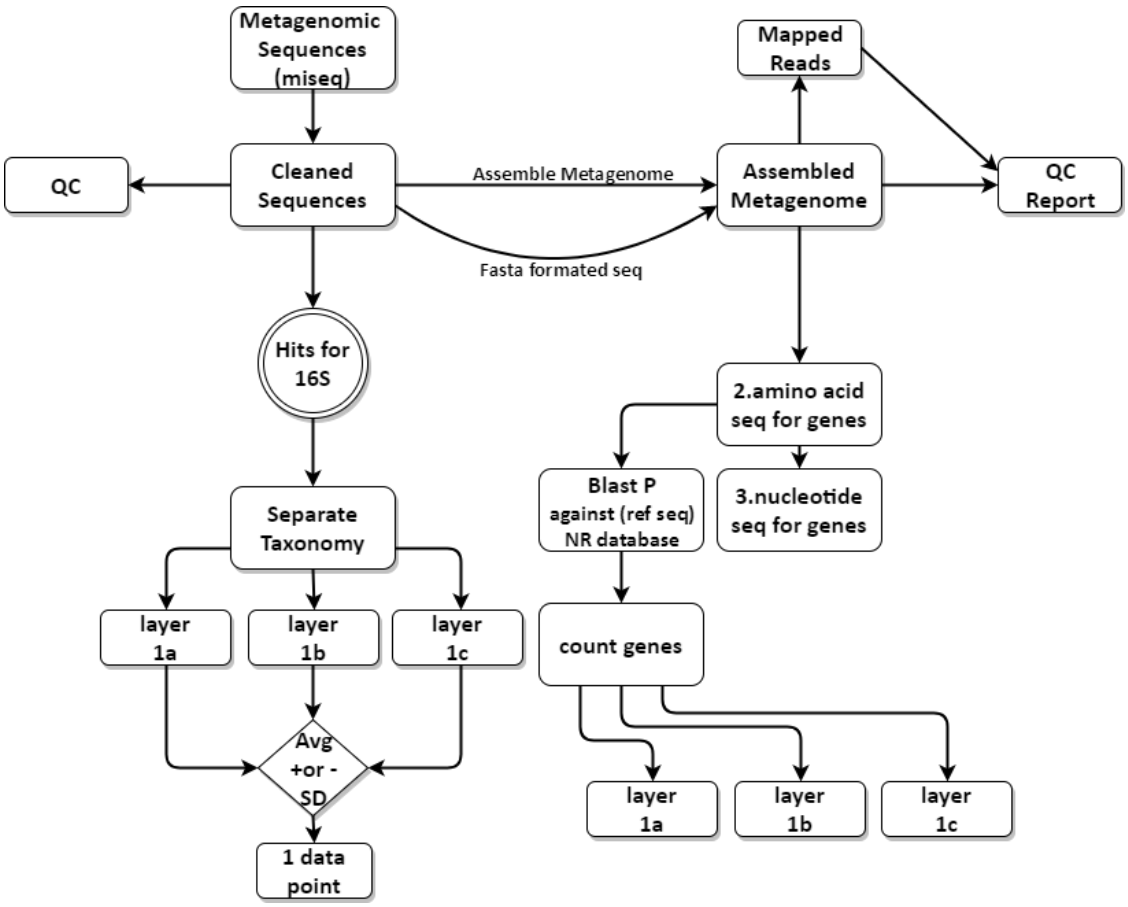

Figure 4.1. Overview of the workflow implemented in the metagenome sequence analysis for this study. Two distinct steps are carried out for 1) community composition comparison based on 16S rRNA taxonomy, and 2) Functional assignment of the metagenome.

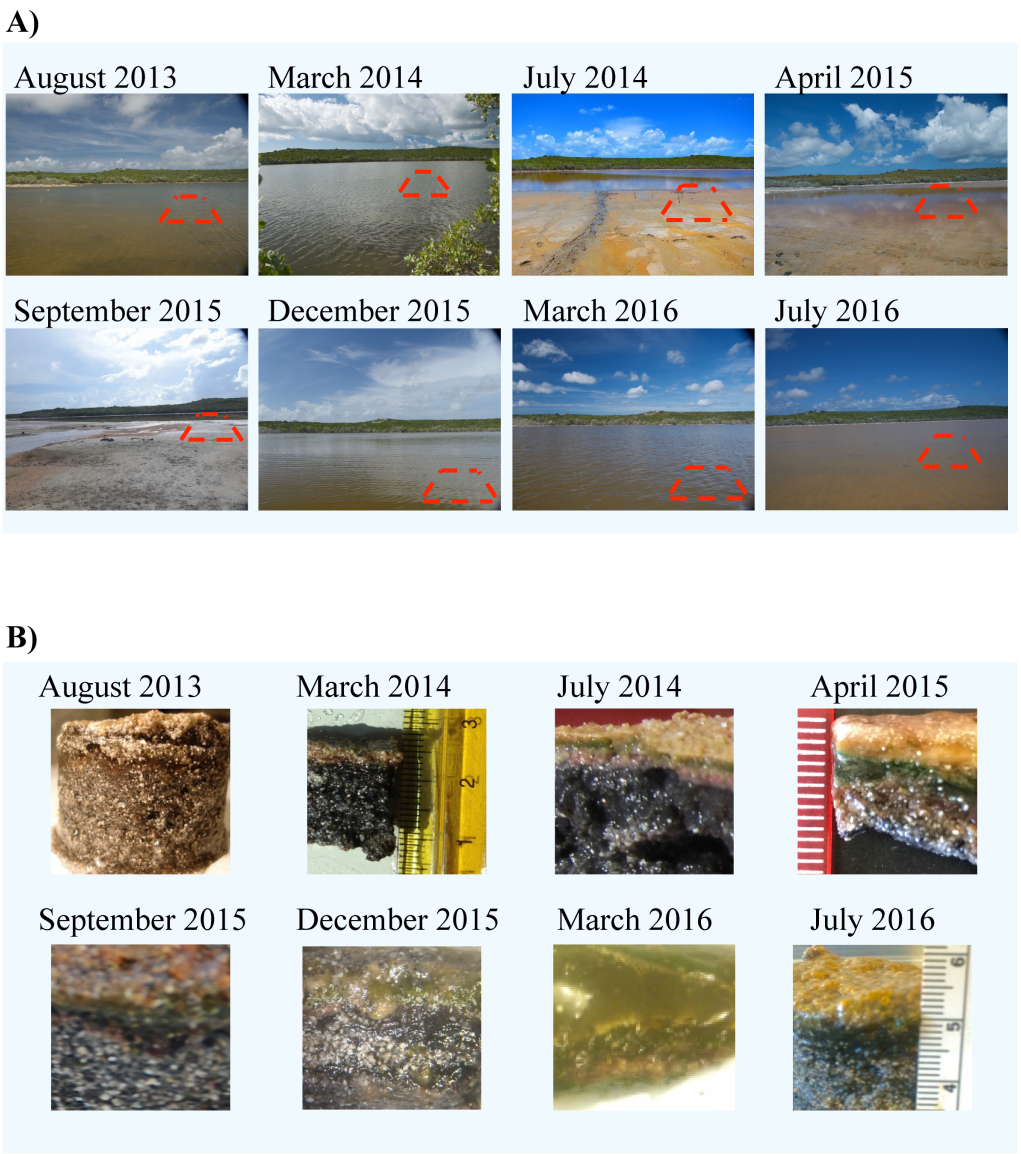

Figure 4.2. A) Photos of Salt Pond Sample side (approximate location of sampling side laid out in red box) from all time points of the study. **B)** Representative of microbial mat vertical cross section taken at each sampling event from the in A) outlined sampling side.

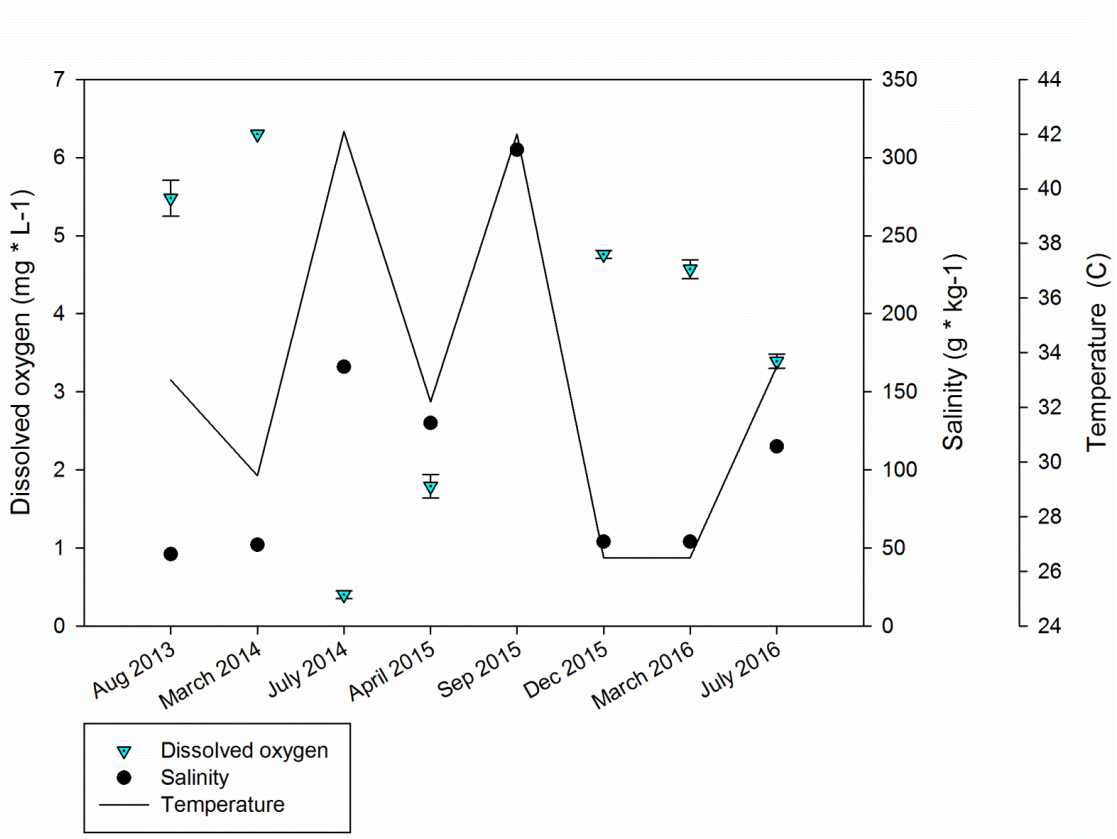

Figure 4.3. Dissolved oxygen concentrations (y-axis, mg L^{-1}) in Salt Pond water (green upside down triangle), versus salinity (second y-axis, black dot, g kg^{-1}) and temperature (black line, °C). X-axis represents the sampling time point (month, year). Dissolved oxygen concentration values represent the average (n=3), with standard deviations.

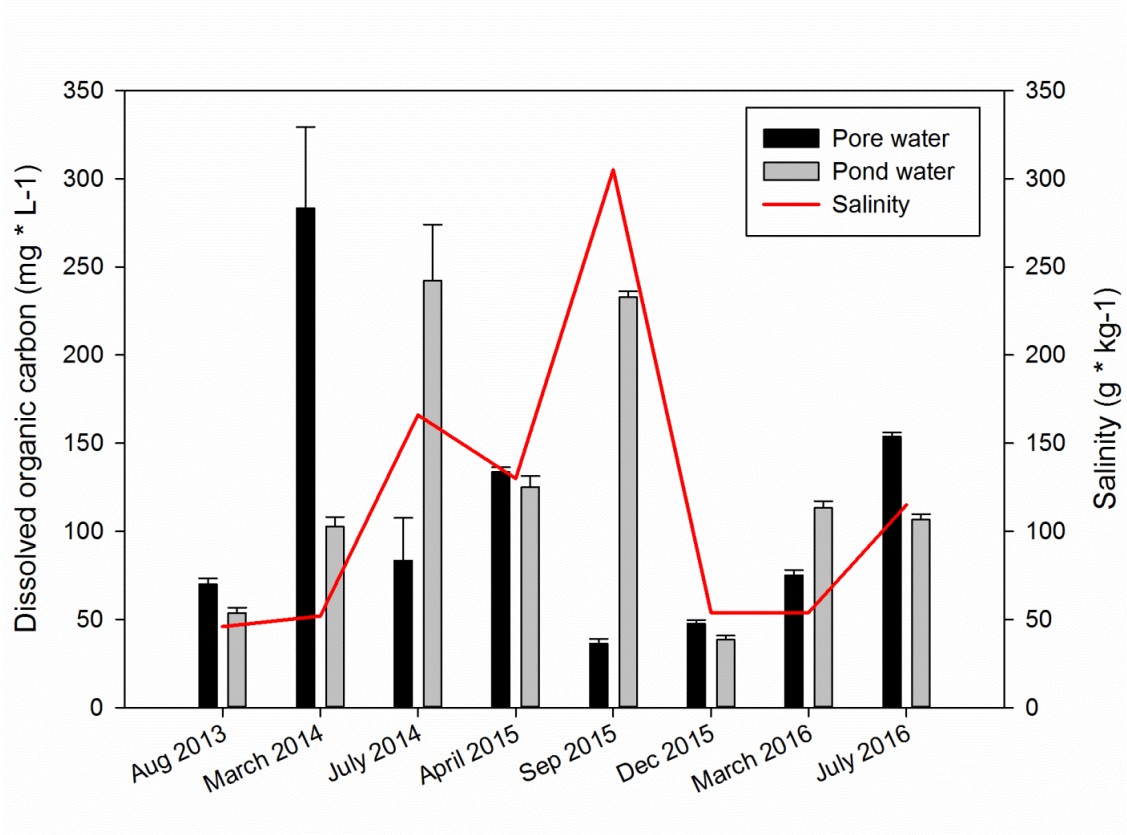

Figure 4.4. Dissolved organic carbon (DOC) concentrations (y-axis, mg L^{-1}) in Salt Pond pore (black bar) and pond (grey bar) water measured at each time point (x-axis, month and year). Second y-axis represents the salinity measurements (red line, g kg^{-1}) at each time point. DOC concentration values represent the average (n=3), with standard deviations.

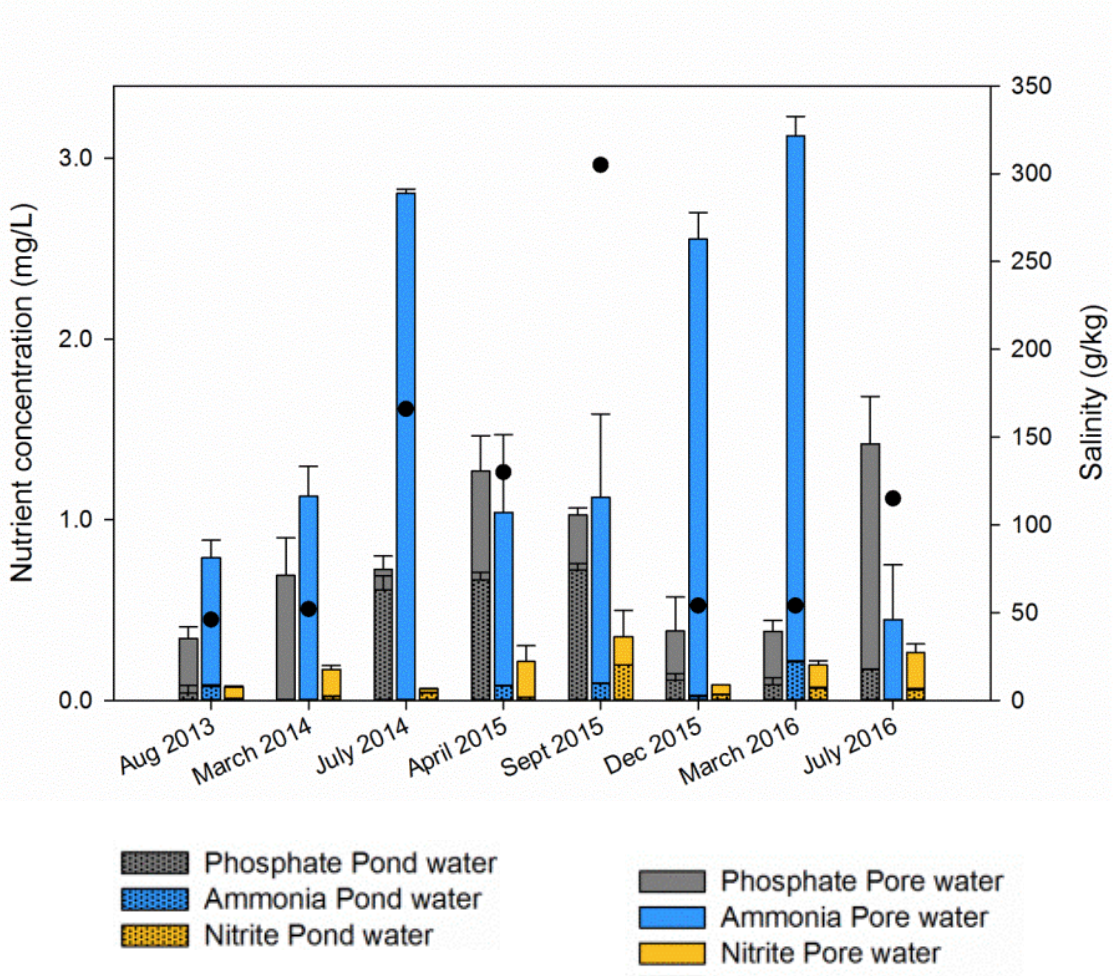

Figure 4.5. Nutrient concentrations in Salt Pond. Y-axis represents the concentration (mg L^{-1}) of each nutrient, Phosphate (grey), Ammonia (blue), and Nitrite (yellow), in pore and pond (shaded bars) water. Second y-axis to the right side shows the salinity (black dot, g kg^{-1}) measured at each time point. X-axis shows the time of sampling (month and year). Nutrient concentration values represent the average (n=3), with standard deviations.

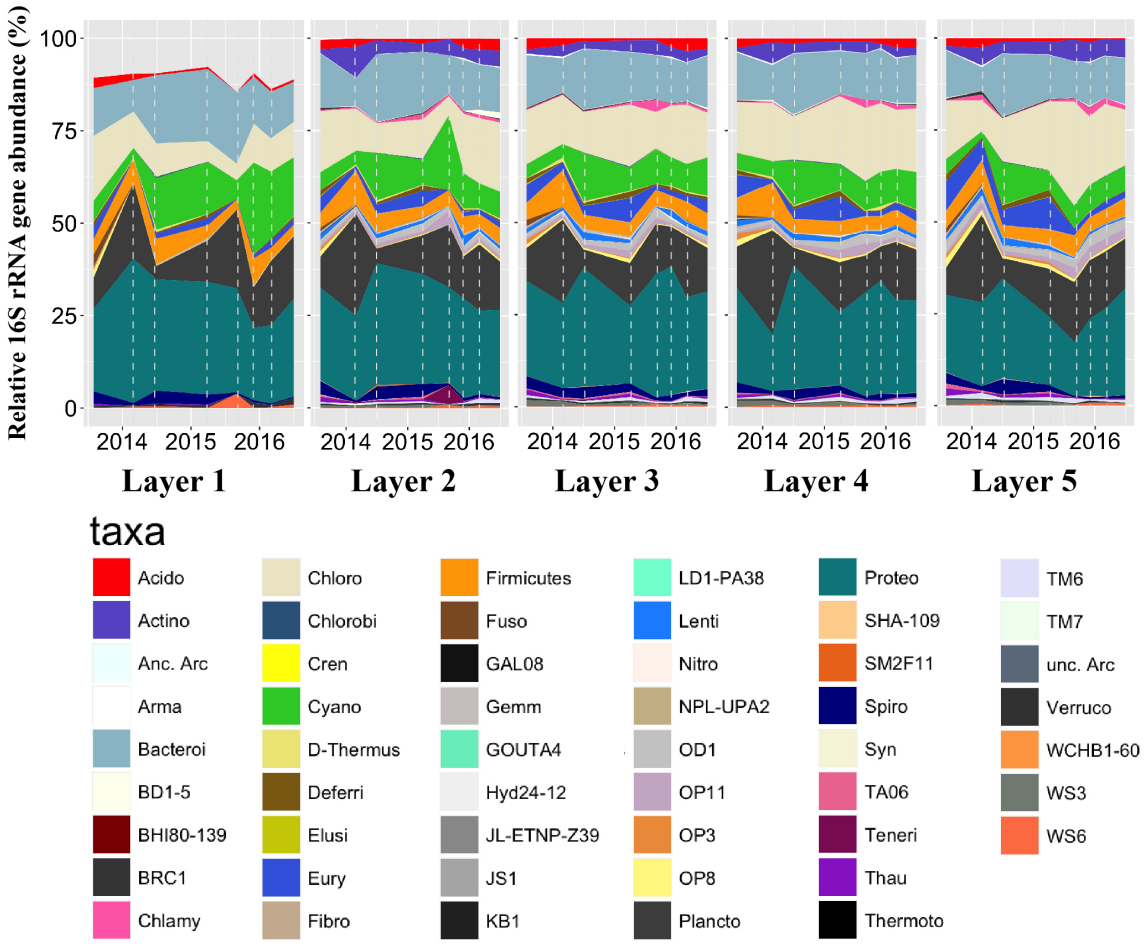

Figure 4.6. Microbial community composition over the course of the study (white dashed line in graph indicates time point) in each layer (1-5). Sequence hits were sorted by taxonomic classification on phyla level of all Archaea and bacteria 16S rRNA genes and mean relative abundance was calculated (y-axis, n=3).

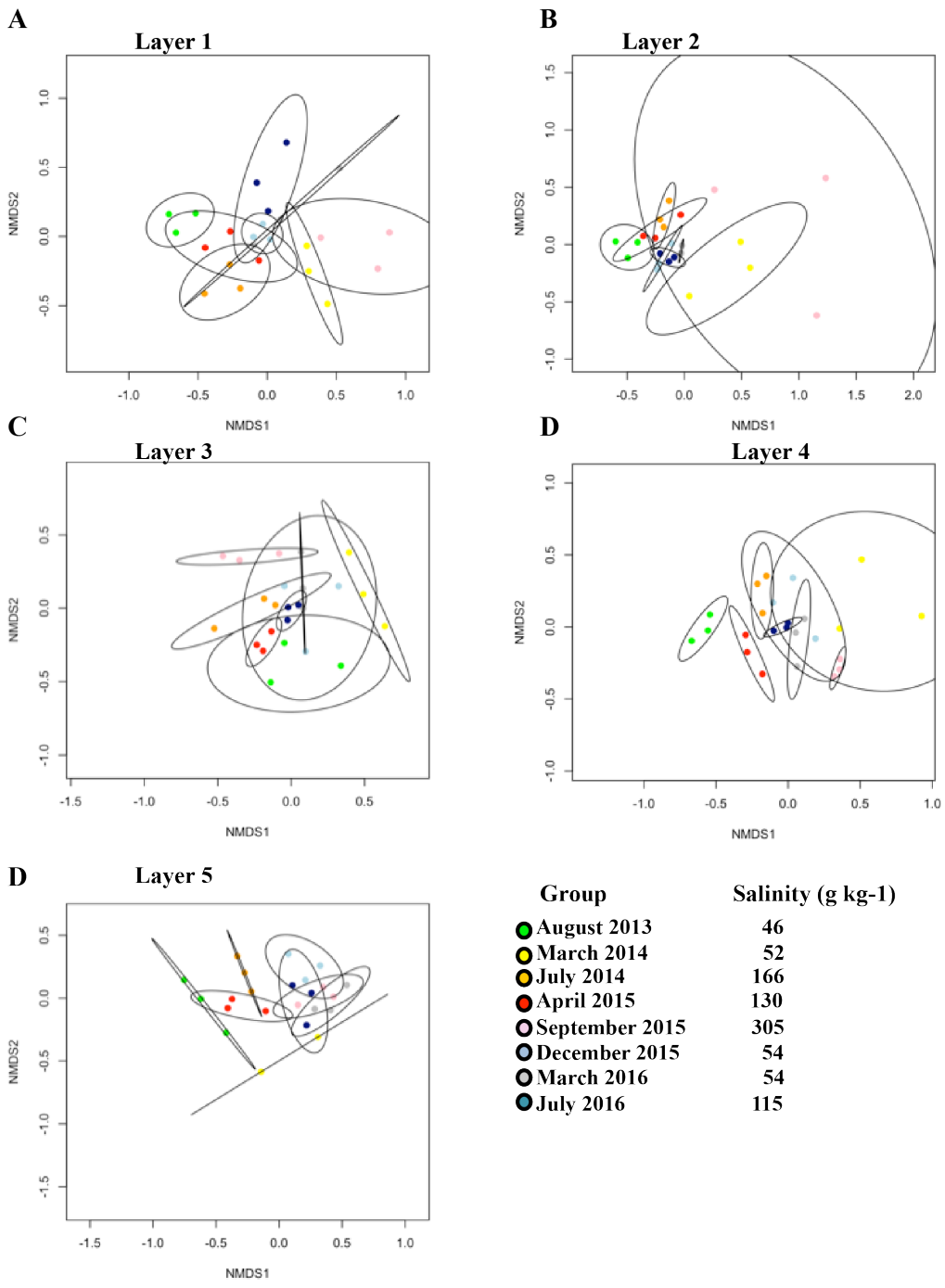

Figure 4.7. Non-metric multidimensional scaling (NMDS) ordination plot of Bray-Curtis community dissimilarities based on taxonomy of 16S rRNA gene pulled out from the metagenome. NMDS plots show microbial mat community at each individual time point in the different layers of the mat (layer1 – 5). Each dot represents an area of ~ 39.5 cm^2 microbial mat. Ellipsoids are defined by a 95% confidence interval surrounding each group.

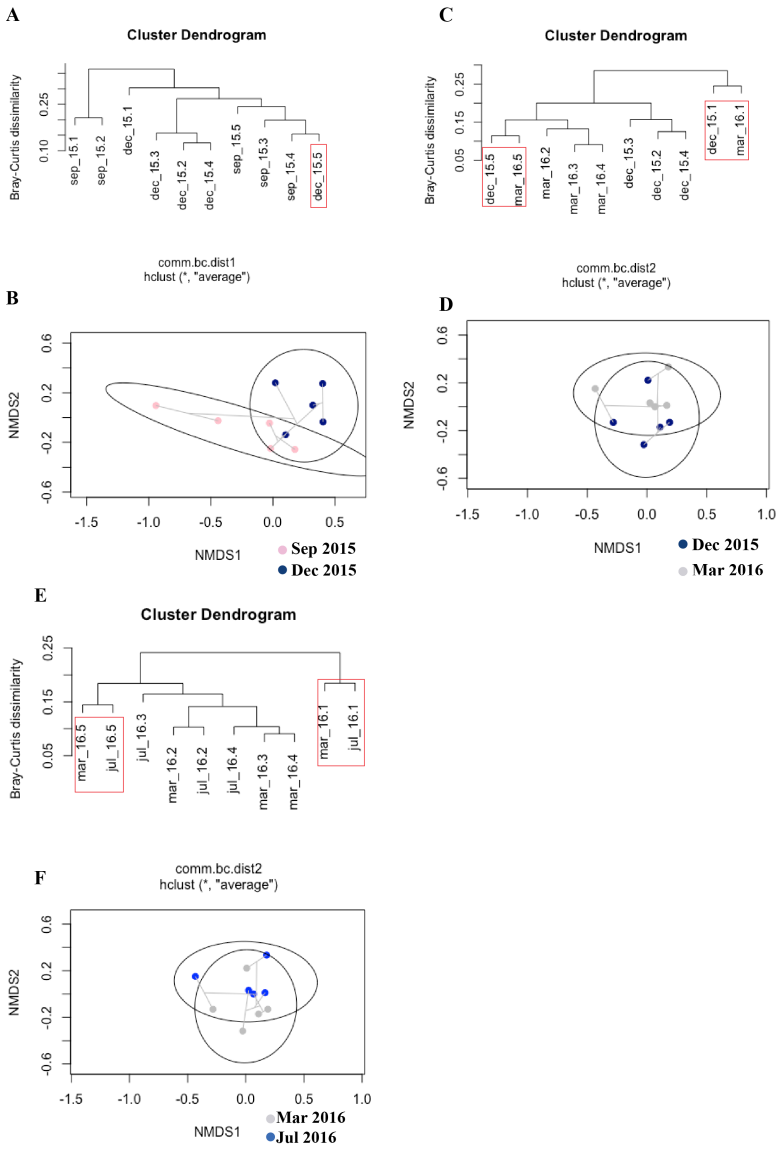

Figure 4.8. Beta diversity analysis of taxonomic classification based on class level. Bray-Curtis dissimilarities were visualized using cluster dendograms (**A**, **C**, and **E**) and NMDS plots (**B**, **D**, and **F**) for the pre-post hurricane time points (September 2015 and December 2015), and the subsequent two time points (March 2016, and July 2016).

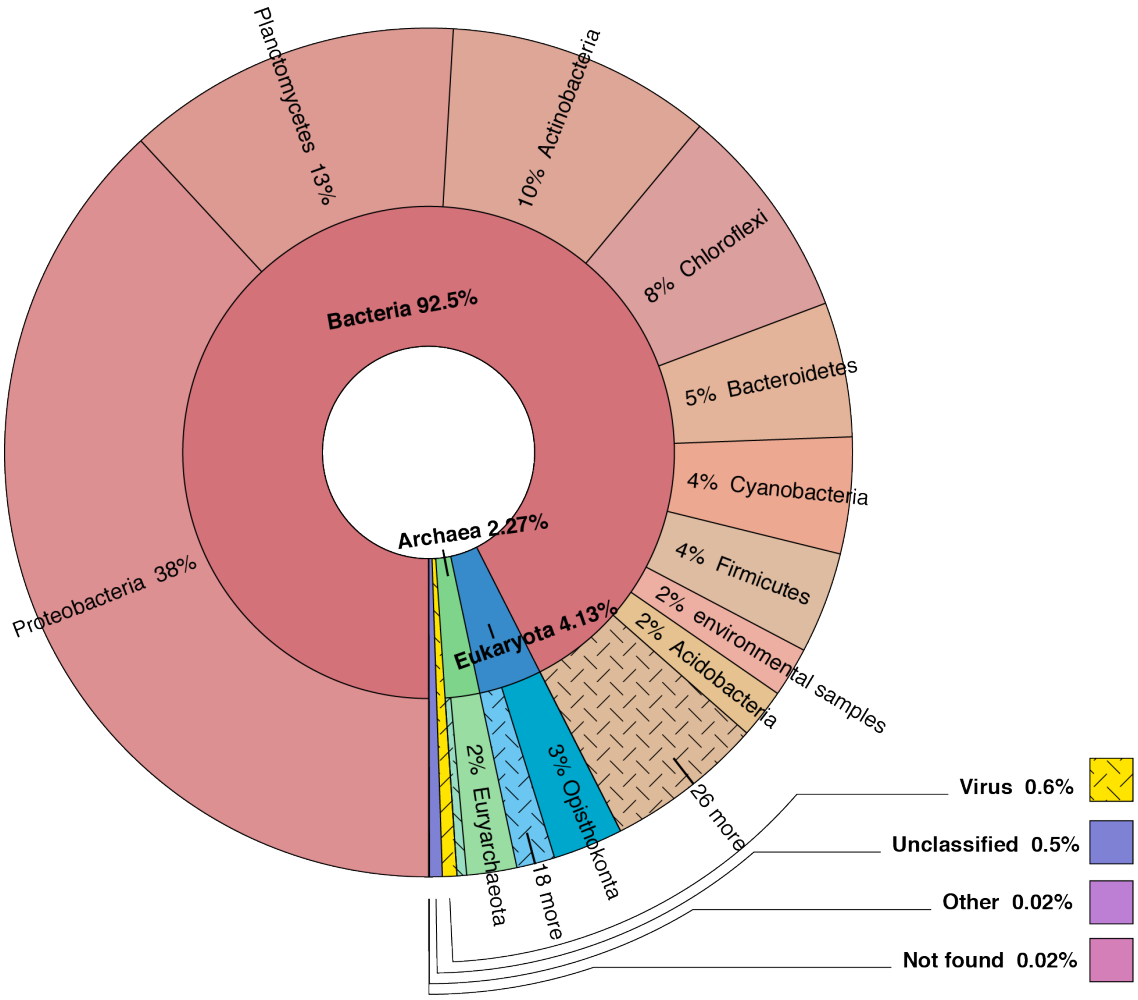

Figure 4.9. Krona graphical representation of the relative percentage of bases from the assembly belonging to the different lineages, Archaea, Bacteria, Eukaryota, Viruses, Unclassified sequences, as well as Other sequences, and sequences not found in the database.

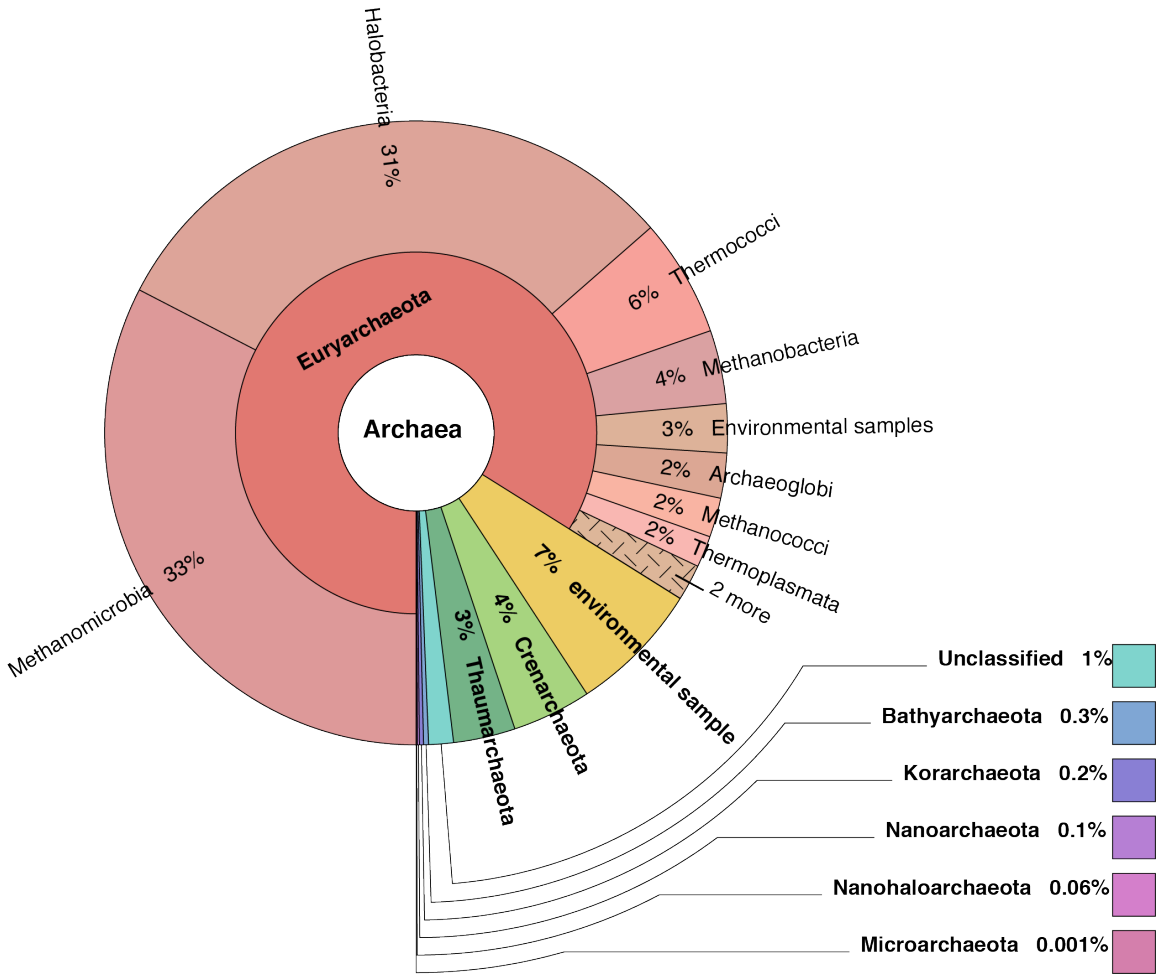

Figure 4.10. Archaea lineage: Breakdown of bases from assembly based on phyla and class level.

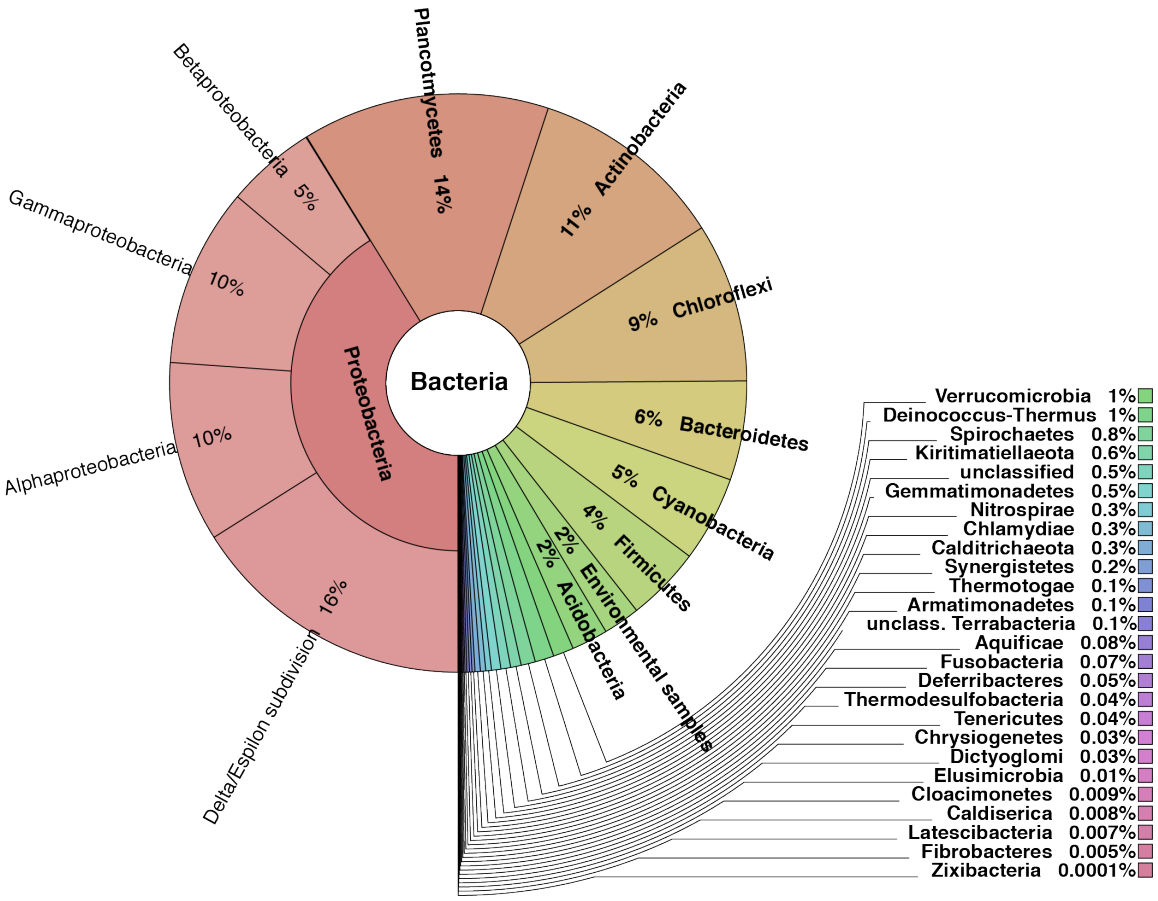

Figure 4.11. Bacteria lineage: Breakdown of bases from assembly based on phyla and class level.

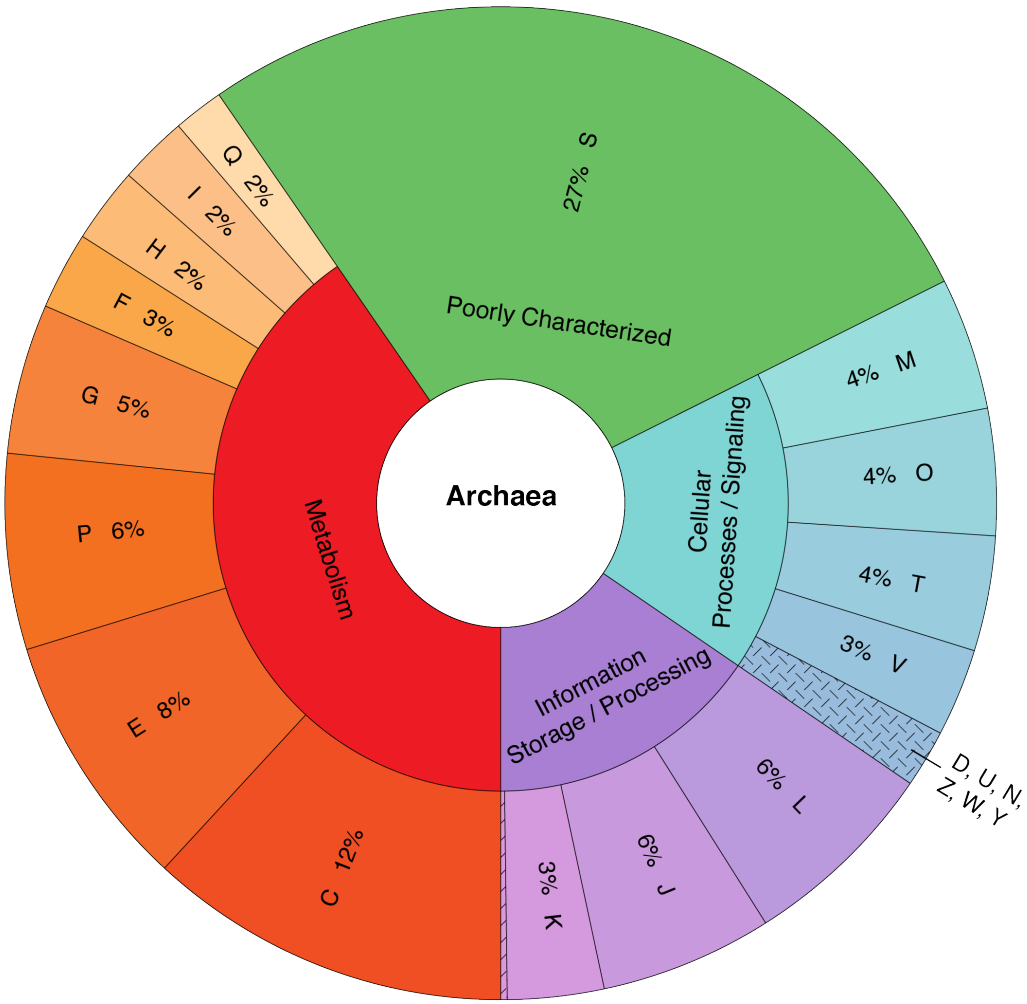

Information Storage and Processing
A RNA processing and modification
B Chromatin structure and dynamics
J Transaltion, ribosomal structure and biogenesis
K Transcription
L Replication, recombination and repair

Metabolism
H Coenzyme transport and metabolism
I Lipid transport and Metabolism
D Cell cycle control, cell division, chromosome partitioning
F Nucleotide transport and metabolism
E Amino acid transport and metabolism
Q Secondary metabolites biosynthesis, transport & catabolism
C Energy production and conversion
P Inorganic ion transport and metabolism
G Carbohydrate transport and metabolism

Cellular Processes and Signaling
M Cell wall/membrane/envelope biogenesis
N Cell motility
O Posttranslational modification, protein turnover, chaperons
T Signal transduction metabolism
U Intracellular trafficking, secretion, and vesicular transport
V Defese mechanism
W Extracellular structures
Y Nuclear structure
Z Cytoskeleton

Poorly Characterized
S Function unknown

Figure 4.12. Prodigal called genes (amino acid sequences) from overall archaea metagenomic assembly that were annotated through eggNOG (Huerta-Cepas *et al.*, 2016). Orthologous groups were annotated based on functional categories using the Clusters of Orthologous Groups (COG) protein database.

Information Storage and Processing

A RNA processing and modification
B Chromatin structure and dynamics
J Transaltion, ribosomal structure and biogenesis
K Transcription
L Replication, recombination and repair

Metabolism

H Coenzyme transport and metabolism
I Lipid transport and Metabolism
D Cell cycle control, cell division, chromosome partitioning
F Nucleotide transport and metabolism
E Amino acid transport and metabolism
Q Secondary metabolites biosynthesis, transport & catabolism
C Energy production and conversion
P Inorganic ion transport and metabolism
G Carbohydrate transport and metabolism

Cellular Processes and Signaling

M Cell wall/membrane/envelope biogenesis
N Cell motility
O Posttranslational modification, protein turnover, chaperons
T Signal transduction metabolism
U Intracellular trafficking, secretion, and vesicular transport
V Defese mechanism
W Extracellular structures
Y Nuclear structure
Z Cytoskeleton

Poorly Characterized

S Function unknown

Figure 4.13. Prodigal called genes (amino acid sequences) from overall bacteria metagenomic assembly that were annotated through eggNOG (Huerta-Cepas *et al.*, 2016). Orthologous groups were annotated based on functional categories using the Clusters of Orthologous Groups (COG) protein database.

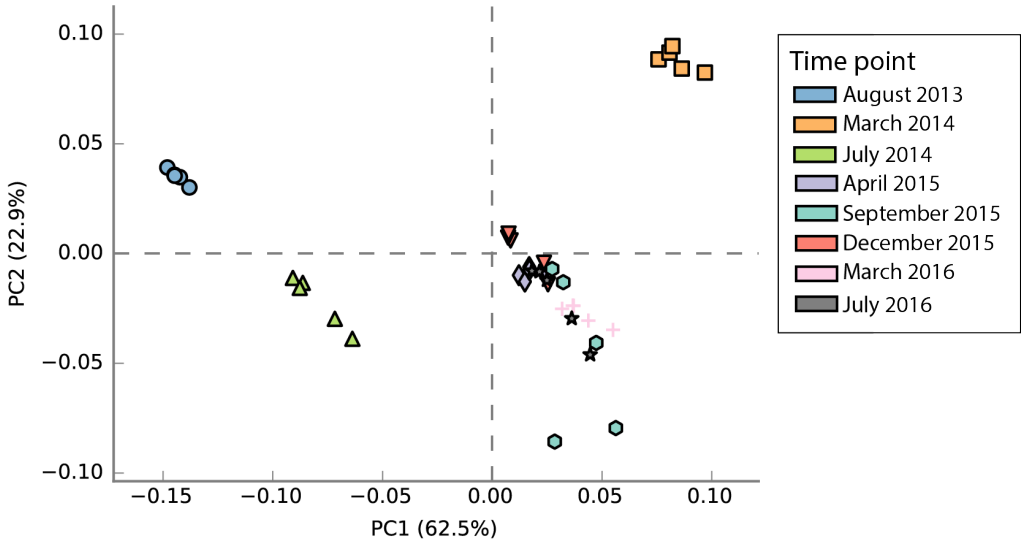

Figure 4.14. Principal component analysis (PCA) plot comparing functional profiles for Archaea between time points (for each time point, n=5) using STAMP.

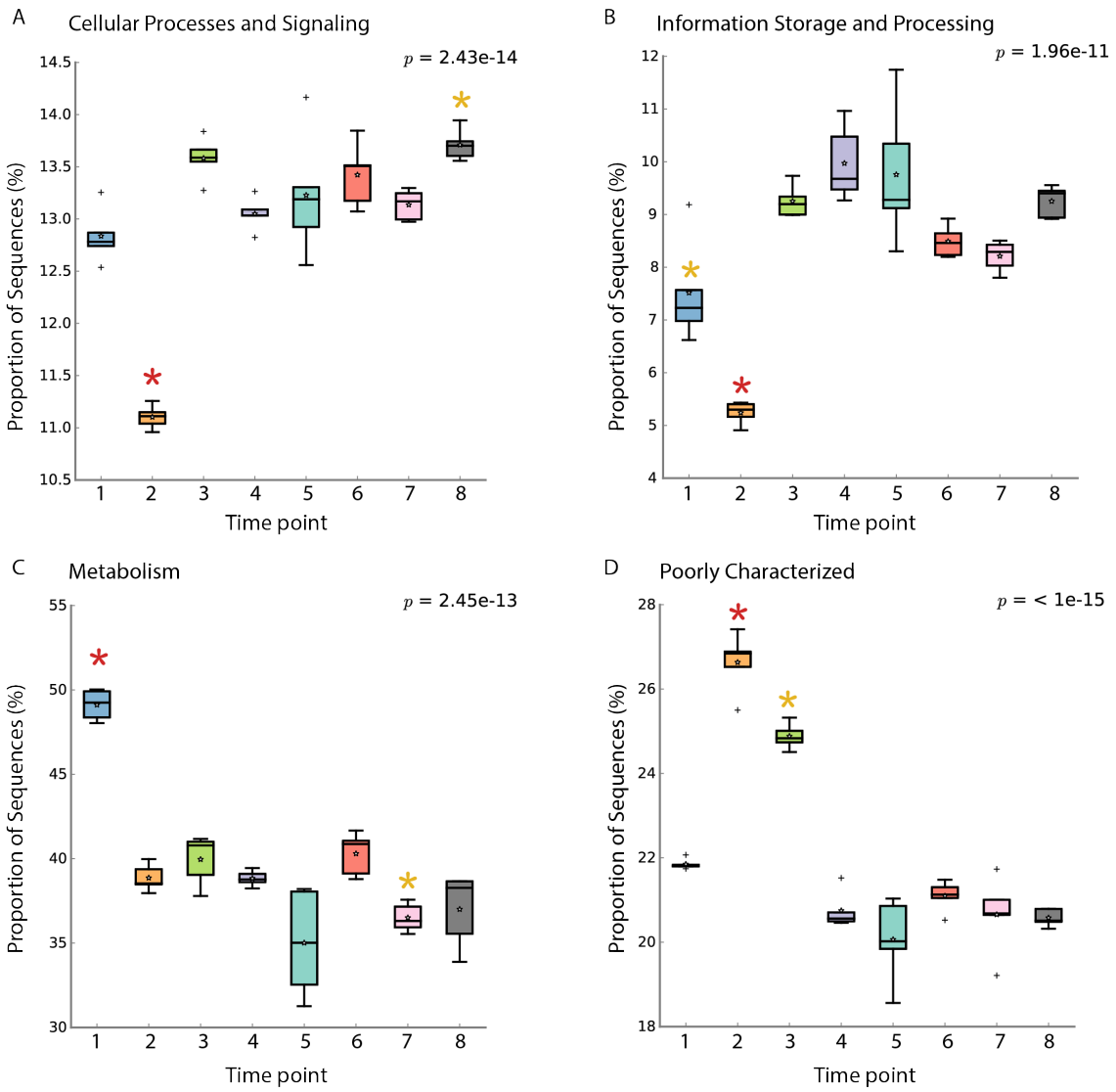

Figure 4.15. Analysis of variance comparison of Archaea assigned COG categories between time points (August 2013 – July 2016). Boxplots of proportion of Sequences (Archaea genes) that were assigned to a specific COG category for each time point (n = 15). COG Categories: **A** Cellular Processes and Signaling, **B** Information Storage and Processing, **C** Metabolism, and **D** Poorly Characterized. * indicates significant difference ($p<0.01$) of that time point to all other time points, * indicates significant difference ($p<0.01$) of that time point to at least 3 other time points.

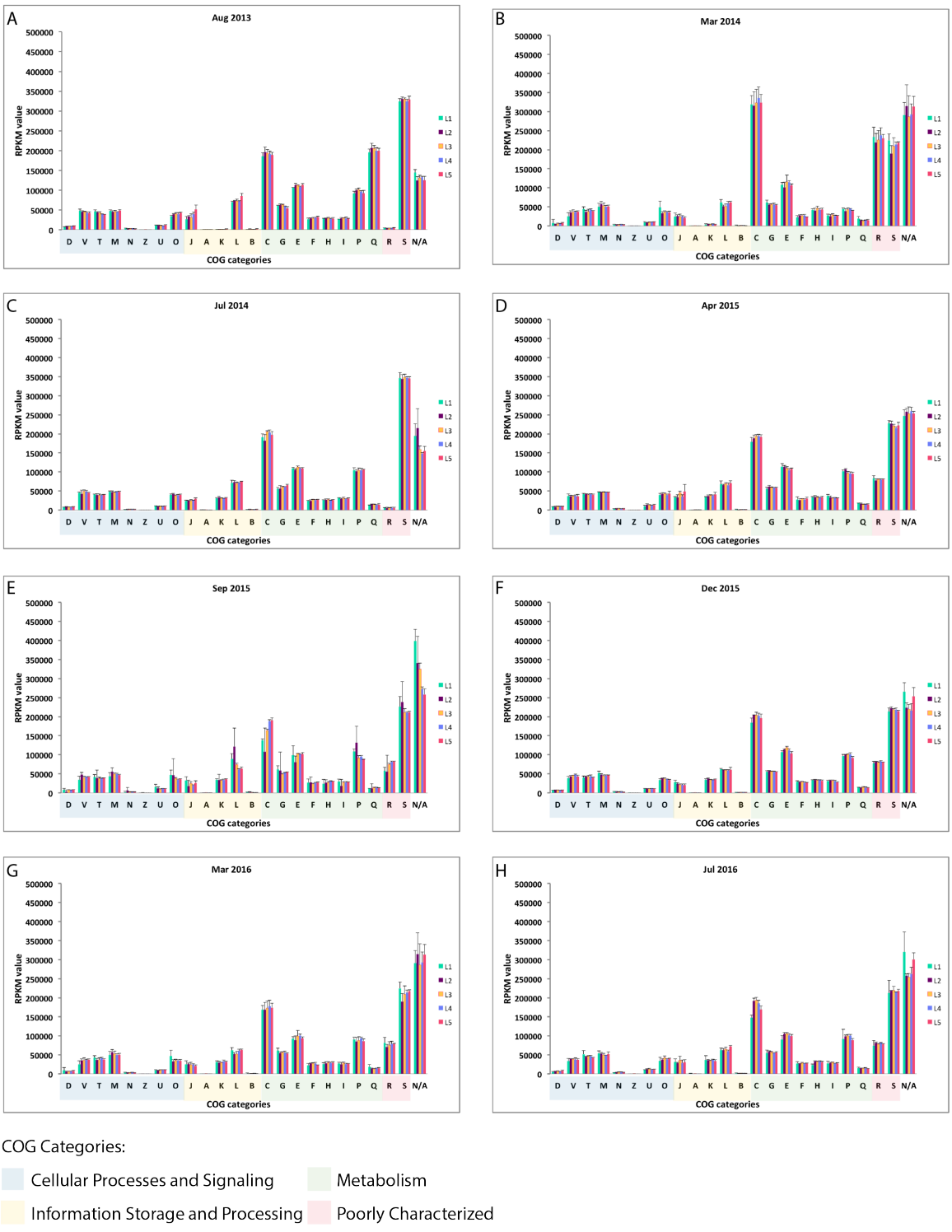

Figure 4.16. Archaea comparison of protein functions based on COG categories in different layers and over time. Y-axis shows the reads per kilobase million (RPKM value) of each layer with its standard deviation (layer 1-5, n=3) for the different functions of the COG categories (x-axis) for each time point (**A** – **H**).

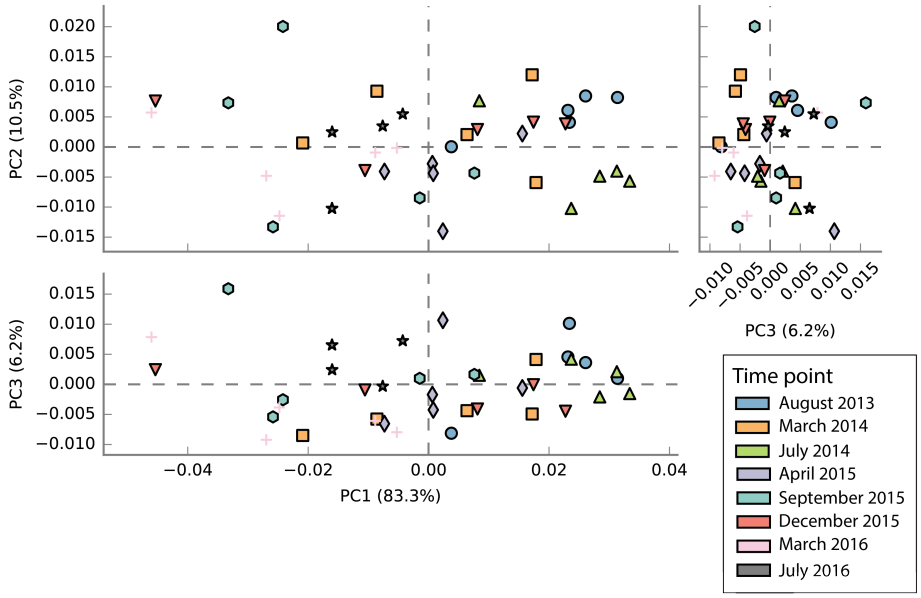

Figure 4.17. Principal component analysis (PCA) plot comparing functional profiles for Bacteria between time points (for each time point, n=5) using STAMP.

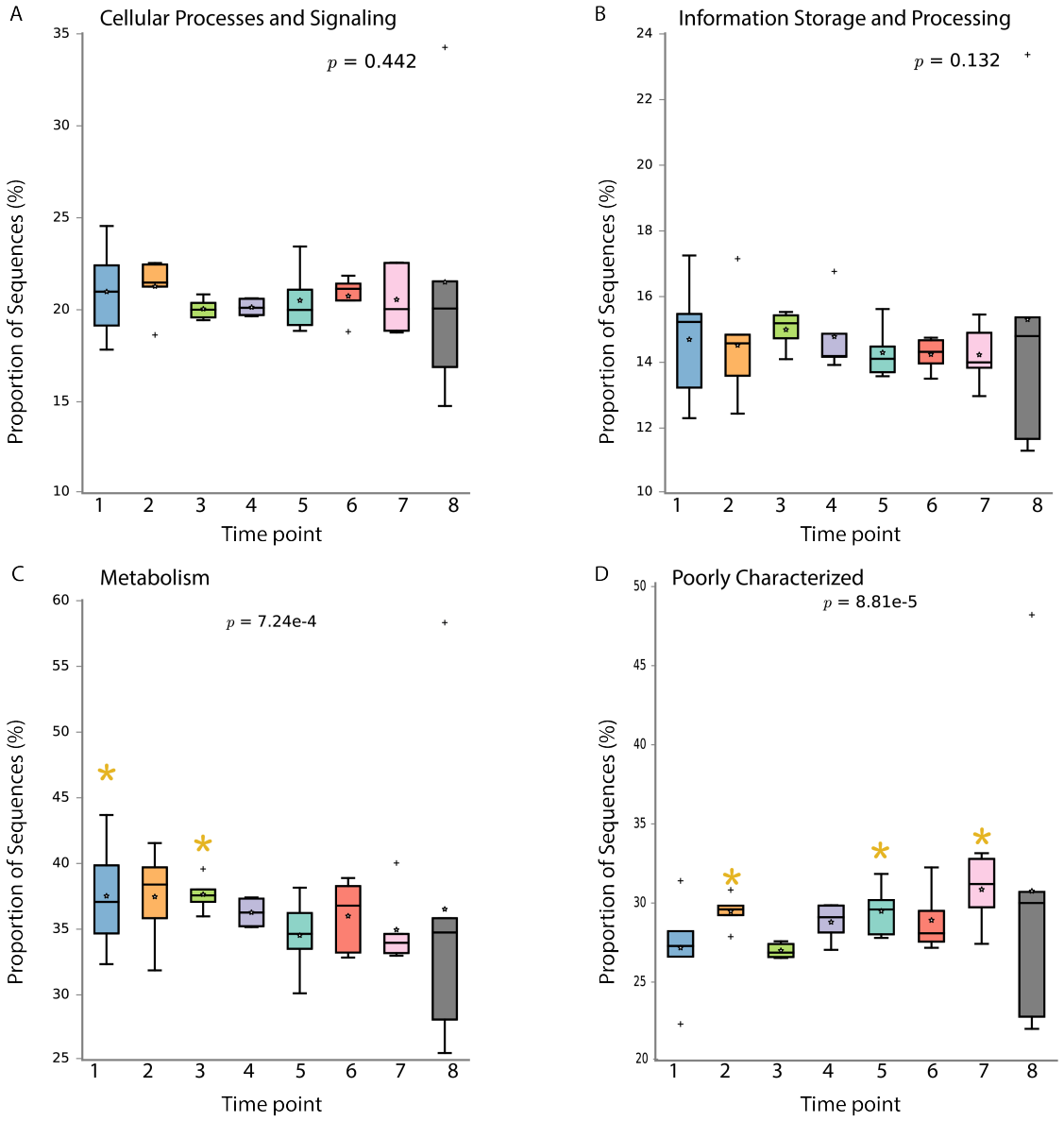

Figure 4.18. Analysis of variance comparison of Bacteria assigned COG categories between time points (August 2013 – July 2016). Boxplots of proportion of Sequences (Bacteria genes) that were assigned to a specific COG category for each time point (n = 15). COG Categories: **A** Cellular Processes and Signaling, **B** Information Storage and Processing, **C** Metabolism, and **D** Poorly Characterized. * indicates significant difference ($p<0.05$) of that time point to at least 2 other time points.

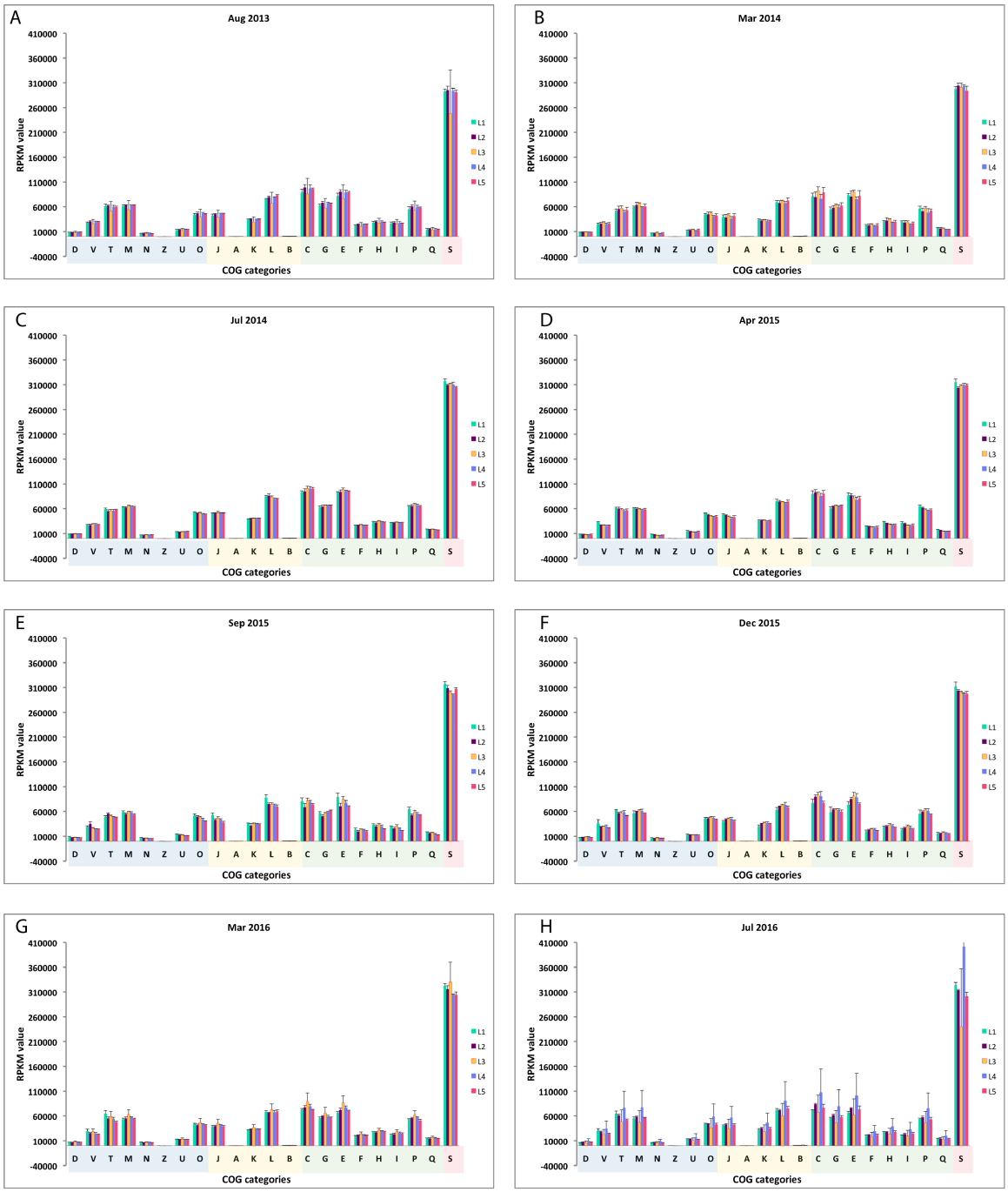

Figure 4.19. Bacteria comparison of protein functions based on COG categories in different layers and over time. Y-axis shows the reads per kilobase million (RPKM value) of each layer with its standard deviation (layer 1-5, n=3) for the different functions of the COG categories (x-axis) for each time point (**A** – **H**).

CHAPTER 5

CONCLUSION

The microbial mat ecosystem of Salt Pond on San Salvador Island, The Bahamas, investigated in this study showed compositional variation depending on the location of the mat within the pond. Near and far shore mats were found to be in different growth cycles with two distinct phototrophic communities. This study revealed that there is a need to stay in the same location of the pond when collecting samples for comparative studies over time.

The microbial mat examined in this study is located within a coastal lagoon ecosystem that experiences routine but wide ranging seasonal variation in environmental conditions. The extensive variability of this system may select for a highly diverse microbial community that provides ecosystem stability following weather-driven disturbances. The ecosystem-level pulse disturbance generated by Hurricane Irene significantly reduced local salinity by 72%, subsequently resulting in Archaea to Bacterial domain shifts. Detailed analysis of this broader trend showed significant shifts among taxa within rare and abundant archaeal and bacterial populations, with less than 1% of taxa remaining abundant. In both archaeal and bacterial communities, the majority of taxa had low PSP across salinities; however, post-disturbance samples showed an increase in the overall microbial mat community PSP, with significant shifts occurring among abundant and rare taxa across and within phyla. While changes in the abundance

and PSP of specific taxa can not be linked to individual biogeochemical processes, overall post-disturbance shifts in community structure enhanced expression of genes involved in N and S cycling. Together, these data show the compositional and functional sensitivity of a microbial mat ecosystem to environmental change but also suggest that rare taxa provide a reservoir of genetic diversity that may enhance the functional flexibility of the ecosystem following environmental disturbances. This is one of the first studies to address how disturbance affects the complex links between microbial diversity and ecosystem processes within hypersaline microbial mat ecosystems, to further defining the ecological principles a more detailed study over the course of four years including eight time points was done. In this study a comparative metagenomic approach was used to address community compositional changes, community resistance, stability and resilience to environmental seasonal and pulse disturbance. Functional annotation of archaeal and bacterial metagenomes were used to address the response of ecosystem function to environmental disturbance. Findings suggest that similar to our previous study, the time frame of one year was not enough for the community of the first four layers to return to its pre-disturbed state. However, the deepest layer showed resistant to environmental disturbance and did not significantly change in community composition. Functional analysis of the metagenome indicated that there was a response to seasonal and pulse disturbance for bacterial and archaeal genes. For aechaeal functional genes, the vertical distribution in the microbial mat was more homogeneous for all time points, while for bacteria functional genes, layer 1, 2 and 5 showed significant changes in gene abundance suggesting stratification within the mat. Significant increases in abundance of archaeal and bacterial functional genes within the metabolism group after the pulse

disturbance suggest that they likely have a much more important role in microbial genome response to perturbation events.

REFERENCES

Aanderud ZT, Jones SE, Fierer N, Lennon JT. (2015). Resuscitation of the rare biosphere contributes to pulses of ecosystem activity. *Front Microbiol* **6**: 24.

Aanderud ZT, Vert JC, Lennon JT, Magnusson TW, Breakwell DP, Harker AR. (2016). Bacterial dormancy is more prevalent in freshwater than hypersaline lakes. *Front Microbiol* **7**. e-pub ahead of print, doi: 10.3389/fmicb.2016.00853.

Afiahayati, Sato K, Sakakibara Y. (2015). MetaVelvet-SL: an extension of the Velvet assembler to a de novo metagenomic assembler utilizing supervised learning. *DNA Res* **22**: 69–77.

Agrawal AA. (2001). Phenotypic Plasticity in the Interactions and Evolution of Species. *Science (80-)* **294**: 321–326.

Akob DM, Lee SH, Sheth M, Küsel K, Watson DB, Palumbo A V, *et al.* (2012). Gene Expression Correlates with Process Rates Quantified for Sulfate- and Fe(III)-Reducing Bacteria in U(VI)-Contaminated Sediments. *Front Microbiol* **3**: 280.

Allen MA, Goh F, Burns BP, Neilan BA. (2009). Bacterial, archaeal and eukaryotic diversity of smooth and pustular microbial mat communities in the hypersaline lagoon of Shark Bay. *Geobiology* **7**: 82–96.

Allen TFH, Hoekstra TW. (1992). Toward a unified ecology. Columbia University Press.

Allison SD, Martiny JBH. (2008). Colloquium paper: resistance, resilience, and

redundancy in microbial communities. *Proc Natl Acad Sci U S A* **105 Suppl**: 11512–9.

Altschul SF, Gish W, Miller W, Myers EW, Lipman DJ. (1990). Basic local alignment search tool. *J Mol Biol* **215**: 403–410.

Altschul SF, Madden TL, Schäffer AA, Zhang J, Zhang Z, Miller W, *et al.* (1997). Gapped BLAST and PSI-BLAST: a new generation of protein database search programs. *Nucleic Acids Res* **25**: 3389–402.

Amaral-Zettler LA, Rocca JD, Lamontagne MG, Dennett MR, Gast RJ. (2008). Changes in microbial community structure in the wake of Hurricanes Katrina and Rita. *Environ Sci Technol* **42**: 9072–8.

Auguet J-C, Barberan A, Casamayor EO. (2010). Global ecological patterns in uncultured Archaea. *ISME J* **4**: 182–90.

Avrahami S, Liesack W, Conrad R. (2003). Effects of temperature and fertilizer on activity and community structure of soil ammonia oxidizers. *Environ Microbiol* **5**: 691–705.

Babbin AR, Ward BB. (2013). Controls on nitrogen loss processes in Chesapeake Bay sediments. *Environ Sci Technol* **47**: 4189–4196.

Bak F, Cypionka H. (1987). A novel type of energy metabolism involving fermentation of inorganic sulphur compounds. *Nature* **326**: 891–892.

Balmonte JP, Arnosti C, Underwood S, McKee BA, Teske A. (2016). Riverine Bacterial Communities Reveal Environmental Disturbance Signatures within the Betaproteobacteria and Verrucomicrobia. *Front Microbiol* **7**: 1441.

Bateson MM, Ward DM. (1988). Photoexcretion and fate of glycolate in a hot spring cyanobacterial mat. *Appl Environ Microbiol* **54**: 1738–43.

Baumgartner LK, Reid RP, Dupraz C, Decho AW, Buckley DH, Spear JR, *et al.* (2006). Sulfate reducing bacteria in microbial mats: Changing paradigms, new discoveries. *Sediment Geol* **185**: 131–145.

Beman JM, Chow C-E, King AL, Feng Y, Fuhrman JA, Andersson A, *et al.* (2011). Global declines in oceanic nitrification rates as a consequence of ocean acidification. *Proc Natl Acad Sci* **108**: 208–213.

Benlloch S, Lopez-Lopez A, Casamayor EO, Ovreas L, Goddard V, Daae FL, *et al.* (2002). Prokaryotic genetic diversity throughout the salinity gradient of a coastal solar saltern. *Environ Microbiol* **4**: 349–360.

Benlloch S, RodrÃ-guez-Valera F, Martinez-Murcia AJ. (1995). Bacterial diversity in two coastal lagoons deduced from 16S rDNA PCR amplification and partial sequencing. *FEMS Microbiol Ecol* **18**: 267–279.

Berga M, Székely AJ, Langenheder S. (2012). Effects of disturbance intensity and frequency on bacterial community composition and function. *PLoS One* **7**: e36959.

Bernhard AE, Landry ZC, Blevins A, de la Torre JR, Giblin AE, Stahl DA. (2010). Abundance of ammonia-oxidizing archaea and bacteria along an estuarine salinity gradient in relation to potential nitrification rates. *Appl Environ Microbiol* **76**: 1285–9.

Blankenship RE, Olson JM, Miller M. (1995). Antenna Complexes from Green Photosynthetic Bacteria. In: *Anoxygenic Photosynthetic Bacteria*. Kluwer Academic Publishers: Dordrecht, pp 399–435.

Blazewicz SJ, Barnard RL, Daly RA, Firestone MK. (2013). Evaluating rRNA as an indicator of microbial activity in environmental communities: limitations and uses. *ISME J* **7**: 2061–2068.

Boujelben I, Gomariz M, Martínez-García M, Santos F, Peña A, López C, *et al.* (2012). Spatial and seasonal prokaryotic community dynamics in ponds of increasing salinity of Sfax solar saltern in Tunisia. *Antonie Van Leeuwenhoek* **101**: 845–57.

Bowen JL, Babbin AR, Kearns PJ, Ward BB. (2014). Connecting the dots: linking nitrogen cycle gene expression to nitrogen fluxes in marine sediment mesocosms. *Front Microbiol* **5**: 429.

Bowen JL, Ward BB, Morrison HG, Hobbie JE, Valiela I, Deegan LA, *et al.* (2011). Microbial community composition in sediments resists perturbation by nutrient enrichment. *ISME J* **5**: 1540–8.

Braithwaite CJR, Whitton BA. (1987). Gypsum and halite associated with the cyanobacterium Entophysalis. *Geomicrobiol J* **5**: 43–55.

Brochier-Armanet C, Boussau B, Gribaldo S, Forterre P. (2008). Mesophilic Crenarchaeota: proposal for a third archaeal phylum, the Thaumarchaeota. *Nat Rev Microbiol* **6**: 245–52.

Brocke HJ, Wenzhoefer F, de Beer D, Mueller B, van Duyl FC, Nugues MM. (2015). High dissolved organic carbon release by benthic cyanobacterial mats in a Caribbean reef ecosystem. *Sci Rep* **5**: 8852.

Brown M, Fuhrman J. (2005). Marine bacterial microdiversity as revealed by internal transcribed spacer analysis. *Aquat Microb Ecol* **41**: 15–23.

Bru D, Ramette A, Saby NPA, Dequiedt S, Ranjard L, Jolivet C, *et al.* (2011). Determinants of the distribution of nitrogen-cycling microbial communities at the landscape scale. *ISME J* **5**: 532–42.

Buckling A, Kassen R, Bell G, Rainey PB. (2000). Disturbance and diversity in

experimental microcosms. *Nature* **408**: 961–964.

Bushnell B. (2015). BBMap. sourceforge.net/projects/bbmap/.

Canfield D, Des Marais D. (1991). Aerobic sulfate reduction in microbial mats. *Science (80-)* **251**: 1471–1473.

Canfora L, Bacci G, Pinzari F, Lo Papa G, Dazzi C, Benedetti A, *et al.* (2014). Salinity and bacterial diversity: to what extent does the concentration of salt affect the bacterial community in a saline soil? Ibekwe AM (ed). *PLoS One* **9**: e106662.

Caumette P, Baulaigue R, Matheron R. (1988). Characterization of Chromatium salexigens sp. nov., a Halophilic Chromatiaceae Isolated from Mediterranean Salinas. *Syst Appl Microbiol* **10**: 284–292.

Chen L, Hu M, Huang L, Hua Z, Kuang J, Li S, *et al.* (2015). Comparative metagenomic and metatranscriptomic analyses of microbial communities in acid mine drainage. *ISME J* **9**: 1579–1592.

Chen YB, Dominic B, Mellon MT, Zehr JP. (1998). Circadian rhythm of nitrogenase gene expression in the diazotrophic filamentous nonheterocystous cyanobacterium Trichodesmium sp. strain IMS 101. *J Bacteriol* **180**: 3598–605.

Church MJ, Short CM, Jenkins BD, Karl DM, Zehr JP. (2005). Temporal Patterns of Nitrogenase Gene (nifH) Expression in the Oligotrophic North Pacific Ocean. *Appl Environ Microbiol* **71**: 5362–5370.

Claire Horner-Devine M, Leibold MA, Smith VH, Bohannan BJM. (2003). Bacterial diversity patterns along a gradient of primary productivity. *Ecol Lett* **6**: 613–622.

Cohen Y, Castenholz R, Halvorson H. (1984). No Title. New York, NY.

Cohen Y, Rosenberg E, American Society for Microbiology., Batsheva de Rothschild

Foundation for the Advancement of Science in Israel. (1989). Microbial mats : physiological ecology of benthic microbial communities. American Society for Microbiology.

Colón-López MS, Sherman DM, Sherman LA. (1997). Transcriptional and translational regulation of nitrogenase in light-dark- and continuous-light-grown cultures of the unicellular cyanobacterium Cyanothece sp. strain ATCC 51142. *J Bacteriol* **179**: 4319–27.

Comte J, del Giorgio PA. (2009). Links between resources, C metabolism and the major components of bacterioplankton community structure across a range of freshwater ecosystems. *Environ Microbiol* **11**: 1704–1716.

Coveley S, Elshahed MS, Youssef NH. (2015). Response of the rare biosphere to environmental stressors in a highly diverse ecosystem (Zodletone spring, OK, USA). *PeerJ* **3**: e1182.

Cutler NA, Arróniz-Crespo M, Street LE, Jones DL, Chaput DL, DeLuca TH. (2017). Long-Term Recovery of Microbial Communities in the Boreal Bryosphere Following Fire Disturbance. *Microb Ecol* **73**: 75–90.

Cypionka H. (1995). Solute Transport and Cell Energetics. In: *Sulfate-Reducing Bacteria*. Springer US: Boston, MA, pp 151–184.

D'Amelio ED, Des Marais DJ, Cohen J. (1989). Comparative functional ultrastructure of two hypersaline submerged cyanobacterial mats - Guerrero Negro, Baja California Sur, Mexico, and Solar Lake, Sinai, Egypt. https://ntrs.nasa.gov/search.jsp?R=19890057883 (Accessed April 20, 2018).

Decho A. (1990). Microbial exopolymer secretions in ocean environments: their role (s) in food webs and marine processes. *Ocean Mar Biol Annu Rev* **28**: 73–153.

DeLong EF, Wickham GS, Pace NR. (1989). Phylogenetic stains: ribosomal RNA-based probes for the identification of single cells. *Science* **243**: 1360–3.

Denef VJ, Fujimoto M, Berry MA, Schmidt ML. (2016). Seasonal Succession Leads to Habitat-Dependent Differentiation in Ribosomal RNA:DNA Ratios among Freshwater Lake Bacteria. *Front Microbiol* **7**: 606.

Desnues C, Michotey VD, Wieland A, Zhizang C, Fourçans A, Duran R, *et al.* (2007). Seasonal and diel distributions of denitrifying and bacterial communities in a hypersaline microbial mat (Camargue, France). *Water Res* **41**: 3407–3419.

Dick GJ, Andersson AF, Baker BJ, Simmons SL, Thomas BC, Yelton AP, *et al.* (2009). Community-wide analysis of microbial genome sequence signatures. *Genome Biol* **10**: R85.

Dillon JG, Carlin M, Gutierrez A, Nguyen V, McLain N. (2013). Patterns of microbial diversity along a salinity gradient in the Guerrero Negro solar saltern, Baja CA Sur, Mexico. *Front Microbiol* **4**: 399.

Dixon P. (2003). VEGAN, a package of R functions for community ecology. *J Veg Sci* **14**: 927–930.

Dubinin A V., V. GM, Gerasimenko L. M. (1992). Physiological features of a strain of Microcoleus chthonoplastes from a hypersaline reservoir. *Mikrobiol (English Transl* 47–51.

Dupraz C, Visscher PT. (2005). Microbial lithification in marine stromatolites and hypersaline mats. *Trends Microbiol* **13**: 429–438.

Edwards U, Rogall T, Blöcker H, Emde M, Böttger EC. (1989). Isolation and direct complete nucleotide determination of entire genes. Characterization of a gene coding for 16S ribosomal RNA. *Nucleic Acids Res* **17**: 7843–53.

Eloe EA, Fadrosh DW, Novotny M, Zeigler Allen L, Kim M, Lombardo M-J, *et al.* (2011). Going Deeper: Metagenome of a Hadopelagic Microbial Community Rodriguez-Valera F (ed). *PLoS One* **6**: e20388.

Falkowski PG. (1997). Evolution of the nitrogen cycle and its influence on the biological sequestration of CO2 in the ocean. *Nature* **387**: 272–275.

Falkowski PG, Fenchel T, Delong EF. (2008). The microbial engines that drive Earth's biogeochemical cycles. *Science* **320**: 1034–9.

Fan H, Bolhuis H, Stal LJ. (2015). Drivers of the dynamics of diazotrophs and denitrifiers in North Sea bottom waters and sediments. *Front Microbiol* **6**: 738.

Feazel LM, Spear JR, Berger AB, Harris JK, Frank DN, Ley RE, *et al.* (2008). Eucaryotic diversity in a hypersaline microbial mat. *Appl Environ Microbiol* **74**: 329–32.

Fegatella F, Lim J, Kjelleberg S, Cavicchioli R. (1998). Implications of rRNA operon copy number and ribosome content in the marine oligotrophic ultramicrobacterium Sphingomonas sp. strain RB2256. *Appl Environ Microbiol* **64**: 4433–8.

Fenchel T. (1998). Formation of laminated cyanobacterial mats in the absence of benthic fauna. *Aquat Microb Ecol* **14**: 235–240.

Fierer N, Allen AS, Schimel JP, Holden PA. (2003). Controls on microbial CO2 production: a comparison of surface and subsurface soil horizons. *Glob Chang Biol* **9**: 1322–1332.

Francis CA, Beman JM, Kuypers MMM. (2007). New processes and players in the

nitrogen cycle: the microbial ecology of anaerobic and archaeal ammonia oxidation. *ISME J* **1**: 19–27.

Francis CA, Roberts KJ, Beman JM, Santoro AE, Oakley BB. (2005). Ubiquity and diversity of ammonia-oxidizing archaea in water columns and sediments of the ocean. *Proc Natl Acad Sci U S A* **102**: 14683–8.

Franks J, Stolz JF. (2009). Flat laminated microbial mat communities. *Earth-Science Rev* **96**: 163–172.

Fraterrigo JM, Rusak JA. (2008). Disturbance-driven changes in the variability of ecological patterns and processes. *Ecol Lett* **11**: 756–70.

Fuhrman JA. (2009). Microbial community structure and its functional implications. *Nature* **459**: 193–199.

Galand PE, Casamayor EO, Kirchman DL, Lovejoy C. (2009). Ecology of the rare microbial biosphere of the Arctic Ocean. *Proc Natl Acad Sci U S A* **106**: 22427–32.

van Gemerden H. (1993). Microbial mats: A joint venture. *Mar Geol* **113**: 3–25.

van Gemerden H. (1980). Survival of Chromatium vinosum at low light intensities. *Arch Microbiol* **125**: 115–121.

Gentile G, Giuliano L, D'Auria G, Smedile F, Azzaro M, De Domenico M, *et al.* (2006). Study of bacterial communities in Antarctic coastal waters by a combination of 16S rRNA and 16S rDNA sequencing. *Environ Microbiol* **8**: 2150–2161.

Glasby TM, Underwood AJ. (1996). Sampling to differentiate between pulse and press perturbations. *Environ Monit Assess* **42**: 241–52.

Gomes NCM, Cleary DFR, Pinto FN, Egas C, Almeida A, Cunha A, *et al.* (2010). Taking root: enduring effect of rhizosphere bacterial colonization in mangroves. *PLoS One* **5**:

e14065.

Green SJ, Blackford C, Bucki P, Jahnke LL, Prufert-Bebout L. (2008). A salinity and sulfate manipulation of hypersaline microbial mats reveals stasis in the cyanobacterial community structure. *ISME J* **2**: 457–70.

Grimm V, Wissel C. (1997). Babel, or the ecological stability discussions: an inventory and analysis of terminology and a guide for avoiding confusion. *Oecologia* **109**: 323–334.

Gu C, Laverman AM, Pallud CE. (2012). Environmental controls on nitrogen and sulfur cycles in surficial aquatic sediments. *Front Microbiol* **3**: 45.

Gubry-Rangin C, Kratsch C, Williams TA, McHardy AC, Embley TM, Prosser JI, *et al.* (2015). Coupling of diversification and pH adaptation during the evolution of terrestrial Thaumarchaeota. *Proc Natl Acad Sci U S A* **112**: 9370–5.

Hallin S, Jones CM, Schloter M, Philippot L. (2009). Relationship between N-cycling communities and ecosystem functioning in a 50-year-old fertilization experiment. *ISME J* **3**: 597–605.

Handelsman J, Rondon MR, Brady SF, Clardy J, Goodman RM. (1998). Molecular biological access to the chemistry of unknown soil microbes: a new frontier for natural products. *Chem Biol* **5**: R245-9.

Harris JK, Caporaso JG, Walker JJ, Spear JR, Gold NJ, Robertson CE, *et al.* (2013). Phylogenetic stratigraphy in the Guerrero Negro hypersaline microbial mat. *ISME J* **7**: 50–60.

Hattori T, Shiba H, Ashiki K, Araki T, Nagashima Y, Yoshimatsu K, *et al.* (2016). Anaerobic Growth of Haloarchaeon Haloferax volcanii by Denitrification Is Controlled

by the Transcription Regulator NarO. *J Bacteriol* **198**: 1077–86.

Häusler S, Weber M, Siebert C, Holtappels M, Noriega-Ortega BE, De Beer D, *et al.* (2014). Sulfate reduction and sulfide oxidation in extremely steep salinity gradients formed by freshwater springs emerging into the Dead Sea. *FEMS Microbiol Ecol* **90**: 956–69.

Headd B, Engel AS. (2013). Evidence for niche partitioning revealed by the distribution of sulfur oxidation genes collected from areas of a terrestrial sulfidic spring with differing geochemical conditions. *Appl Environ Microbiol* **79**: 1171–82.

Henry S, Baudoin E, López-Gutiérrez JC, Martin-Laurent F, Brauman A, Philippot L. (2004). Quantification of denitrifying bacteria in soils by nirK gene targeted real-time PCR. *J Microbiol Methods* **59**: 327–35.

Henry S, Bru D, Stres B, Hallet S, Philippot L. (2006). Quantitative detection of the nosZ gene, encoding nitrous oxide reductase, and comparison of the abundances of 16S rRNA, narG, nirK, and nosZ genes in soils. *Appl Environ Microbiol* **72**: 5181–9.

Holling CS. (1996). Engineering resilience versus ecological resilience. In: Gunderson LH, Allen CR, Holling CS (eds). *Foundations of Ecological Resilience*. Island Press, pp 51–66.

Holling CS. (1973). RESILIENCE AND STABILITY.

Hollister EB, Engledow AS, Hammett AJM, Provin TL, Wilkinson HH, Gentry TJ. (2010). Shifts in microbial community structure along an ecological gradient of hypersaline soils and sediments. *ISME J* **4**: 829–38.

Huerta-Cepas J, Szklarczyk D, Forslund K, Cook H, Heller D, Walter MC, *et al.* (2016). eggNOG 4.5: a hierarchical orthology framework with improved functional annotations

for eukaryotic, prokaryotic and viral sequences. *Nucleic Acids Res* **44**: D286–D293.

Huson DH, Auch AF, Qi J, Schuster SC. (2007). MEGAN analysis of metagenomic data. *Genome Res* **17**: 377–386.

Hyatt D, Chen G-L, Locascio PF, Land ML, Larimer FW, Hauser LJ. (2010). Prodigal: prokaryotic gene recognition and translation initiation site identification. *BMC Bioinformatics* **11**: 119.

Jiménez DJ, Andreote FD, Chaves D, Montaña JS, Osorio-Forero C, Junca H, *et al.* (2012). Structural and Functional Insights from the Metagenome of an Acidic Hot Spring Microbial Planktonic Community in the Colombian Andes Badger JH (ed). *PLoS One* **7**: e52069.

Jones CM, Hallin S. (2010). Ecological and evolutionary factors underlying global and local assembly of denitrifier communities. *ISME J* **4**: 633–641.

Jones SE, Chiu C-Y, Kratz TK, Wu J-T, Shade A, McMahon KD. (2008). Typhoons initiate predictable change in aquatic bacterial communities. *Limnol Oceanogr* **53**: 1319–1326.

Jones SE, Lennon JT. (2010). Dormancy contributes to the maintenance of microbial diversity. *Proc Natl Acad Sci U S A* **107**: 5881–5886.

Jonsson V, Österlund T, Nerman O, Kristiansson E. (2016). Statistical evaluation of methods for identification of differentially abundant genes in comparative metagenomics. *BMC Genomics* **17**: 78.

Jørgensen BB, Revsbech NP. (1985). Diffusive boundary layers and the oxygen uptake of sediments and detritus1. *Limnol Oceanogr* **30**: 111–122.

Josephson KL, Gerba CP, Pepper IL. (1993). Polymerase chain reaction detection of

nonviable bacterial pathogens. *Appl Environ Microbiol* **59**: 3513–5.

Kawaguchi T, Decho AW. (2002). ISOLATION AND BIOCHEMICAL CHARACTERIZATION OF EXTRACELLULAR POLYMERIC SECRETIONS (EPS) FROM MODERN SOFT MARINE STROMATOLITES (BAHAMAS) AND ITS INHIBITORY EFFECT ON CACO $_3$ PRECIPITATION. *Prep Biochem Biotechnol* **32**: 51–63.

Kemp PF, Lee S, Laroche J. (1993). Estimating the growth rate of slowly growing marine bacteria from RNA content. *Appl Environ Microbiol* **59**: 2594–601.

Kerkhof L, Ward BB. (1993). Comparison of Nucleic Acid Hybridization and Fluorometry for Measurement of the Relationship between RNA/DNA Ratio and Growth Rate in a Marine Bacterium. *Appl Environ Microbiol* **59**: 1303–9.

Kim K, Zhang Y, Roberts GP. (1999). Correlation of activity regulation and substrate recognition of the ADP-ribosyltransferase that regulates nitrogenase activity in Rhodospirillum rubrum. *J Bacteriol* **181**: 1698–702.

Kirk Harris J, Gregory Caporaso J, Walker JJ, Spear JR, Gold NJ, Robertson CE, *et al.* (2012). Phylogenetic stratigraphy in the Guerrero Negro hypersaline microbial mat. *ISME J* **7**: 50–60.

Koike I, Hattori A. (1975). Energy yield of denitrification: an estimate from growth yield in continuous cultures of Pseudomonas denitrificans under nitrate-, nitrite- and oxide-limited conditions. *J Gen Microbiol* **88**: 11–9.

Könneke M, Bernhard AE, de la Torre JR, Walker CB, Waterbury JB, Stahl DA. (2005). Isolation of an autotrophic ammonia-oxidizing marine archaeon. *Nature* **437**: 543–546.

Kozich JJ, Westcott SL, Baxter NT, Highlander SK, Schloss PD. (2013). Development of

a dual-index sequencing strategy and curation pipeline for analyzing amplicon sequence data on the MiSeq Illumina sequencing platform. *Appl Environ Microbiol* **79**: 5112–20.

Kristiansson E, Hugenholtz P, Dalevi D. (2009). ShotgunFunctionalizeR: an R-package for functional comparison of metagenomes. *Bioinformatics* **25**: 2737–2738.

Kulp TR, Han S, Saltikov CW, Lanoil BD, Zargar K, Oremland RS. (2007). Effects of imposed salinity gradients on dissimilatory arsenate reduction, sulfate reduction, and other microbial processes in sediments from two California soda lakes. *Appl Environ Microbiol* **73**: 5130–7.

Lam P, Kuypers MMM. (2011). Microbial nitrogen cycling processes in oxygen minimum zones. *Ann Rev Mar Sci* **3**: 317–45.

Lee S-H, Sorensen JW, Grady KL, Tobin TC, Shade A. (2017). Divergent extremes but convergent recovery of bacterial and archaeal soil communities to an ongoing subterranean coal mine fire. *ISME J* **11**: 1447–1459.

van de Leemput IA, Veraart AJ, Dakos V, de Klein JJM, Strous M, Scheffer M. (2011). Predicting microbial nitrogen pathways from basic principles. *Environ Microbiol* **13**: 1477–87.

Lefebvre O, Vasudevan N, Thanasekaran K, Moletta R, Godon JJ. (2006). Microbial diversity in hypersaline wastewater: the example of tanneries. *Extremophiles* **10**: 505–513.

Lennon JT, Jones SE. (2011). Microbial seed banks: the ecological and evolutionary implications of dormancy. *Nat Rev Microbiol* **9**: 119–30.

Ley RE, Harris JK, Wilcox J, Spear JR, Miller SR, Bebout BM, *et al.* (2006). Unexpected diversity and complexity of the Guerrero Negro hypersaline microbial mat. *Appl Environ*

Microbiol **72**: 3685–3695.

Li D, Liu C-M, Luo R, Sadakane K, Lam T-W. (2015). MEGAHIT: an ultra-fast single-node solution for large and complex metagenomics assembly via succinct de Bruijn graph. *Bioinformatics* **31**: 1674–1676.

Liu H, Buskey EJ. (2000). Hypersalinity enhances the production of extracellular polymeric substance (eps) in the texas brown tide alga, aureoumbra lagunensis (pelagophyceae). *J Phycol* **36**: 71–77.

Liu Y, Beer LL, Whitman WB. (2012). Sulfur metabolism in archaea reveals novel processes. *Environ Microbiol* **14**: 2632–44.

Liu Y, Priscu JC, Xiong J, Conrad R, Vick-Majors T, Chu H, *et al.* (2016). Salinity drives archaeal distribution patterns in high altitude lake sediments on the Tibetan Plateau. *FEMS Microbiol Ecol* **92**. e-pub ahead of print, doi: 10.1093/femsec/fiw033.

Logares R, Lindström ES, Langenheder S, Logue JB, Paterson H, Laybourn-Parry J, *et al.* (2013). Biogeography of bacterial communities exposed to progressive long-term environmental change. *ISME J* **7**: 937–48.

Long A, Heitman J, Tobias C, Philips R, Song B. (2013). Co-occurring anammox, denitrification, and codenitrification in agricultural soils. *Appl Environ Microbiol* **79**: 168–76.

López-López a., Richter M, Peña a., Tamames J, Rosselló-Móra R. (2013). New insights into the archaeal diversity of a hypersaline microbial mat obtained by a metagenomic approach. *Syst Appl Microbiol* **36**: 205–214.

López-López A, Yarza P, Richter M, Suárez-Suárez A, Antón J, Niemann H, *et al.* (2010). Extremely halophilic microbial communities in anaerobic sediments from a solar

saltern. *Environ Microbiol Rep* **2**: 258–71.

Love MI, Huber W, Anders S. (2014). Moderated estimation of fold change and dispersion for RNA-seq data with DESeq2. *Genome Biol* **15**: 550.

Lozupone CA, Knight R. (2007). Global patterns in bacterial diversity. *Proc Natl Acad Sci U S A* **104**: 11436–40.

Ludwig D, Walker B, Holling CS. (1996). Sustainability, Stability, and Resilience. *Conserv Ecol* **1**: 1–27.

Des Marais DJ. (1990). Microbial mats and the early evolution of life. *Trends Ecol Evol* **5**: 140–144.

Marshall CW, Ross DE, Fichot EB, Norman RS, May HD. (2012). Electrosynthesis of commodity chemicals by an autotrophic microbial community. *Appl Environ Microbiol* **78**: 8412–20.

Marusina AI, Boulygina ES, Kuznetsov BB, Tourova TP, Kravchenko IK, Gal'chenko VF. (2001). A System of Oligonucleotide Primers for the Amplification of nifH Genes of Different Taxonomic Groups of Prokaryotes. *Microbiology* **70**: 73–78.

Marxsen J, Zoppini A, Wilczek S. (2010). Microbial communities in streambed sediments recovering from desiccation. *FEMS Microbiol Ecol* **71**: 374–386.

Maturrano L, Santos F, Rosselló-Mora R, Antón J. (2006). Microbial diversity in Maras salterns, a hypersaline environment in the Peruvian Andes. *Appl Environ Microbiol* **72**: 3887–95.

Mesbah NM, Abou-El-Ela SH, Wiegel J. (2007). Novel and unexpected prokaryotic diversity in water and sediments of the alkaline, hypersaline lakes of the Wadi An Natrun, Egypt. *Microb Ecol* **54**: 598–617.

Mikheenko A, Saveliev V, Gurevich A. (2016). MetaQUAST: evaluation of metagenome assemblies. *Bioinformatics* **32**: 1088–1090.

Mills HJ, Martinez RJ, Story S, Sobecky PA. (2005). Characterization of microbial community structure in Gulf of Mexico gas hydrates: comparative analysis of DNA- and RNA-derived clone libraries. *Appl Environ Microbiol* **71**: 3235–47.

Moeseneder MM, Arrieta JM, Herndl GJ. (2005). A comparison of DNA- and RNA-based clone libraries from the same marine bacterioplankton community. *FEMS Microbiol Ecol* **51**: 341–352.

Mohit V, Archambault P, Lovejoy C. (2015). Resilience and adjustments of surface sediment bacterial communities in an enclosed shallow coastal lagoon, Magdalen Islands, Gulf of St. Lawrence, Canada. *FEMS Microbiol Ecol* **91**: fiv038.

Mouné S, Caumette P, Matheron R, Willison JC. (2003). Molecular sequence analysis of prokaryotic diversity in the anoxic sediments underlying cyanobacterial mats of two hypersaline ponds in Mediterranean salterns. *FEMS Microbiol Ecol* **44**: 117–130.

Müller AK, Westergaard K, Christensen S, Sørensen SJ. (2002). The diversity and function of soil microbial communities exposed to different disturbances. *Microb Ecol* **44**: 49–58.

Muyzer G, Stams AJM. (2008). The ecology and biotechnology of sulphate-reducing bacteria. *Nat Rev Microbiol* **6**: 441.

Mylroie JR, Mylroie JE. (2007). DEVELOPMENT OF THE CARBONATE ISLAND KARST MODEL. *J Cave Karst Stud* **69**: 59–75.

Najjari A, Elshahed MS, Cherif A, Youssef NH. (2015). Patterns and Determinants of Halophilic Archaea (Class Halobacteria) Diversity in Tunisian Endorheic Salt Lakes and

Sebkhet Systems. **81**: 4432–4441.

Namiki T, Hachiya T, Tanaka H, Sakakibara Y. (2012). MetaVelvet: an extension of Velvet assembler to de novo metagenome assembly from short sequence reads. *Nucleic Acids Res* **40**: e155–e155.

Nazaries L, Murrell JC, Millard P, Baggs L, Singh BK. (2013). Methane, microbes and models: fundamental understanding of the soil methane cycle for future predictions. *Environ Microbiol* **15**: 2395–2417.

NCBI Resource Coordinators. (2017). Database Resources of the National Center for Biotechnology Information. *Nucleic Acids Res* **45**: D12–D17.

Nercessian O, Fouquet Y, Pierre C, Prieur D, Jeanthon C. (2005). Diversity of Bacteria and Archaea associated with a carbonate-rich metalliferous sediment sample from the Rainbow vent field on the Mid-Atlantic Ridge. *Environ Microbiol* **7**: 698–714.

Nogales B, Timmis KN, Nedwell DB, Osborn AM. (2002). Detection and Diversity of Expressed Denitrification Genes in Estuarine Sediments after Reverse Transcription-PCR Amplification from mRNA. *Appl Environ Microbiol* **68**: 5017–5025.

Nübel U, Garcia-Pichel F, Kühl M, Muyzer G. (1999). Quantifying microbial diversity: morphotypes, 16S rRNA genes, and carotenoids of oxygenic phototrophs in microbial mats. *Appl Environ Microbiol* **65**: 422–30.

Oakley BB, Francis CA, Roberts KJ, Fuchsman CA, Srinivasan S, Staley JT. (2007). Analysis of nitrite reductase (nirK and nirS) genes and cultivation reveal depauperate community of denitrifying bacteria in the Black Sea suboxic zone. *Environ Microbiol* **9**: 118–30.

Ochsenreiter T, Pfeifer F, Schleper C. (2002). Diversity of Archaea in hypersaline

environments characterized by molecular-phylogenetic and cultivation studies. *Extremophiles* **6**: 267–74.

Odom. (1993). What is an Asset? In: Vol. 7. *American Accounting Association*. pp 66–70.

Oksanen L, Fretwell SD, Arruda J, Niemela P. (1981). Exploitation Ecosystems in Gradients of Primary Productivity. *Am Nat* **118**: 240–261.

Ondov BD, Bergman NH, Phillippy AM. (2013). Krona: Interactive Metagenomic Visualization in a Web Browser. In: *Encyclopedia of Metagenomics*. Springer New York: New York, NY, pp 1–8.

Oren A. (1999). Bioenergetic aspects of halophilism. *Microbiol Mol Biol Rev* **63**: 334–48.

Oren A. (2013). Life in Magnesium- and Calcium-Rich Hypersaline Environments: Salt Stress by Chaotropic Ions. In: Springer, Dordrecht, pp 215–232.

Oren A. (2008). Microbial life at high salt concentrations: phylogenetic and metabolic diversity. *Saline Systems* **4**: 2.

Oren A. (2011). Thermodynamic limits to microbial life at high salt concentrations. *Environ Microbiol* **13**: 1908–23.

Øvreås L, Torsvik V. (1998). Microbial Diversity and Community Structure in Two Different Agricultural Soil Communities. *Microb Ecol* **36**: 303–315.

Paerl H, Joye S, Fitzpatrick M. (1993). Evaluation of nutrient limitation of C02 and N2 fixation in marine microbial mats. *Mar Ecol Prog Ser* **101**: 297–306.

Paerl HW, Fulton RS, Moisander PH, Dyble J. (2001). Harmful freshwater algal blooms, with an emphasis on cyanobacteria. *ScientificWorldJournal* **1**: 76–113.

Paerl HW, Steppe TF, Buchan KC, Potts M. (2003). Hypersaline cyanobacterial mats as

indicators of elevated tropical hurricane activity and associated climate change. *Ambio* **32**: 87–90.

Paerl HW, Yannarell AC. (2010). Environmental dynamics, community structure and function in a hypersaline microbial mat. In: *Microbial Mats*. Springer Netherlands, pp 421–442.

Parks DH, Tyson GW, Hugenholtz P, Beiko RG. (2014). STAMP: statistical analysis of taxonomic and functional profiles. *Bioinformatics* **30**. e-pub ahead of print, doi: 10.1093/bioinformatics/btu494.

Paul K, Nonoh JO, Mikulski L, Brune A. (2012). "Methanoplasmatales," Thermoplasmatales-related archaea in termite guts and other environments, are the seventh order of methanogens. *Appl Environ Microbiol* **78**: 8245–53.

Pedrós-Alió C. (2006). Marine microbial diversity: can it be determined? *Trends Microbiol* **14**: 257–263.

Peng Y, Leung HCM, Yiu SM, Chin FYL. (2011). Meta-IDBA: a de Novo assembler for metagenomic data. *Bioinformatics* **27**: i94-101.

Pester M, Bittner N, Deevong P, Wagner M, Loy A. (2010). A 'rare biosphere' microorganism contributes to sulfate reduction in a peatland. *ISME J* **4**: 1591–602.

Pester M, Schleper C, Wagner M. (2011). The Thaumarchaeota: an emerging view of their phylogeny and ecophysiology. *Curr Opin Microbiol* **14**: 300–6.

Petri R, Podgorsek L, Imhoff JF. (2001). Phylogeny and distribution of the sox B gene among thiosulfate-oxidizing bacteria. *FEMS Microbiol Lett* **197**: 171–178.

Philippot L, Hallin S. (2005). Finding the missing link between diversity and activity using denitrifying bacteria as a model functional community. *Curr Opin Microbiol* **8**:

234–239.

Pimm SL. (1984). The complexity and stability of ecosystems. *Nature* **307**: 321–326.

Pinckney J, Long R, Paerl H. (2011). Structural and functional responses of microbial mats to reductions in nutrient and salinity stressors in a Bahamian hypersaline lagoon. *Aquat Microb Ecol* **62**: 289–298.

Pinckney J, Paerla HW, Beboutb BM. (1995). Salinity control of benthic microbial mat community production in a Bahamian hypersaline lagoon. **187**: 223–237.

Pinckney JL, Paerl HW. (1997). Anoxygenic photosynthesis and nitrogen fixation by a microbial mat community in a bahamian hypersaline lagoon. *Appl Environ Microbiol* **63**: 420–6.

Pookhao N, Sohn MB, Li Q, Jenkins I, Du R, Jiang H, *et al.* (2015). A two-stage statistical procedure for feature selection and comparison in functional analysis of metagenomes. *Bioinformatics* **31**: 158–165.

Postgate J. (1998). The origins of the unit of nitrogen fixation at the University of Sussex. *Notes Rec R Soc* **52**: 355–362.

Poulsen LK, Ballard G, Stahl DA. (1993). Use of rRNA fluorescence in situ hybridization for measuring the activity of single cells in young and established biofilms. *Appl Environ Microbiol* **59**: 1354–60.

Preisner EC, Fichot EB, Norman RS. (2016). Microbial Mat Compositional and Functional Sensitivity to Environmental Disturbance. *Front Microbiol* **7**: 1632.

Prosser JI. (1997). Microbial processes witin te soil. In: Dekker M (ed). *Modern soil microiology*. New York, NY, pp 183–213.

Quast C, Pruesse E, Yilmaz P, Gerken J, Schweer T, Yarza P, *et al.* (2013). The SILVA

ribosomal RNA gene database project: improved data processing and web-based tools. *Nucleic Acids Res* **41**: D590-6.

R Development Core Team. (2015). R: a language and environment for statistical computing. https://www.gbif.org/tool/81287/r-a-language-and-environment-for-statistical-computing (Accessed August 23, 2017).

Reed HE, Martiny JBH. (2007). Testing the functional significance of microbial composition in natural communities. *FEMS Microbiol Ecol* **62**: 161–170.

Revsbech NP, Jmgensen BB, Blackburn TH, Cohen Y. (1983). Microelectrode studies of the photosynthesis and 02 , H & 5 , and pH profiles of a microbial mat1. **28**: 1062–1074.

Rietz D., Haynes R. (2003). Effects of irrigation-induced salinity and sodicity on soil microbial activity. *Soil Biol Biochem* **35**: 845–854.

Risgaard-Petersen N, Langezaal AM, Ingvardsen S, Schmid MC, Jetten MSM, Op den Camp HJM, *et al.* (2006). Evidence for complete denitrification in a benthic foraminifer. *Nature* **443**: 93–96.

Robertson CE, Spear JR, Harris JK, Pace NR. (2009). Diversity and stratification of archaea in a hypersaline microbial mat. *Appl Environ Microbiol* **75**: 1801–1810.

Robinson MD, McCarthy DJ, Smyth GK. (2010). edgeR: a Bioconductor package for differential expression analysis of digital gene expression data. *Bioinformatics* **26**: 139–40.

Rodriguez-Brito B, Rohwer F, Edwards RA. (2006). An application of statistics to comparative metagenomics. *BMC Bioinformatics* **7**: 162.

Rondon MR, August PR, Bettermann AD, Brady SF, Grossman TH, Liles MR, *et al.* (2000). Cloning the soil metagenome: a strategy for accessing the genetic and functional

diversity of uncultured microorganisms. *Appl Environ Microbiol* **66**: 2541–7.

Rosenzweig ML. (1999). Evolutionary ecology research. Evolutionary Ecology.

Rotthauwe J, Witzel K. (1997). The ammonia monooxygenase structural gene amoA as a functional marker : molecular fine-scale analysis of natural ammonia-oxidizing populations . The Ammonia Monooxygenase Structural Gene amoA as a Functional Marker : Molecular Fine-Scale Analysis of Natur.

Ruiz B, Chávez A, Forero A, García-Huante Y, Romero A, Sánchez M, *et al.* (2010). Production of microbial secondary metabolites: Regulation by the carbon source. *Crit Rev Microbiol* **36**: 146–167.

Russ L, Speth DR, Jetten MSM, Op den Camp HJM, Kartal B. (2014). Interactions between anaerobic ammonium and sulfur-oxidizing bacteria in a laboratory scale model system. *Environ Microbiol* **16**: 3487–98.

Rykiel EJ. (1985). Towards a definition of ecological disturbance. *Aust J Ecol* **10**: 361–365.

Sanli K, Karlsson FH, Nookaew I, Nielsen J. (2013). FANTOM: Functional and taxonomic analysis of metagenomes. *BMC Bioinformatics* **14**: 38.

Schäfer H, Muyzer G. (2001). Denaturing gradient gel electrophoresis in marine microbial ecology. *Methods Microbiol* **30**: 425–468.

Scheffer M, Carpenter S, Foley JA, Folke C, Walker B. (2001). Catastrophic shifts in ecosystems. *Nature* **413**: 591–6.

Schloss PD, Handelsman J. (2005). Metagenomics for studying unculturable microorganisms: cutting the Gordian knot. *Genome Biol* **6**: 229.

Schloss PD, Westcott SL, Ryabin T, Hall JR, Hartmann M, Hollister EB, *et al.* (2009).

Introducing mothur: open-source, platform-independent, community-supported software for describing and comparing microbial communities. *Appl Environ Microbiol* **75**: 7537–41.

Schneider D, Arp G, Reimer A, Reitner J, Daniel R. (2013). Phylogenetic analysis of a microbialite-forming microbial mat from a hypersaline lake of the Kiritimati atoll, Central Pacific. *PLoS One* **8**: e66662.

Sealey N. (2017). THE CLIMATE OF THE BAHAMAS. 1–13.

Segata N, Izard J, Waldron L, Gevers D, Miropolsky L, Garrett WS, *et al.* (2011). Metagenomic biomarker discovery and explanation. *Genome Biol* **12**: R60.

Severin I, Confurius-Guns V, Stal LJ. (2012). Effect of salinity on nitrogenase activity and composition of the active diazotrophic community in intertidal microbial mats. *Arch Microbiol* **194**: 483–91.

Severin I, Lindström ES, Östman Ö, Vrede K, Karlsson J. (2014). Relationships between Bacterial Community Composition, Functional Trait Composition and Functioning Are Context Dependent – but What Is the Context? Antonopoulos DA (ed). *PLoS One* **9**: e112409.

Severin I, Stal LJ. (2010). NifH expression by five groups of phototrophs compared with nitrogenase activity in coastal microbial mats. *FEMS Microbiol Ecol* **73**: 55–67.

Shade A, Peter H, Allison SD, Baho DL, Berga M, Bürgmann H, *et al.* (2012a). Fundamentals of microbial community resistance and resilience. *Front Microbiol* **3**: 417.

Shade A, Read JS, Welkie DG, Kratz TK, Wu CH, McMahon KD. (2011). Resistance, resilience and recovery: aquatic bacterial dynamics after water column disturbance. *Environ Microbiol* **13**: 2752–67.

Shade A, Read JS, Youngblut ND, Fierer N, Knight R, Kratz TK, *et al.* (2012b). Lake microbial communities are resilient after a whole-ecosystem disturbance. *ISME J* **6**: 2153–67.

Sharpton TJ. (2014). An introduction to the analysis of shotgun metagenomic data. *Front Plant Sci* **5**: 209.

Shen J, Hirayama O. (1991). Hydrogen photoproduction and denitrification by photosynthetic bacteria isolated from Lake Nakaumi and its vicinity. *J Ferment Bioeng* **72**: 338–342.

Shrader-Frechette KS. (1993). Method in Ecology: Strategies for Conservation. In: *The Quarterly Review of Biology*. Cambridge University Press. e-pub ahead of print, doi: 10.1086/418924.

Sinigalliano CD, Gidley ML, Shibata T, Whitman D, Dixon TH, Laws E, *et al.* (2007). Impacts of Hurricanes Katrina and Rita on the microbial landscape of the New Orleans area. *Proc Natl Acad Sci U S A* **104**: 9029–34.

Smith JM, Ogram A. (2008). Genetic and functional variation in denitrifier populations along a short-term restoration chronosequence. *Appl Environ Microbiol* **74**: 5615–20.

Sogin ML, Morrison HG, Huber JA, Mark Welch D, Huse SM, Neal PR, *et al.* (2006). Microbial diversity in the deep sea and the underexplored 'rare biosphere'. *Proc Natl Acad Sci U S A* **103**: 12115–20.

Sorensen KB, Canfield DE, Oren A. (2004). Salinity Responses of Benthic Microbial Communities in a Solar Saltern (Eilat, Israel). *Appl Environ Microbiol* **70**: 1608–1616.

Sorensen KB, Canfield DE, Teske AP, Oren A. (2005). Community Composition of a Hypersaline Endoevaporitic Microbial Mat. *Appl Environ Microbiol* **71**: 7352–7365.

Sorokin DY, Berben T, Melton ED, Overmars L, Vavourakis CD, Muyzer G. (2014). Microbial diversity and biogeochemical cycling in soda lakes. *Extremophiles* **18**: 791–809.

Sousa WP. (1984). The Role of Disturbance in Natural Communities. *Annu Rev Ecol Syst* **15**: 353–391.

Stahl DA, de la Torre JR. (2012). Physiology and diversity of ammonia-oxidizing archaea. *Annu Rev Microbiol* **66**: 83–101.

Stal LJ. (1994). Microbial mats in coastal environments. In: *Microbial Mats*. Springer Berlin Heidelberg: Berlin, Heidelberg, pp 21–32.

STAL LJ. (1995). Physiological ecology of cyanobacteria in microbial mats and other communities. *New Phytol* **131**: 1–32.

Stal LJ, Gemerden H, Krumbein WE. (1985). Structure and development of a benthic marine microbial mat. *FEMS Microbiol Lett* **31**: 111–125.

States DJ, Gish W. (1994). Combined use of sequence similarity and codon bias for coding region identification. *J Comput Biol* **1**: 39–50.

Steppe TF, Pinckney JL, Dyble J, Paerl HW. (2001). Diazotrophy in Modern Marine Bahamian Stromatolites. *Microb Ecol* **41**: 36–44.

Steunou A-S, Jensen SI, Brecht E, Becraft ED, Bateson MM, Kilian O, *et al.* (2008). Regulation of nif gene expression and the energetics of N2 fixation over the diel cycle in a hot spring microbial mat. *ISME J* **2**: 364–78.

Strous M, Kuenen JG, Jetten MS. (1999). Key physiology of anaerobic ammonium oxidation. *Appl Environ Microbiol* **65**: 3248–50.

Su X, Pan W, Song B, Xu J, Ning K. (2014). Parallel-META 2.0: Enhanced

Metagenomic Data Analysis with Functional Annotation, High Performance Computing and Advanced Visualization Zhang Z (ed). *PLoS One* **9**: e89323.

Tansley AG. (1935). The Use and Abuse of Vegetational Concepts and Terms. *Ecology* **16**: 284–307.

Teske A, Ramsing NB, Habicht K, Fukui M, Küver J, Jørgensen BB, *et al.* (1998). Sulfate-reducing bacteria and their activities in cyanobacterial mats of solar lake (Sinai, Egypt). *Appl Environ Microbiol* **64**: 2943–51.

Thiel H. (1994). Gene E. Likens: The 'Ecosystem Approach: Its Use and Abusein: Excellence in Ecology. O. Kinne (Ed.). Publisher: Ecology Institute, Nordbünte 23, 21385 Oldendorf, FRG. 1992. ISSN 0932–2205. DM 59,-. *Int Rev der gesamten Hydrobiol und Hydrogr* **79**: 323–324.

Throbäck IN, Enwall K, Jarvis A, Hallin S. (2004). Reassessing PCR primers targeting nirS, nirK and nosZ genes for community surveys of denitrifying bacteria with DGGE. *FEMS Microbiol Ecol* **49**: 401–17.

Tomlinson GA, Jahnke LL, Hochstein LI. (1986). Halobacterium denitrificans sp. nov., an extremely halophilic denitrifying bacterium. *Int J Syst Bacteriol* **36**: 66–70.

Trigui H, Masmoudi S, Brochier-Armanet C, Barani A, Grégori G, Denis M, *et al.* (2011). Characterization of heterotrophic prokaryote subgroups in the Sfax coastal solar salterns by combining flow cytometry cell sorting and phylogenetic analysis. *Extremophiles* **15**: 347–358.

Tripathi S, Kumari S, Chakraborty A, Gupta A, Chakrabarti K, Bandyapadhyay BK. (2005). Microbial biomass and its activities in salt-affected coastal soils. *Biol Fertil Soils* **42**: 273–277.

Turk-Kubo KA, Achilles KM, Serros TRC, Ochiai M, Montoya JP, Zehr JP. (2012). Nitrogenase (nifH) gene expression in diazotrophic cyanobacteria in the Tropical North Atlantic in response to nutrient amendments. *Front Microbiol* **3**: 386.

Tyson GW, Chapman J, Hugenholtz P, Allen EE, Ram RJ, Richardson PM, *et al.* (2004). Community structure and metabolism through reconstruction of microbial genomes from the environment. *Nature* **428**: 37–43.

Visscher PT, Gritzer RF, Leadbetter ER. (1999). Low-molecular-weight sulfonates, a major substrate for sulfate reducers in marine microbial mats. *Appl Environ Microbiol* **65**: 3272–8.

Visscher PT, Reid RP, Bebout BM, Hoeft SE, Macintyre IG, Thompson JA. (1998). Formation of lithified micritic laminae in modern marine stromatolites (Bahamas); the role of sulfur cycling. *Am Mineral* **83**: 1482–1493.

Visscher PT, Stolz JF. (2005). Microbial mats as bioreactors: populations, processes, and products. *Palaeogeogr Palaeoclimatol Palaeoecol* **219**: 87–100.

Wagner M, Loy A, Klein M, Lee N, Ramsing NB, Stahl DA, *et al.* (2005). Functional marker genes for identification of sulfate-reducing prokaryotes. *Methods Enzymol* **397**: 469–89.

Wagner M, Roger AJ, Flax JL, Brusseau GA, Stahl DA. (1998). Phylogeny of dissimilatory sulfite reductases supports an early origin of sulfate respiration. *J Bacteriol* **180**: 2975–82.

Warnes G, Bolker B, Bonebakker L, Gentleman R, Hubert W, Liaw A, *et al.* (2012). gplots: Various R programming tools for plotting data. http://cran.r-project.org/package=gplots.

Webster G, O'Sullivan LA, Meng Y, Williams AS, Sass AM, Watkins AJ, *et al.* (2015). Archaeal community diversity and abundance changes along a natural salinity gradient in estuarine sediments. *FEMS Microbiol Ecol* **91**: 1–18.

Wertz S, Degrange V, Prosser JI, Poly F, Commeaux C, Guillaumaud N, *et al.* (2007). Decline of soil microbial diversity does not influence the resistance and resilience of key soil microbial functional groups following a model disturbance. *Environ Microbiol* **9**: 2211–2219.

Wetzel RG. (2001). Limnology: Lake and River Ecosystems. Academic Press: San Diego.

White JR, Nagarajan N, Pop M, Purdom E, Dethlefsen L. (2009). Statistical Methods for Detecting Differentially Abundant Features in Clinical Metagenomic Samples Ouzounis CA (ed). *PLoS Comput Biol* **5**: e1000352.

Whitehead T. (1999). Phylogenetic diversity of methanogenic archaea in swine waste storage pits. *FEMS Microbiol Lett* **179**: 223–226.

Williams RJ, Howe A, Hofmockel KS. (2014). Demonstrating microbial co-occurrence pattern analyses within and between ecosystems. *Front Microbiol* **5**: 358.

Woebken D, Burow LC, Behnam F, Mayali X, Schintlmeister A, Fleming ED, *et al.* (2015). Revisiting N_2 fixation in Guerrero Negro intertidal microbial mats with a functional single-cell approach. *ISME J* **9**: 485–96.

Wong HL, Smith D-L, Visscher PT, Burns BP. (2015). Niche differentiation of bacterial communities at a millimeter scale in Shark Bay microbial mats. *Sci Rep* **5**: 15607.

Worrall F, Burt TP. (2010). Has the composition of fluvial DOC changed? Spatiotemporal patterns in the DOC-color relationship. *Global Biogeochem Cycles* **24**:

n/a-n/a.

Yang J, Jiang H, Dong H, Wang H, Wu G, Hou W, *et al.* (2013). amoA-encoding archaea and thaumarchaeol in the lakes on the northeastern Qinghai-Tibetan Plateau, China. *Front Microbiol* **4**: 329.

Yannarell AC, Steppe TF, Paerl HW. (2007). Disturbance and recovery of microbial community structure and function following Hurricane Frances. **9**: 576–583.

Yeo SK, Huggett MJ, Eiler A, Rappé MS, Falsen E. (2013). Coastal Bacterioplankton Community Dynamics in Response to a Natural Disturbance Kirchman DL (ed). *PLoS One* **8**: e56207.

Yoshimatsu K, Sakurai T, Fujiwara T. (2000). Purification and characterization of dissimilatory nitrate reductase from a denitrifying halophilic archaeon, Haloarcula marismortui. *FEBS Lett* **470**: 216–220.

Youssef NH, Ashlock-Savage KN, Elshahed MS. (2012). Phylogenetic Diversities and Community Structure of Members of the Extremely Halophilic Archaea (Order Halobacteriales) in Multiple Saline Sediment Habitats. *Appl Environ Microbiol* **78**: 1332–1344.